SVENSKA GEOFYSISKA FÖRENINGEN

VOLUME 10, NUMBER 2 **Tellus** MAY 1958

A QUARTERLY JOURNAL OF GEOPHYSICS

Some Examples of Stationary Planetary Flow Patterns in Bounded Basins[1]

By HENRY STOMMEL, A. B. ARONS and A. J. FALLER

Woods Hole Oceanographic Institution, Massachusetts

(Manuscript received August 22, 1957)

Abstract

A simple regime of fluid flow is defined. This regime can occur in a homogeneous layer of fluid (i) of uniform depth on a rotating sphere and bounded by meridional barriers (ii) of uniform depth on a betaplane and bounded by barriers running north-south (iii) of radially non-uniform depth on a rotating plane and bounded by radial barriers. The essential elements defining the regime are: (a) the flow in the whole layer is steady and geostrophic except and only (b) at the western boundary where a narrow, intense western boundary current is permitted to depart markedly from geostrophy, and (c) the system, which would otherwise be at rest, is driven by a distribution of sources and sinks of fluid (this includes driving agents such as the wind, which can be expressed in terms of source and sink distributions).

Predictions concerning patterns of flow have been deduced from the defined regime and verified experimentally on a rotating model of type (iii). Certain results obtained were by no means intuitively obvious from *a priori* considerations.

Introduction

It is generally recognized that the specific results obtained in theoretical hydrodynamics are not achieved deductively from the general hydrodynamical equations, but on the contrary, are derived deductively only from very much simplified fluid models (or, to say the same thing, an abbreviated set of equations). For example, there is a large range of problems where the so-called perfect fluid idealization proves an adequate representation of what is observed; another range in which laminar viscous flow is adequate. Hydraulic engineers have invented even simpler sets of equations to describe gradually varied flow and flow in transitions. The justification for applying such simplified equations to any particular set of problems is largely *a posteriori;* that is, we judge the reasonableness of the simplified regime of fluid flow by its results.

In meteorology and oceanography there is a constant search for such simple regimes. As an example from meteorology, Rossby's recognition of the essential dynamical elements of the long waves in the westerlies has led to formulation of a barotropic regime of atmospheric flow—and a simple set of equations—which meteorologists hope may describe major features of the atmospheric circulation and perhaps even be useful for prediction. In oceanography there has gradually emerged a conception of a regime of fluid flow which seems to be peculiarly applicable to large scale stationary oceanic flow patterns (for a summary see STOMMEL, 1957). This regime can occur in a homogeneous layer of fluid (i) of uniform depth on a rotating sphere and bounded by meridional barriers (ii) of uniform depth on a beta-plane and bounded by barriers running north-south (iii) of radially non-uniform depth on a rotating plane and bounded by radial barriers. The essential elements which define this simplified regime are: (a) the flow in the whole layer is steady and geostrophic except and only

[1] Contribution No. 939 of the Woods Hole Oceanographic Institution.

(b) at the western boundary where a narrow, intense western boundary current is permitted to depart markedly from geostrophy; and moreover, (c) this system, which would otherwise be at rest, is driven by a distribution of sources and sinks of fluid (various driving agents such as the wind can be expressed in terms of source and sink distributions, so this is no real restriction).

Although our main interest in this regime of planetary flow is in its possible applicability to oceanic circulation, we felt that some of its implications were so bizarre and contrary to intuition that it would be reassuring if they could be partially tested by model experiments. Thus, the model experiments are not meant as »scale models» of what perhaps occurs in the real ocean. We conceive of them as being tests of the internal consistency of the conceptual elements (a, b, c) which define the regime. The notion that such a regime can exist is mainly built on plausibility arguments. The elements which make up the regime are susceptible to quantitative mathematical description; hence, given the distribution of sources and sinks, the circulation pattern can be deduced. If, in comparing the predicted circulation pattern with that observed in a model experiment with a rotating basin, a large discrepancy should arise, it would suggest, among other things, that there were hidden inconsistencies or contradictions in the formulation of the regime. On the other hand, if the experiments with the basin verify the predictions, especially for flow patterns which do not seem intuitively obvious, the belief that such a simple regime might be applicable to the ocean is strengthened, although of course not confirmed. One then, however, feels encouraged to undertake the labor involved in constructing theoretical models and pursuing their implications, the ultimate validation lying in agreement between predictions of the theory and observable phenomena in the ocean.

A priori predictions for a particular rotating model

The model used in this work was a pie-shaped sector of a rotating basin of fluid (Fig. 1). The bottom of the basin is level. The free surface is a paraboloidal cylinder with axis vertical, concave upward. The undisturbed

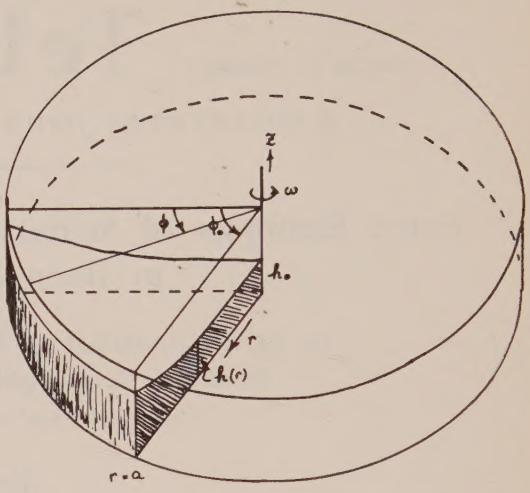

Fig. 1. Schematic diagram of rotating sector showing notation used in theoretical formulation.

depth varies radially from a minimum at the center to a maximum at the rim. The top is covered with a sheet of glass to prevent the air in the room from exerting a stress on the water surface. After the basin has been rotating for some time the fluid in the sector is completely at rest with respect to the basin. In a geometrical configuration of this kind it is clear that any radial component of geostrophic flow is horizontally divergent due to the radial variation in depth of the fluid. A radially outward (inward) component of flow in the interior can therefore only occur if there is a local source (sink) of water. Components of geostrophic flow along circles of constant radius are permissible without divergence, except where blocked by radial barriers.

Before we had carried out any mathematical analysis or experimental work we could see that our regime led qualitatively to some rather remarkable deductions. For example, consider the circulation induced by a point source ⊕ and sink ⊖ of equal intensity placed near to the eastern boundary of the sector (the absolute sense of rotation of the basin in Fig. 2, as viewed from above is counterclockwise, as in the northern hemisphere on the earth) at different radii. Since there are no distributed sources or sinks over the remainder of the basin, all radial geostrophic flow is prohibited in the interior. We deduce that the only permissible circulation pattern, according to the rules of the regime, is one in which zonal geostrophic flow

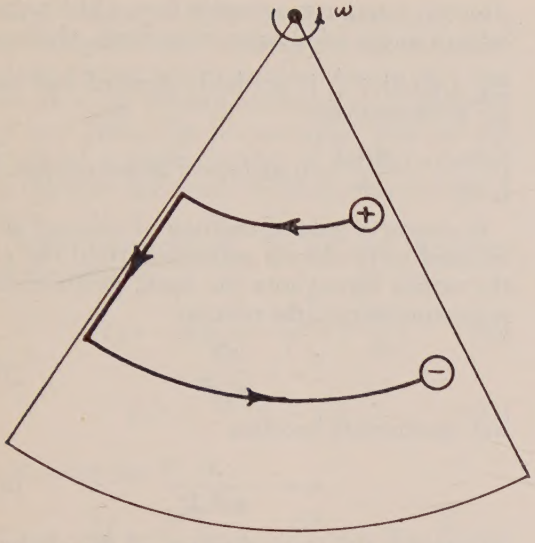

Fig. 2. Diagram of circulation induced in rotating sector by source ⊕ and sink ⊖ positioned as shown.

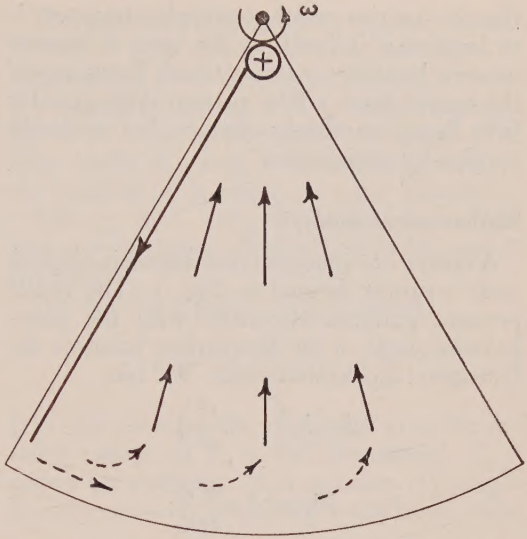

Fig. 3. Sketch of flow pattern expected with source ⊕ at apex of sector, surface of fluid rising uniformly. (Dashed arrows are sketched in to indicate portions of flow not given by elementary theory but evidently required by continuity.)

extends from the source to the western boundary, thence down the western boundary in a narrow, intense boundary current to the radius of the sink, and thence, in another zonal geostrophic flow to the sink. This flow pattern is very circuitous as compared to what occurs in the absence of rotation and non-uniform depth. It was the first flow pattern which we attempted to verify by an actual experiment.

From the point of view of our interest in the eventual application of the regime to oceanic circulation patterns it was desirable to make some deductions and experiments involving distributed sources and sinks. It is easy to obtain a uniform sink (source) over the whole fluid surface by allowing the tank slowly to fill up (empty), thus producing an overall rise (drop) of the free equilibrium surface. As an example, consider the flow pattern induced by an isolated source at the apex of the sector (Fig. 3). Since there is no point sink provided, the free surface rises uniformly—the equivalent of a uniformly distributed sink over the entire sector. Hence, qualitatively, one would expect an inward directed radial component of geostrophic velocity everywhere in the sector, connected to the source by a western boundary current, as sketched in Fig. 3. This is indeed rather surprising: the basin fills up from the rim, although water is added at the apex. But a quantitative analysis (see below) reveals even more surprising features. When the sector is allowed to fill up from an isolated source at the western edge of the rim (Fig. 4), the interior geostrophic flow is again toward the center, but the mathematical development indicates

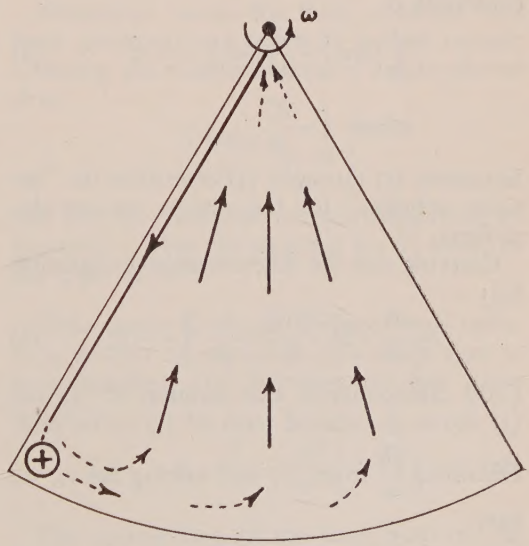

Fig. 4. Sketch of flow pattern expected with source ⊕ at western edge of rim, surface of fluid rising uniformly.

that the interior radial geostrophic transport is so large that it feeds. at the apex, a narrow western boundary current which flows *toward* the source. Such a flow pattern (Fig. 4) is far from being intuitively obvious, but is clearly verified by experiment.

Mathematical analysis

A system of cylindrical coordinates is adopted with notation defined in Fig. 1. The radial pressure gradient associated with the paraboloidal shape of the free surface balances the centripetal acceleration term. We take

$$h = h_0\left(1 + l\frac{r^2}{a^2}\right) \tag{1}$$

$$\text{where } l = \frac{\omega^2 a^2}{2gh_0};$$

h denotes the height of the unpertubed paraboloidal surface. Assuming hydrostatic equilibrium in the vertical direction and denoting by ζ the vertical displacement associated with steady geostrophic flow, the equations of motion (neglecting inertial terms) take the form

$$2\omega v_\varphi = g\frac{\partial \zeta}{\partial r} \tag{2}$$

$$-2\omega v_r = \frac{g}{r}\frac{\partial \zeta}{\partial \varphi} \tag{3}$$

Neglecting ζ relative to h, the equation of continuity is

$$\frac{\partial}{\partial r}(hrv_r) + \frac{\partial}{\partial \varphi}(hv_\varphi) = -r\dot{\zeta} \tag{4}$$

$$\text{where } \dot{\zeta} = \frac{\partial \zeta}{\partial t}$$

Equations (1) throught (4) determine the "interior solution" for the regime we are describing.

Carrying out the differentiation in equation (4):

$$rv_r\frac{dh}{dr} + h\left[\frac{\partial(rv_r)}{\partial r} + \frac{\partial v_\varphi}{\partial \varphi}\right] = -r\dot{\zeta} \tag{5}$$

Cross differentiation and addition of (2) and (3) shows the second term of (5) to be zero. Obtaining $\frac{dh}{dr}$ from (1) and solving for v_r, we have:

$$v_r = -\frac{\dot{\zeta}a^2}{2h_0 lr} \tag{6}$$

Thus the interior geostrophic flow which arises when a source adds water to the basin, producing a positive $\dot{\zeta}$, is northerly directed and has no φ component.

$$\left[\frac{\partial v_\varphi}{\partial \varphi} = -\frac{\partial(rv_r)}{\partial r} = 0, \text{ and } v_\varphi = 0 \text{ at eastern edge.}\right]$$

If sources S (rate of addition of volume) are assumed to produce a uniform vertical rise of the surface throughout the basin, geometrical requirements give the relation:

$$\dot{\zeta} = -\frac{2S}{\varphi_0 a^2}, \tag{7}$$

and equation (6) becomes

$$v_r = -\frac{S}{\varphi_0 h_0 lr} \tag{8}$$

Consider the water budget of the shaded sector defined by $r = r$ in Fig. 5. T_I represents the transport into the sector by the interior geostrophic flow; T_v represents the vertical transport associated with $\dot{\zeta}$; S_0 denotes the source transport; and T_w denotes the western boundary transport. We have postulated the existence of T_w as one of the elements of the regime, and we solve for it on the basis of the mass conservation requirement:

$$T_w + T_I + S_0 + T_v = 0 \tag{9}$$

The ambiguity implied in the term T_w should be carefully noted. This is *not* a dyna-

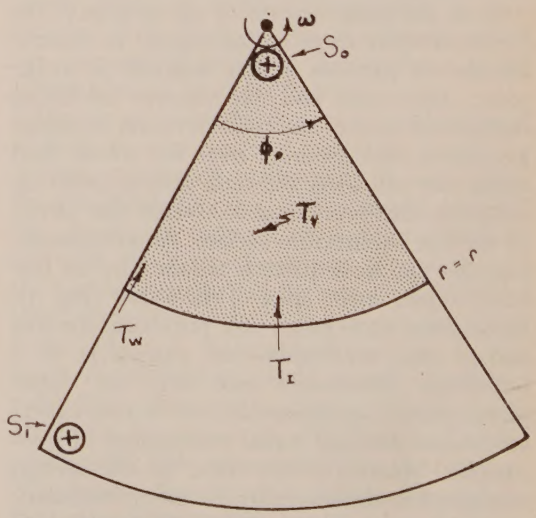

Fig. 5. Notation for analyzing water budget of the shaded sector $T_w + T_I + T_v + S_0 = 0$

mical solution; T_w is simply postulated as a *net* transport. There is nothing in the definition of the regime which precludes more than one stream at the western boundary or meandering of any kind. The net transport may be the result of a single current, of parallel currents in opposite directions, or some other combination.

From equations (7), (8) and the geometry of the system:

$$T_I = -hr\varphi_0 v_r = \frac{S}{l}\left(1 + \frac{lr^2}{a^2}\right) \qquad (10)$$

$$T_v = -\frac{\varphi_0 r^2}{2}\dot{\zeta} = -S\frac{r^2}{a^2} \qquad (11)$$

Solving for T_w:

$$T_w = -\frac{S}{l}\left(1 + \frac{lr^2}{a^2}\right) - S_0 + \frac{Sr^2}{a^2} = -S_0 - \frac{S}{l} \qquad (12)$$

where, for the general case depicted in Fig. 5,

$$S = S_0 + S_1$$

We can now interpret the results for T_w for various specific cases:

Case 1. S_0 positive, $S_1 = 0$. (Fig. 3).

For this case equation (12) becomes:

$$T_w = -S_0\left(1 + \frac{1}{l}\right) \qquad (13)$$

The mathematical analysis of the postulated regime thus predicts a southerly transport at the western boundary of the model. The transport is *larger* than the input of the source at the apex by the amount S_0/l, l being the parameter characterizing the slope of the equilibrium paraboloidal surface. If the angular velocity ω is such that $h(a) = 2h_0$, $l = 1$, and the total boundary transport is *twice* the transport of the source. The transport is independent of r and the boundary current must therefore flow undiminished to the outer rim of the basin, turn to the eastward at the outer rim, and from that region feed the north-bound interior geostrophic flow. Part of the boundary current (the amount S_0/l) represents a *recirculation flow* of water originally in the basin.

Case 2. $S_0 = 0$, S_1 positive (Fig. 4).

For this case equation (12) becomes:

$$T_w = -\frac{S_1}{l} \qquad (14)$$

This predicts a flow pattern essentially similar to that of Case 1, but the result is even more surprising. If $l = 1$, the regime requires a *southerly* boundary current with a transport *equal to that at the source* in the southwest corner! (The same result, of course, is obtained regardless of the position of S_1 along the outer boundary.)

Case 3. $S_0 = -xS_1$, S positive. (i.e. a fraction x of the input is drained off at the apex of the model.)

For this case equation (12) becomes:

$$T_w = \frac{S_1}{l}\left[x(l+1) - 1\right] \qquad (15)$$

In this situation the ambiguity as to the detailed nature of T_w is well dramatized. T_w is only a *net* transport. Thus equation (15) might be interpreted as describing a southerly transport of magnitude $\frac{S_1}{l}$ paralleling a northerly transport $\frac{S_1 x}{l}$ $(l+1)$, or as a single transport either north or south (changing direction when $x = \frac{1}{l+1}$), or as some other combination leading to the same *net* T_w.

Order of magnitude of approximations in the theory

Numerical values for flow, rotation, and basin geometry are given in a later section. Utilizing the numerical data, it can be shown that:

$$\frac{\zeta \text{ max.}}{h} \sim 10^{-4}$$

and that the fractional transport neglected by dropping ζ from the equation for T_I is also of the order of 10^{-4}.

If the sector is cut off at some small radius $r = a_0$ instead of extending to a sharp apex at $r = 0$, equation (12) becomes, to first order terms:

$$T_w = -S_0 - \frac{S}{l} - S\frac{a_0^2}{a^2}\left(1 + \frac{1}{l}\right) \qquad (16)$$

The contribution of the third term on the right hand side is of the order of 10% when a_0/a is about 0.2.

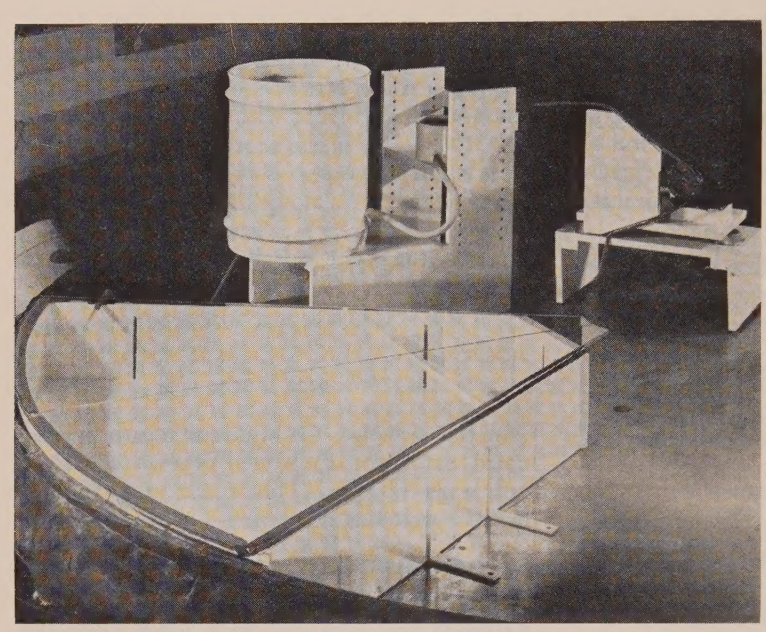

Fig. 6. A photograph of the rotating tank showing the 60° sector with 1/4-inch slots at various positions in the walls for the introduction or extraction of mass. When not in use the slots are sealed with tape. The glass cover prevents wind stress on the free surface of the water. A controlled flow rate is obtained by adjusting the level of the small can (with an overflow) into which water is pumped continuously. A constant head of water is thereby maintained in the large can containing the dyed source water.

The Laboratory Experiments

To check and demonstrate the principles of the foregoing theory and quantitative notions concerning the flow in a simple laboratory model, the 7-ft. diameter rotating tank previously employed for oceanographic models (VON ARX, 1952) was used. For these studies a truncated sector of 60° width (Fig. 6) was isolated by wooden partitions with several vertical slots in the walls for the introduction or extraction of mass. An alternate source was direct injection of the fluid through a vertical glass tube at any desired point in the interior of the sector.

The rate of in flow of mass was an important consideration and was adjusted so that the Rossby number for the western boundary current was of the same order of magnitude as that for the Gulf Stream system. Similar values of the Rossby number (defined by $R_0 = v/\omega R = = .001$ where v is a representative velocity and ωR is the tangential speed of rotation) are obtained when the circulations have approximately the same degree of geostrophy. The ratio of depth at the rim to that at the center (h_a/h_0) was set at approximately 2 in all cases, a value corresponding to $l = 1$ in the theoretical discussion. Other significant parameters were $\omega = 1.05$ sec.$^{-1}$, $a = 100$ cm., and $\bar{h} = 8$ cm.

Fig. 7 shows a sequence of photographs of an experiment which corresponded approximately to the situation of Fig. 2. Dyed water entered through the slot at the upper right and showed the path followed by the water in migrating zonally across the tank, down the western boundary, and zonally across the tank to the exit slot at the eastern wall of the sector. The flow was not as simple as that of the idealized diagram primarily because only 5/6 S_0 passed through the exit slot and 1/6 S_0 was used to raise the level of water in the sector. By the preceding theoretical arguments, there should have been a slow radially inward (poleward) flow over the interior of the tank and this was manifest in the poleward spread of dye from both of the zonal currents. In addition to the southward flowing western boundary current of strength S_0, the theory also predicts an additional component of 1/6 S_0 which is required by continuity and is associated with the distributed sink of 1/6 S_0. This "recirculation" was not made up of source water and must have been drawn from the interior of the basin. We interpret the thin streak of clear water (Figs. 8b, c) between the primary current near the western wall and the poleward flowing mass in the interior as evidence for the "recirculation" flow.

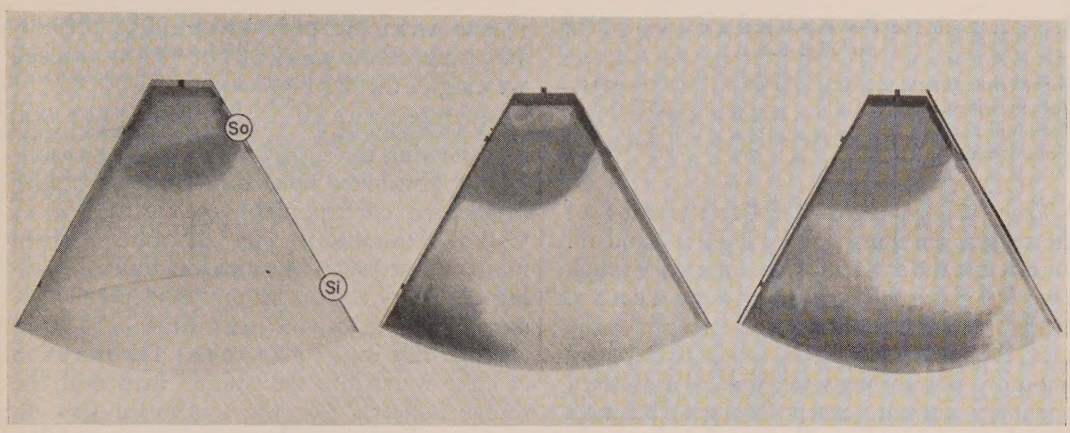

Fig. 7. Photographs at 20, 80, and 220 minutes after the introduction of dye, showing the path followed by the source water ($S_0 = 50$ cc./min.) in flowing from a slot in the eastern wall near the apex to the sink ($S_1 = 5/6\ S_0$) in the same wall near the rim (corresponding to Fig. 2).

Fig. 8 illustrates the circulation with the source at the apex of the sector and with no external sink, i.e., with a uniform rise of the water level in the tank (a uniformly distributed sink). (Compare with Fig. 3 and Case 1. of the mathematical analysis.) In accord with the theory, the interior of the basin filled from the rim and continuity was maintained by an intense western current S_0 from the source, which was augmented by a recirculation (theoretically of strength S_0 for $l = 1$) from the interior water. Evidence for this recirculation is the clear streak in Figs. 8b, c which penetrates toward the rim into the dyed fluid near the western wall. By evaluating the volume of fluid-containing dye, the transport of the total western boundary current has been determined for comparison with the source strength. The data of Table I show that: a) at 20 minutes the dyed fluid was composed almost entirely of source water, b) at 60 minutes the dyed fluid occupied twice the total volume of the input, which implies mixing with an equal volume of clear water (presumably that from the recirculated component of the boundary current), and c) at 125 minutes the dyed volume was less than twice that of the source input, a fact which is consistent with the decrease in the factor l as the mean depth of the fluid ($\bar{h}$) gradually increased. These results are in rough agreement with the quantitative predictions of the theory.

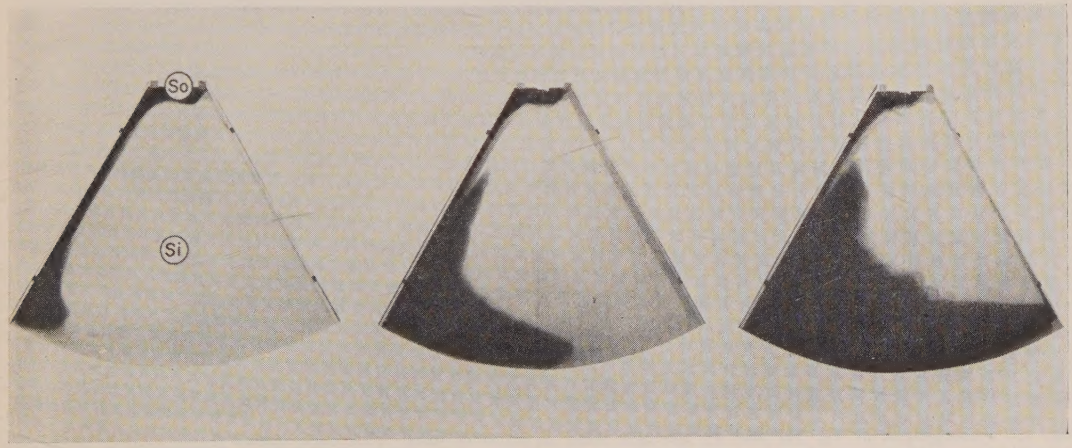

Fig. 8. Photographs at 20, 60, and 80 minutes with $S_0 = 120$ cc./min. The source was at the apex and there was no external sink (corresponding to Fig. 3).

Table 1. Data for the experiment corresponding to Fig. 8.

Elapsed time (minutes)	20	60	125
Volume with dye (liters)	1.9	14.6	27.4
Total input from source	2.4	7.2	15.0
Mean depth (h), (cm)	7.7	8.2	10.3

The situations discussed in Cases 2. and 3. of the analysis are illustrated by Figures 9 and 10. In each case the dyed mass was injected through a vertical glass tube in the southwestern corner. In Fig. 9, with a sink of equal strength at the apex, the greater part of the source mass passed smoothly out through the sink as a western boundary current, except for protuberances caused by inertial oscillations in the tank. (These were the product of slight periodic variations of the rotation rate due to uneven wearing of the driving belt.)

By eliminating the external sink at the apex and allowing the surface to rise slowly (a uniformly distributed sink) as in Fig. 10, we have a situation corresponding to Fig. 4 and to Case 2. of the analysis. Figs. 10b and 10c (three minutes apart) show the rapid southward flowing boundary stream by means of permanganate dye from crystals that were introduced through slits in the glass cover. The intrusion of clear water into the colored mass near the source indicates that the southward flowing current mixed with the source mass, and the

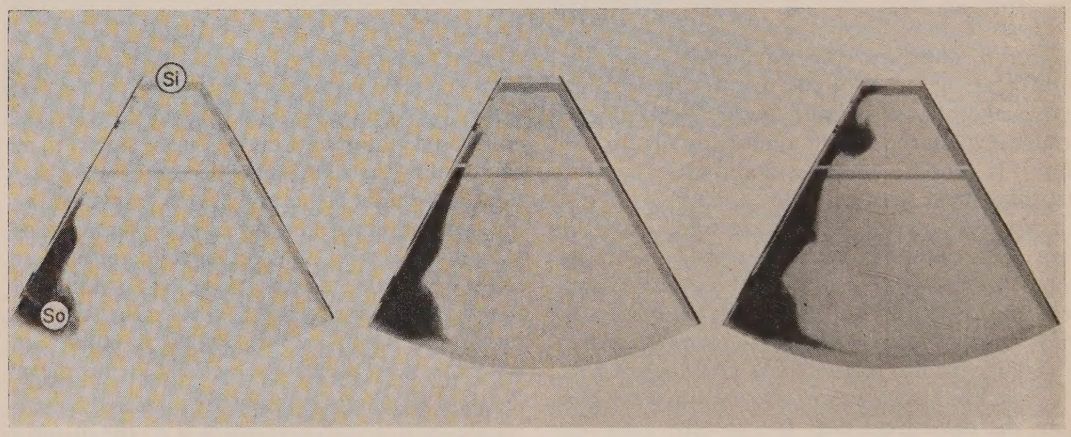

Fig. 9. Photographs at 5, 10, and 20 minutes with $S_0 = 100$ cc./min. The dyed fluid was injected through a vertical glass tube in the southwest corner of the tank and the sink was at the apex.

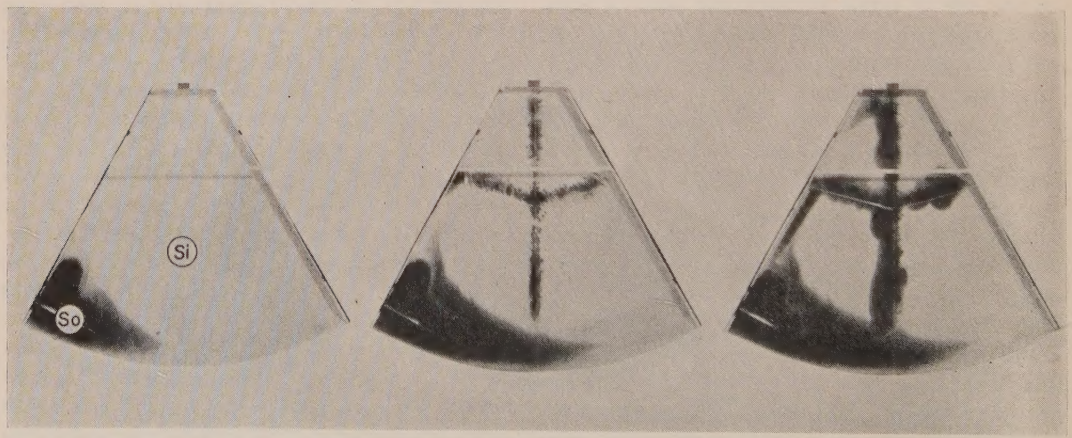

Fig. 10. Photographs at 15, 32, and 35 minutes with $S_0 = 100$ cc./min. This experiment corresponded to fig. 4 and was identical to that of Fig. 9 except that the external sink at the apex was eliminated. Potassium permanganate dye from crystals introduced through slits in the glass cover showed the southward flowing western boundary current.

mixture gradually spread across the tank near the rim. (The anomalous apparent southward flow of permanganate dye in the interior (Fig. 10c) was due to the dense concentration of heavy dye near the botton and antitriptic outward flow toward surfaces of lower "geopotential". The bottom surface of the model was not an equipotential surface, and the introduction of density gradients destroys the simple interpretation of the simulation of the "β" effect by a radial variation of depth.)

REFERENCES

STOMMEL, HENRY, 1957: A survey of ocean current theory. *Deep-Sea Research* **4**, pp. 149-184.

VON ARX W. S., 1952: A laboratory study of the wind-driven ocean circulation. *Tellus*, **4**, pp. 311—318.

On the Global Balance of Water Vapor and the Hydrology of Deserts

By V. P. STARR, Massachusetts Institute of Technology[1]
and
J. P. PEIXOTO, University of Lisbon and the
National Meteorological Service of Portugal

(Manuscript received December 15, 1956)

Abstract

An attempt is made to measure the horizontal divergence of the vertically integrated moisture flux over the northern hemisphere for the calendar year of 1950. This is done through the evaluation of daily data for some 90 upper air stations at several levels up to 500 mb. The final map obtained indicates strong maxima of divergence not only over certain oceanic regions, but also over three separate arid regions. Such a result implies an unexpectedly large excess of evaporation over precipitation in these latter areas, which must be balanced by convergence of liquid water on and below the ground surface, unless the year studied was rather completely different from normal, this not being so likely, however.

1. Introduction

With the advent of more plentiful observations concerning the troposphere from stations distributed over the northern hemisphere, it has become feasible to treat many problems associated with the terrestrial hydrological cycle on a hemispheric basis. Previously many such questions could be approached, if at all, only on a regional basis with corresponding limitations in the significance of results when the general circulation processes and other global questions are at issue. Even when more local investigations are intended the simultaneous consideration of hemispheric conditions imparts a sense of perspective not otherwise obtainable. The importance of the last remark is illustrated by various features of the material which follows.

Probably one of the first truly hemispheric attempts to measure directly from winds and humidities the effect of atmospheric motions in transporting water vapor across latitude circles was that of WHITE (1951), in an effort to include the contribution of latent heat to the earth's energy balance. These efforts were much amplified by STARR and WHITE (1954), again especially from the viewpoint of the energy balance of the general circulation. Oceanographical and climatological aspects were later touched upon in some still further extensions of this work by STARR and WHITE (1955).

All of the papers referred to involve the assessment of the net vapor flux across latitude circles, following the pattern of tech-

[1] The research resulting in this work has been sponsored by the Geophysics Research Directorate of the Air Force Cambridge Research Center, under Contract No. AF 19 (604)-1000.

niques evolved for the similar evaluation of the momentum flux in general circulation studies. In the case of these latter endeavors, BUCH (1954) has shown that air data for the northern hemisphere are sufficient not only for the calculation of zonal averages of the momentum flux, but also for the drawing of reasonable hemispheric yearly and seasonal maps of a number of quantities involved in the observational treatment of this flux. It was therefore decided that the comparable maps for the water vapor flux problem should be drawn for the same time interval as was used by Buch, namely the calendar year 1950. The feasibility of this plan was also suggested by the studies of moisture flux over North America made by BENTON and ESTOQUE (1954). This aim necessitated extensive recomputation and augmentation of data tabulations previously compiled by the General Circulation Project at the Massachusetts Institute of Technology.

At the present writing this task has been accomplished, and the results will be published *in extenso* as soon as time permits. In the meantime, a survey of the material is being presented by PEIXOTO (1958). Also, certain special aspects are treated by STARR, PEIXOTO and LIVADAS (1958), and by PEIXOTO and SALTZMAN (1957). The present paper is still another such discussion dealing with the hydrological significance of the results, especially for some of the principal desert areas of the hemisphere.

2. Procedures and results

The zonal and meridional components of the horizontal total flux of water vapor above a point on the earth's surface may be represented by the expressions

$$Q_\lambda = \frac{1}{g}\int\int qu\ dp\ dt; \qquad Q_\varphi = \frac{1}{g}\int\int qv\ dp\ dt, \quad (1)$$

where g is gravity, q specific humidity, p pressure, t time and u and v are the zonal and meridional wind components counted positive eastward and northward. Use has here been made of the hydrostatic relation. The pressure integration extends from zero to the value of pressure at the surface, while the time integration extends for a period of one year, in the present instance. It is clear that the expressions (1) are the components of a vector, conveniently denoted by $\vec{Q}$, which defines a two-dimensional vector field over the earth's surface. It follows that one may take the (horizontal) divergence of $\vec{Q}$ and express it in terms of a convenient system of coordinates—spherical polar in our case. We thus have

$$\nabla \cdot \vec{Q} = \frac{1}{R\cos\phi} \times \left\{\frac{\partial}{\partial\lambda}(Q_\lambda)\frac{\partial}{\partial\phi}(Q_\varphi \cos\phi)\right\} \quad (2)$$

Here R is the earth's radius assumed constant, λ is longitude and ϕ latitude.

From the magnitudes encountered in the atmosphere, such as that for the precipitable water vapor contained in a typical column of air, it must be concluded that the storage effects are sufficiently small so that the water lost in regions of positive divergence must be resupplied and that concentrated into regions of convergence must be removed. Since such corrections as the horizontal transport of liquid water are small, the divergence must, for all practical purposes then be numerically equal to the annual excess of evaporation over precipitation.

In the evaluations from data, the station network presented by STARR and WHITE (1955) was significantly extended especially in Africa and elsewhere. Some stations near to the equator in the southern hemisphere were used as an aid in the drawing of maps. The augmented key station distribution is shown in Fig. 1. Many of the procedures followed are the same as those described in the reference given. Thus, for instance, the advection was computed wherever possible from radio winds although a number of pilot-balloon stations again had to be resorted to. Unlike the previous study, the evaluation of the expressions (1) was carried out independently for each station, using wind and humidity data reported daily from the levels: surface, 1000 mb, 850 mb, 700 mb and 500 mb, except where elevation of the earth's surface interfered. Above 500 mb the moisture transports are much too small to be of practical concern.

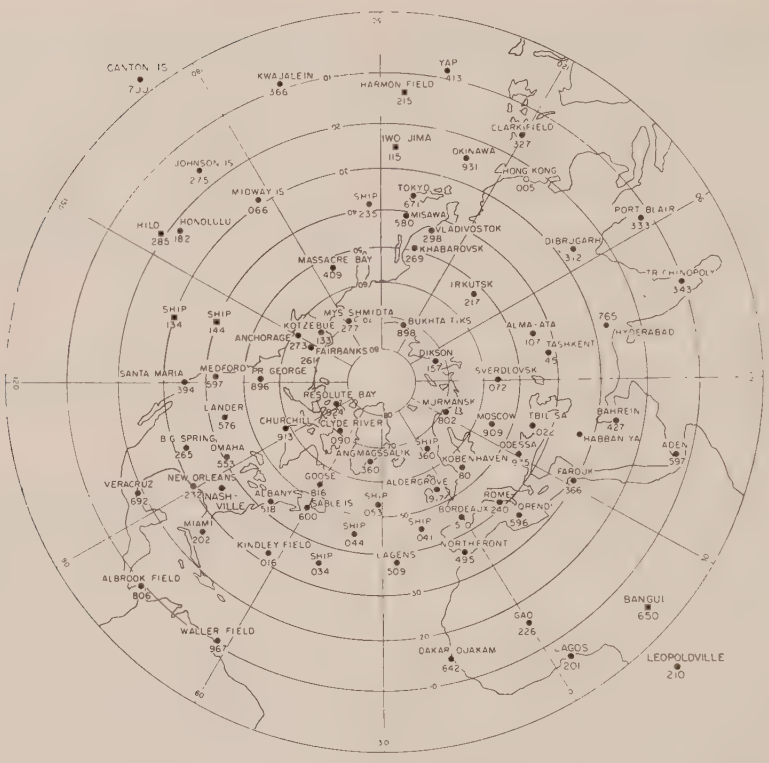

Fig. 1. The distribution of key stations over the northern hemisphere (and slightly beyond the equator) used in the investigation of the atmospheric water vapor transport. A few additional stations which are not shown were also used at times as alternates.

Two maps were then constructed and analyzed, one for each of the quantities Q_λ and Q_φ. Using data read off from these charts for every 10° of latitude and longitude, $\nabla \cdot \vec{Q}$ was computed through the use of equation (2), measuring the derivatives by finite difference approximations. In this way a value of the divergence was obtained for each 10° interval zonally and meridionally. These were plotted on a third map and analyzed, the resulting picture being that shown in Fig. 2. An approximate representation of the field of $\vec{Q}$ itself is given in Fig. 3.

3. General discussion

It is to be understood at the outset that the character of observations at our disposal, and the consequent methods which must be resorted to in performing calculations of the present kind, prevent the reproduction of a vast amount of detail which, without a doubt, is present in the true picture. Viewing the result then only as a general, first approximation to actuality, the writers have concluded that it nevertheless possesses much that challenges one's scientific imagination and raises many questions which deserve something more than mere facile answers. The following list of topics includes several such subjects.

a. By and large, the areas of divergence and convergence balance for the hemisphere so that there is but little net flow across the equator. Zonal averages along other latitudes agree with corresponding climatological estimates secured by independent means (see STARR, PEIXOTO and LIVADAS 1958).

b. Large centers of convergence are to be found in the general vicinity of the headwaters and drainage basins of many large rivers. Such convergence is found over the northwestern United States and western Canada (Columbia,

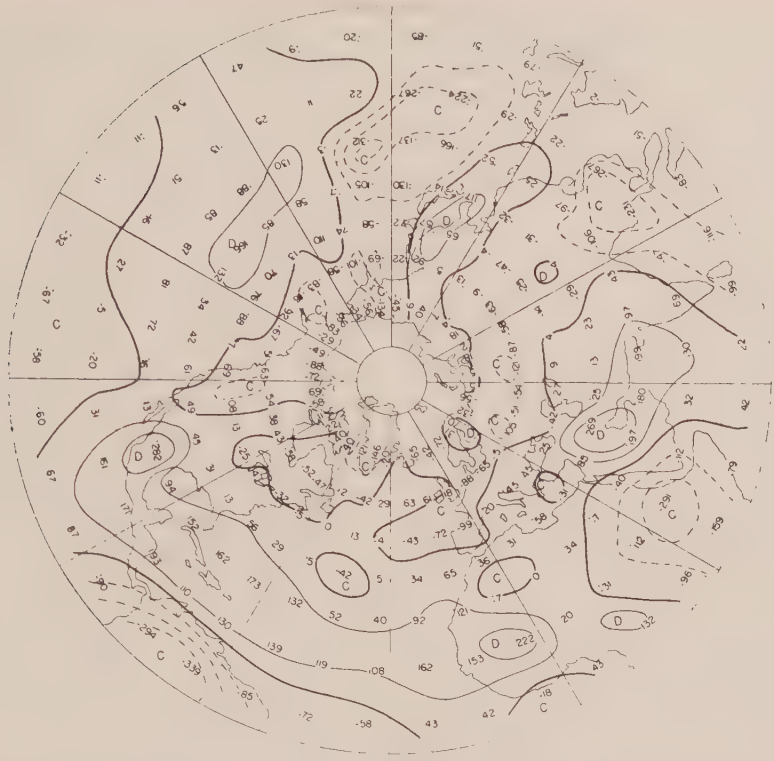

Fig. 2. Distribution of the horizontal divergence of the vertically integrated total annual flux of water vapor for the year 1950. The units are the equivalent depth of liquid water in centimeters per year. The isopleths (full lines for divergence and dashed for convergence) are entered for intervals of 100 cm per year.

Mississippi, Colorado, Mackenzi, Saskatchewan and Rio Grande rivers); over northern South America (Magdalena, Orinoco, and Amazon rivers); over eastern Africa (Nile, Congo, Juba and Scebeli rivers); over eastern India, Burma and Indo-China (Ganges, Brahmaputra, Irrawaddy, Salween, Yangtze, Si Kiang and Mekong rivers). In the case of some rivers of large size, no particularly marked convergence areas seem to manifest themselves; e.g., the Indus river—a quite possible result of deficient reports from central Asia where it rises.

c. Convergence centers are to be found over ocean areas as for example, the one in the western Pacific. Since the addition of such large amounts of fresh water are involved, the resulting dilution of the mineral salts in sea water is a matter of consequence in oceanographic studies.

d. Several areas of strong divergence are located over the oceans; notably, over the southern Atlantic and the Gulf of Mexico, and in the mid-Pacific. These then are major sources for atmospheric moisture as seems reasonable enough on general meteorological grounds. From the standpoint of oceanography, the effect of the resulting concentration of salinity in such locations has been considered.[2]

e. One of the more striking and puzzling features of Fig. 2 is the delineation of strong divergence centers over a number of (but not all) deserts. This is indicated over northern Mexico and the southwestern United States, over the western Sahara and over the general region of Arabia, Iraq and Iran. The eastern Sahara and the Gobi are exceptions, although the meager reports from central Asia may again be involved in the latter instance. Ac-

[2] From Fig. 2. by - and - large greater surface salinities should be expected in the North Atlantic than in the North Pacific. A more detailed study of this subject is now in progress.

Fig. 3. Approximate distribution of the net moisture transport vector averaged for the year 1950. It should be stressed that the interdiurnal variability of this quantity is large and that because of this large standard deviation the rough streamlines suggested by this map cannot be regarded as being also the trajectories of individual water vapor particles. It is of pertinence to note the good agreement of this map with the analogous one drawn by Benton and Estoque (1954) for the North American sector from data for the calendar year 1949.

cepting the magnitudes shown, it is tempting to draw the somewhat startling conclusion that desert areas are on a par with oceans as major sources of moisture for our hemispheric regime of precipitation. Many questions are however raised immediately, and several of these will be enumerated in the following section.

f. The divergence pattern is most directly related to the difference between the evaporation and precipitation, as has already been explained. On the whole, some relation should exist with the (annual) precipitation itself, nevertheless. It follows that a better analyzed set of isopleths might have been drawn in Fig. 2 by making explicit use of a precipitation chart for the hemisphere. This was not done for several reasons, the lines having been sketched without at least deliberate deference to the rainfall distribution. Since the grid-point values are given, this allows each reader to make such adjustments as seem reasonable to him, the process being inherently subjective. In such attempts, it should be kept in mind that the divergence pattern for 1950 need not be exactly normal, and likewise that the precipitation for this one year may depart from the longer term average values at many points. The large area of convergence in the western Pacific may not, for example, be a normal feature.

g. To the extent that Fig. 2 resembles the long term mean pattern, it must be accompanied by an equal and opposite divergence of water substance below the base of the atmosphere in the hydrosphere and lithosphere, since continuity must be maintained and secular

changes in long term storage are, no doubt, slow. Liberation of juvenile and connate water and other such effects are to be reckoned with here, but the sum total of their contributions is doubtless small.

This compensatory lower circulation cannot be determined from a knowledge of its divergence alone. At best, the only component of it which can so be determined is an irrotational part, which might nevertheless be of some interest. This could be accomplished by inserting derivatives of a velocity potential for Q_λ and Q_φ in an expression of the form (2) and solving the resulting Poisson equation by finite difference procedures or otherwise. The stipulation of a given flow across the equator completes the specification of a Neumann type problem. The resulting flow would, of course, be indeterminate to the extent of a quite arbitrary additive divergence-free transport.

h. During the preparation of the vast amount of data which went into the end product shown in Fig. 2, averages were also made for shorter time periods. Such seasonal maps are not reproduced here, since it is thought that the annual mean condition already presents a sufficient array of problems without now considering less reliable short term pictures. Plans are now in progress to treat additional years of record, especially the Geophysical Year. Upon the completion of such longer period averages, it may be feasible to return to the consideration of seasonal means.

i. We may pause but briefly here in order to ask philosophical questions concerning our material. The ramifications of the subject are well nigh endless as even slight reflection will confirm. Evaporation fares best under low relative humidities effectively produced by descent of air. Why do we have some of the hottest air on the earth's surface descending? Why, in other places such as southeast of Japan does the warm air ascend so vigorously but not elsewhere over certain other ocean areas with seemingly similar air properties? Why does the moisture evaporate so intensely in the middle of the Pacific south of the Aleutians? Why over northern Korea and eastern Siberia?

Answers to these questions and others exist. In many cases, simple statements of considerable pertinence can, no doubt, be made. But, more generally, the subject is part and parcel of the general circulation problem; to be elucidated fundamentally not otherwise than through a better understanding of the whole system. Fortunately, more sophisticated approaches to general circulation theory are at length gaining popularity, and worthwhile results are forthcoming at an increasing rate.

4. Comments on desert hydrology

It has long been recognized that evaporation far exceeds rainfall in most deserts. What is surprising is the magnitude in Fig. 2 of the evaporation from those arid regions already enumerated. How does the water balance at and below the surface maintain itself in order to permit this large annual loss? Unfortunately, the state of our information here is such that it is possible only to speculate about the processes which may furnish the answer to this and other related questions. The following notes may, it is hoped, at least be suggestive, pending the corroboration of our results from independent data and through other means.

a. Desert areas generally contain evidence of evaporation processes. Thus, residues of salt, gypsum and other deposits left behind are common. Presumably, these materials were leached out from ground substances during the passage of water over or through the lithosphere, although at least occasional contributions from sea water cannot be ruled out. Special phenomena such as the deposition on exposed rock surfaces of "desert varnish" indicate the accumulation of a mineral coating, again through the agency of evaporation (see, e.g., HOLMES 1945).

b. A considerable amount of water is transported by surface flow from surrounding territories of more copious rainfall, since deserts tend to have an internal drainage. Various gorges and wadis mark the sites of ephemeral rivers which on occasion carry torrential streams into the central parts of the depressions formed by wind erosion. Such low areas often are below sea level. In some instances, permanent rivers like the Volga and the Jordan never find their way to the sea, their waters being eventually evaporated in toto. In other cases, as with the Nile and Rio Grande, a sizeable fraction of the flow is evaporated before the remainder is drained into the ocean.

c. The flow of ground water into deserts through aquifers and other means (underground rivers and such) can and, no doubt, usually does take place. If in a circular region one thousand kilometers in diameter, one meter of water is to be evaporated annually, the required inflow through porousmedia, distributed uniformly through a depth of one kilometer around the periphery would be much less than one millimeter per second.

That underground waters are abundant in deserts is commonly recognized because of the presence of oases and the fact that many wells have been constructed. It is said that the Nile receives water from such sources on its way across the arid portions of its course.

d. The problem of how underground water might rise from the water table to the surface either as a liquid or vapor is not known. In places where erosion by the wind has lowered the floor of depressions sufficiently, this question does not occur. Elsewhere, great thicknesses of sand intervene, and studies would have to be made in order to provide an answer. Much might perhaps be learned in this regard from laboratory experiments.

e. Since much remains to be verified as to the manner in which large evaporation in these arid regions may take place, it would be highly instructive to make extensive direct measurements of the vertical water vapor transfer near the ground by the standard methods. Even though these procedures involve questions as to the absolute accuracy which may be obtained, still the order of magnitude of the vertical transport can be determined. Due to the extremes of temperature and relative humidity likely to be encountered, special instrumental problems might have to be considered in some detail in order to achieve success.

f. Without further information it would seem from what has been said that if such intense inflows of water into certain deserts really do take place, some potential economic significance should be involved. The flow might thus be strong enough in order to make it profitable to install additional irrigation stations to intercept it at strategic places depending upon hydrological factors.

Also, it would appear that if a strong vertical flow of water in some form takes place through the ground from the water table, some means might be found for arresting it at or near the top surface. This might result in somewhat improved soil moisture conditions for plant growth.

The writers wish to express their thanks to Professor G. C. Livadas of the University of Thessaloniki for valuable assistance and discussions.

REFERENCES

Benton, G. S and Estoque, M. A., 1954: Water vapor transfer over the North American continent. *J. Meteor.*, **11**, pp. 462—477.

Buch, H., 1954: Hemispheric wind conditions during the year 1950. Final Report Part 2, General Circulation Project, Mass. Institute of Technology.

Holmes, Arthur, 1945: *Principles of Physical Geology*. London, Thomas Nelson and Sons, Ltd., pp. 532.

Peixoto, J. P., 1958: Doctoral dissertation, University of Lisbon.

Peixoto, J. P., and Saltzman, B., 1957: Harmonic analysis of the mean water vapor distribution for the year 1950 (unpublished).

Starr, V. P., Peixoto, J. P., and Livadas, G. C., 1958: Note on the meridional transport of water vapor in the northern hemisphere. *Geofisica pura e applicata* (in press).

Starr, V. P., and White, R. M., 1954: Balance requirements of the general circulation of the atmosphere. Geophysical Research Papers, 35, Geophysics Research Directorate, Cambridge, Mass.

Starr, V. P., and White, R. M., 1955: Direct measurement of the hemispheric poleward flux of water vapor. *J. of Mar. Res.*, **14**, pp. 217—225.

White, R. M., 1951: The meridional eddy flux of energy. *Q. J. R. M. S.*, **77**, pp. 188—199.

Scale Consideration of Planetary Motions of the Atmosphere[1]

By ALEWYN P. BURGER[2]

(Manuscript received August 5, 1957)

Abstract

The application of scale considerations to atmospheric motions indicates that the equations hitherto used in numerical prediction are unfit for detailed prognosis on the planetary (or very large) scale.

It appears that the dominant terms of the vorticity equation in this case are the divergence term and the β-term, which means that the vorticity equation here displays the same quasi-stationary character as the undifferentiated equations of motion. An attempt at expressing more than the quasistationary character of the planetary flow leads to undue complication of the equation, even requiring inclusion of the twisting terms.

As for the application of the geostrophic approximation, it is confirmed that the β-term in the divergence equation is important in the representation of the planetary scale. Further, though metrical terms (containing the reciprocal of the earth's radius) are important on this scale in spherical coordinates, it is shown that, in using the geostrophic approximation and a square grid on a conformal plane projection of the earth's surface, no metrical terms appear.

Remarks are also included on a relation of Prandtl, which loses its validity on the planetary scale, and also on the use of the Richardson number to characterize large-scale atmospheric motion.

1. Introduction

In his classical article of 1948, Charney used scale considerations systematically for determining the relative importance of the different terms in the set of hydrodynamical equations which are supposed to govern the behaviour of the large scale motions of the atmosphere over short periods. As is known, this analysis led to a rational way of using the geostrophic approximation in the equations, and served as a basis for much of the further development of dynamical weather prediction. At a later stage Stümke (1953) applied a similar analysis with a view to improving on the geostrophic approximation in medium scale motions. In both these studies the notion of "large scale" is apparently distinct from what may be called the "very large scale", or, more concisely, the planetary scale. However, this planetary scale, in which the characteristic distance is comparable in magnitude to the earth's radius, is known to be very significantly represented in the spectrum of atmospheric motions (cf. White and Cooley, 1956). It is therefore of some importance to investigate to what extent the equations used in dynamical prediction are applicable to this scale of motion. The present paper aims at making a contribution on this subject.

One instance in which the longest waves have received special attention, was in the

[1] This work was carried out while attached to the South African Weather Bureau, Pretoria. It was also presented as a lecture at the conference on Numerical Weather Prediction in Stockholm, in June, 1957.

[2] Present affiliation: National Physical Research Laboratory (Mathematics Division), Council for Scientific and Industrial Research, Pretoria.

article of CHARNEY and ELIASSEN (1949). In their one-dimensional barotropic model the equation was adjusted to suit the planetary (stationary) waves, by introducing an empirically determined current width; however, this was simply a subterfuge to compensate for the absence of a second space dimension in the model.

Later BOLIN (1955) pointed out that the barotropic model, as used in Stockholm, performs less well on the planetary scale than on the moderately large scale. To remedy this, he proposes the introduction of a divergence term with an empirical coefficient into the barotropic model. The improvement brought about by this means has not yet been thoroughly tested; however, the present analysis will indicate that the planetary scale does require a divergence term to be present in the model and also that it should be supported by a β-term in the divergence equation.

In general we hope to illustrate that the equations currently used in both barotropic and baroclinic models are unsuited to supply reliable specific information on the planetary scale.

The arguments leading to this last statement are based on the fundamental relation (22) between Charney's scale quantities; this and other relations are established in sections 2 and 3 under very unrestrictive assumptions.

In section 4 it is shown how the equations may be simplified with the aid of the above results in the case of the medium-long waves treated by Charney. Here the difficulties attached to the quasi-stationary character of the motion may be overcome by using the vorticity equation.

Section 5 contains the extension of these considerations to the planetary scale, and it appears that in this case even the vorticity equation displays a quasi-stationary character. It turns out that a divergence term, (which may here be geostrophically approximated), is needed in the vorticity equation, while further for good representation the omission of β-terms in the geostrophic formulae for vorticity and divergence is not permitted. Also metrical terms become important in spherical coordinates, but not with the geostrophic approximation and cartesian coordinates on a conformal map. These and other conclusions are listed in the final section.

Included in the material mentioned, are discussions of the direct representation of ordinary and geostrophic divergence (section 4) and of the interrelation of results obtained in the "z-system" and "p-system" of coordinates (section 5). Other matters mentioned in passing are the ceased validity of Prandtl's ratio between horisontal and vertical scales when the planetary scale is considered, and a comparison of the use of the Rossby and Richardson numbers for expressing the quasi-geostrophic character of large-scale motion.

2. Basic assumptions

It is assumed that the short-term behaviour of the atmosphere can be described by the hydrodynamical equations for adiabatic and laminar motion of an ideal fluid, and, following Charney, we shall make use of characteristic scale quantities to represent the relative magnitudes of different terms.

We denote by S and H the respective half-wave-lengths, by V and W the characteristic absolute horizontal and vertical particle speeds and by C the horizontal phase speed of streamline configurations. The use of these quantities to characterize a complicated field of flow, implies that harmonic components, rather than the full observed motion, are treated; further the use of results based on such simplified phenomena treated in isolation, implies the assumption that the non-linear interaction between motions on different scales is considered negligible.

Although actual computations are usually performed using a square grid on a conformal map projection, we shall use spherical coordinates λ, ϕ and r, so that the Eulerian equations of motion are:

$$\left.\begin{aligned} \frac{du}{dt} - \frac{uv}{r}\tan\phi + \frac{uw}{r} + jw - fv &= -\frac{p_x}{\varrho} \\ \frac{dv}{dt} + \frac{u^2}{r}\tan\phi + \frac{vw}{r} + fu &= -\frac{p_y}{\varrho} \\ \frac{dw}{dt} - \frac{1}{r}(u^2+v^2) - ju &= -\frac{p_z}{\varrho} - g \end{aligned}\right\} \quad (1)$$

in which u, v and w are the eastward, northward and upward velocity components respec-

tively, while x, y and z denote differentiation in the corresponding directions, e.g.

$$p_x = \frac{1}{r\cos\phi}\frac{\partial p}{\partial \lambda},\ p_y = \frac{1}{r}\frac{\partial p}{\partial \phi},\ p_z = \frac{\partial p}{\partial r}.$$

Further, f is the coriolis parameter $2\Omega\sin\phi$ and j is $=2\Omega\cos\phi$, where Ω is the earth's angular speed.

As in Charney's paper, we represent the order of magnitude of velocity derivatives by the scale quantities, as follows:

$$u_x \sim v_x \sim u_y \sim v_y \sim \frac{V}{S}$$

$$u_t \sim v_t \sim C\frac{V}{S}$$

$$u_z \sim v_z \sim \frac{V}{H}$$

$$w_x \sim w_y \sim \frac{W}{S}$$

$$w_t \sim C\frac{W}{S}$$

$$w_z \sim \frac{W}{H}$$

and, since the order of H is again taken to be about the depth of the troposphere, the change of pressure and density with height is of the same order as the variables themselves, so that

$$\frac{p_z}{p} \sim \frac{\varrho_z}{\varrho} \sim \frac{1}{H}. \tag{2}$$

Again the horizontal variation of p and ϱ will need more precise treatment.

We now impose a number of restricions on the possible values of the scale quantities, in conformity with observational evidence. For this purpose attention is focussed on medium and large scale synoptic motions in middle latitudes, and we may then evidently write:

$$\left.\begin{aligned} H < S &\lesssim a \\ W &\lesssim V \\ C &\lesssim V \end{aligned}\right\} \tag{3}$$

in which a is the earth's radius. We further note that, in the range of interest (where $S \gtrsim$ 1,000 km, $V \lesssim$ 100 m/sec, and $f \sim 10^{-4}$ sec^{-1}), the Rossby parameter $\frac{V}{fS}$ satisfies

$$\frac{V}{fS} \lesssim 1. \tag{4}$$

If, in addition, the order of H is fixed at 10 km, we may also write

$$\left.\begin{aligned} \frac{V^2}{gH} &<< 1 \\ \frac{fV}{g} \lesssim \frac{H}{a} &<< 1 \end{aligned}\right\} \tag{5}$$

in which the symbol $<<$ indicates that the left-hand side is at most of the order of about one-tenth of the right-hand side.

As far as the variables of state are concerned, restrictions are placed on the vertical variation of temperature and on the horizontal variation of pressure and density. Thus, firstly we require the lapse-rate to be sub-adiabatic, while even a substantial temperature inversion is allowed:

$$-2 \lesssim \frac{\Gamma}{\Gamma_a} < 1 \tag{6}$$

where Γ_a is the adiabatic lapse-rate $\frac{\varkappa g}{R}$; secondly we assume that the pressure force has the same order as the coriolis force:

$$\frac{p_x}{\varrho} \sim \frac{p_y}{\varrho} \sim fV \tag{7}$$

It may be noted that this last assumption, which is well substantiated by observation, is much weaker than the geostrophic approximation, since equality in order of magnitude only is required. It is also in keeping with (4), since the Rossby parameter measures the ratio of horizontal advection terms to coriolis terms in the horizontal equations of motion.

3. Derivation of the basic relations

We may now apply the above relations to the different hydrodynamical equations in order to obtain further relations. Firstly, the third equation of motion reduces at once to the hydrostatic equation, since, by (3) and (5) its entire left-hand side is of lower order than the gravity acceleration g.

Thus

$$\frac{p_z}{\varrho} = -g. \tag{8}$$

Together with (2), this yields

$$RT = \frac{p}{\varrho} \sim \left(\frac{p}{p_z} \cdot \frac{p_z}{\varrho}\right) \sim gH \tag{9}$$

which is consistent with the observation that the absolute temperature is always about 200 or 300 K in the troposphere. Combination of (8) with (2) and the (weak) geostrophic relation (7) yields

$$\frac{p_x}{p} = \frac{p_x}{\varrho} \cdot \frac{\varrho}{p_z} \frac{p_z}{p} \sim \frac{fV}{gH}$$

and similarly for the y-direction. With a little more care we may write, from (9) and (7),

$$\frac{\varrho_x}{\varrho} \sim \frac{1}{\varrho}\left(\frac{p}{gH}\right)_x \sim \frac{1}{gH}\frac{p_x}{\varrho} + \frac{H_x}{H} \sim \frac{1}{gH} \cdot \frac{p_x}{\varrho} \sim \frac{fV}{gH}$$

so that, in summary,

$$(\ln p)_x \sim (\ln p)_y \sim (\ln \varrho)_x \sim (\ln \varrho)_y \sim \frac{fV}{gH}. \tag{10}$$

Our next step is to substitute this into the adiabatic equation, viz. into

$$\frac{1}{\gamma} \cdot \frac{d_h \ln p}{dt} - \frac{d_h \ln \varrho}{dt} = -\sigma w, \tag{11}$$

in which $\gamma = 1.4$ is the ratio of the specific heats, the subscript h indicates that the vertical advection term is to be omitted from the individual time-derivative, while σ is the stability parameter

$$\sigma = \frac{1}{T}\left(T_z + \frac{\varkappa g}{R}\right) = \frac{\varkappa g}{RT}\left(1 - \frac{\Gamma}{\Gamma_a}\right). \tag{12}$$

By (10) the left-hand side of (11) has the order $\frac{fV^2}{gH}$ (unless cancellation of terms occurs), so that we may write

$$\frac{fV^2}{gH} \sim \sigma W. \tag{13}$$

This relation expresses the inhibiting effect of stability on vertical motion. Taking note of (9) and (6) and the value 0.3 for $\varkappa$, the expression for σ may be written as

$$\sigma \sim \frac{\varkappa}{H}\left(1 - \frac{\Gamma}{\Gamma_a}\right) \lesssim \frac{1}{H} \tag{14}$$

so that (13) yields

$$\frac{fV^2}{gH} \lesssim \frac{W}{H}. \tag{15}$$

We can now relate the vertical speed W and the divergence D of the horizontal wind with the aid of the continuity equation

$$\frac{d \ln \varrho}{dt} + D + \frac{2w}{r} + w_z = 0 \tag{16}$$

in which

$$D = u_x + v_y - \frac{v}{r}\tan\phi. \tag{17}$$

From (10) and (15), the first term of (16) satisfies

$$\frac{d \ln \varrho}{dt} \sim \frac{fV^2}{gH} + \frac{W}{H} \sim \frac{W}{H}$$

while w_z is of the same order and $\frac{2w}{r}$ is negligible. Therefore we may write.

$$D \sim \frac{W}{H} \tag{18}$$

This result may be used to relate $\frac{W}{H}$ and $\frac{V}{S}$, by use of the vorticity equation, viz.

$$\frac{d\zeta}{dt} + \beta v + (f+\zeta)\left(D + \frac{2w}{r}\right) + w_x\left(v_z + \frac{v}{r}\right) - w_y\left(u_z + \frac{u}{r} + j\right) = -p_y\left(\frac{1}{e}\right)_x + p_x\left(\frac{1}{\varrho}\right)_y \tag{19}$$

in which

$$\left.\begin{aligned} \beta &= f_y \\ \zeta &= v_x - u_y + \frac{u}{r}\tan\phi \end{aligned}\right\}. \tag{20}$$

By (4) and (18), none of the terms in (19) containing w or D are of higher order than the term fD. The remaining terms on the left-hand side, viz. $\frac{d_h\zeta}{dt}$ and βv, are of the orders

$\frac{V^2}{S^2}$ and $\frac{fV}{a}$ respectively, while the solenoidal terms on the right may be written as

$$\frac{p}{\varrho}\left(\frac{p_y}{p}\cdot\frac{\varrho_x}{\varrho}-\frac{p_x}{p}\cdot\frac{\varrho_y}{\varrho}\right)$$

which, by (9) and (10), is of the order $\frac{f^2V^2}{gH}$. Therefore we have

$$f\frac{W}{H}\sim\frac{V^2}{S^2}+\frac{fV}{a}+\frac{f^2V^2}{gH}. \tag{21}$$

However, by (5), the solenoidal term never exceeds the β-term in order of magnitude, so that (21) becomes

$$\frac{W}{H}\sim\frac{V}{S}\left(\frac{V}{fS}+\frac{S}{a}\right), \tag{22}$$

which is the key-relation on which our subsequent argumentation will be based. We may note at this stage that, from (3) and (4)

$$\frac{W}{H}\lesssim\frac{V}{S}. \tag{23}$$

This implies that the vertical advection terms are not more important than the horizontal advection terms in the horizontal equations of motion, and therefore smallness of the Rossby parameter (representing the ratio of horizontal advection terms and coriolis terms) is sufficient for validating the geostrophic approximation.

4. Application to moderately long waves

Turning now to the interpretation of the key-relation (22), we note that, within the range of its validity, it determines the order of W uniquely in terms of V and S, so that also σ is determined in terms of V and S by (13). Evidently we should distinguish in (22) between the two cases where $\frac{V}{fS}\gtrsim\frac{S}{a}$ and $\frac{V}{fS}\lesssim\frac{S}{a}$, and our aim is to stress the significance of the latter case. In this section, however, we consider the former case. Thus, when

$$\frac{S}{a}\lesssim\frac{V}{fS} \tag{24}$$

the relation (22) becomes

$$\frac{W}{H}\sim\frac{1}{f}\cdot\frac{V^2}{S^2} \tag{25}$$

showing that W increases with increasing V and decreasing S. Substitution of this into (13) yields

$$\frac{S}{H}\sim\frac{\sqrt{g\sigma}}{f}, \tag{26}$$

and this is a fundamental relation for the ratio of the horizontal and vertical scales, which is already implicit in the work of PRANDTL (1936). The condition (24), however, represents definite limits to its applicability. The relation (26) may be written as

$$\sigma H\sim\frac{f^2S^2}{gH} \tag{27}$$

which shows a fast decrease of σ with decreasing S. On substituting from (24), we get

$$\sigma H\lesssim\frac{fVa}{gH} \tag{28}$$

so that, since $V\lesssim 100$ m/sec,

$$\sigma H\lesssim 1$$

in consistence with (14).

In the case treated by Charney, i.e. where $S\sim 1{,}000$ km, the value of σH yielded by (27) is 10^{-1}, in conformity with the value used by Charney. We write (27) as

$$\frac{f^2S^2}{gH}<<1 \tag{29}$$

and therefore

$$\frac{f^2V^2}{gH}<<\frac{V^2}{S^2} \tag{30}$$

which means that the solenoidal terms are negligible against the horizontal advection of vorticity. Further, (13) yields

$$\frac{fV^2}{gH}\sim\frac{W}{H}(\sigma H)<<\frac{W}{H} \tag{31}$$

which shows that the horizontal time derivative of density is negligible in the continuity equation. The fact that here

$$\frac{S}{a} << 1 \tag{32}$$

allows metrical terms containing $\frac{1}{r}$ to be omitted from the equations, and D and ζ may be simplified to

$$\left.\begin{aligned} D &= u_x + v_y \\ \zeta &= v_x - u_y \end{aligned}\right\} \tag{33}$$

Charney's further assumption $V \sim 10$ m/sec now implies

$$\frac{V}{fS} << 1 \tag{34}$$

so that the geostrophic approximation holds and, from (25)

$$\frac{W}{H} << \frac{V}{S} \tag{35}$$

This justifies the omission of terms containing w in the vorticity equation, and also, by (18), incidentally implies that

$$D << \zeta \tag{36}$$

This also means that D is of lower order than its component terms; in fact it is of the same order as the errors in its components, and is therefore very difficult to represent accurately.

At this stage the equations, as simplified under Charney's assumptions, may be directly written down. The equations of motion (1) become the geostrophic and hydrostatic approximations, the adiabatic equation remains unchanged, while the continuity equation becomes

$$\left.\begin{aligned} &D + w(\ln \varrho)_z + w_z = 0 \\ &\text{i.e. } D + \frac{(\varrho w)_z}{\varrho} = 0 \end{aligned}\right\} \tag{37}$$

which supplies an alternative way of representing D. The disappearance of time-derivatives from the equations reflects the quasi-stationary nature of the flow, and, as is well known, constitutes a major difficulty in the application of the primitive equations for prognostic purposes. The value of the vorticity equation (19) lies in the fact that the time-derivative does not drop out; in fact (taking into account $C \sim V$) it becomes

$$\frac{d_h \zeta}{dt} + \beta v + fD = 0 \tag{38}$$

or, if D is eliminated from (37),

$$\frac{d_h \zeta}{dt} + \beta v = \frac{(\varrho w)_z}{\varrho}. \tag{39}$$

In this equation the left-hand side may now be geostrophically approximated. As is known, this is not allowed for D in (38). We may remark in passing that the reason for this is not, as is occasionally stated, "that the geostrophic divergence is nearly zero", but simply that, being of lower order than its individual terms, it is masked by errors in these terms, whether they are geostrophically approximated or not. This may be illustrated by writing down the geostrophic divergence:

$$\left.\begin{aligned} D_g &= \frac{1}{f}\left[-\left(\frac{1}{\varrho}\right)_x p_y + \left(\frac{1}{\varrho}\right)_y p_x\right] - \frac{\beta}{f^2}\cdot\frac{p_x}{\varrho} \\ &= \frac{1}{f}\left[-\left(\frac{1}{\varrho}\right)_x p_y + \left(\frac{1}{\varrho}\right)_y p_x - \beta v_g\right] \\ &\sim \frac{fV^2}{gH} + \frac{V}{a} \end{aligned}\right\} \tag{40}$$

and therefore, because of (5),

$$D_g \sim \frac{V}{a}.$$

From (22) we see that

$$\frac{W}{H} \gtrsim \frac{V}{a}$$

which, by (18), means

$$D \gtrsim D_g.$$

However, it should be noted that in the present case, where $S \sim 1{,}000$ km and $V \sim 10$ m/sec,

$$D \sim D_g.$$

In fact (22) shows that only for larger $\frac{V}{fS}$ $\left(\text{though not exceeding } \frac{S}{a}\right)$, i.e. for small S

and large V where the geostrophic approximation is generally bad, does D_g become small compared to D. However, the results of Landers (1955), who obtains relatively large values of D, are not quite clear in the light of these considerations.

Turing from the vorticity equation to the other popular differentiated form of the equations of motion, viz. the divergence equation, we find that it is again quasi-stationary, being simply equivalent to the geostrophic approximation. Written out in full, the divergence equation is

$$\left.\begin{aligned} &\frac{dD}{dt} + D\left(D + \frac{2w}{r}\right) + 2\left(v_x u_y - u_x v_y\right) + \\ &\quad + w_x\left(u_z + \frac{u}{r} + j\right) + w_y\left(v_z + \frac{v}{r}\right) + \\ &+ 2\tan\phi\left(u u_y + v v_y\right) + \frac{u^2 + v^2}{r^2} - f\zeta + \\ &+ \beta u = -\left(\frac{p_x}{\varrho}\right)_x - \left(\frac{p_y}{\varrho}\right)_y + \frac{p_y}{\varrho}\frac{\tan\phi}{r} \end{aligned}\right\} \quad (41)$$

An alternative form of the right-hand side is

$$-f\zeta_g + \beta u_g \quad (42)$$

where the subscript g again denotes the geostrophic value. These two terms are of orders $\frac{V}{S}$ and $\frac{fV}{a}$ respectively, so that the whole expression is of order $\frac{fV}{S}$. Thus knowing the order of the right-hand side of (41), it may be simplified by being written in the further alternative form:

$$\left.\begin{aligned} &-\frac{1}{\varrho}\left(p_{xx} + p_{yy}\right) + \frac{p_y}{\varrho}\frac{\tan\phi}{r} - \left(\frac{1}{\varrho}\right)_x p_x - \\ &\qquad - \left(\frac{1}{\varrho}\right)_y p_y. \end{aligned}\right\} \quad (43)$$

The middle one of these terms is of order $\frac{fV}{a}$, and therefore negligible in the present case, while the last two, like the solenoidal terms in the vorticity equation, are of the order $\frac{f^2V^2}{gH}$, and therefore, by (30) and (34), also negligible. It is now easily seen that (41) simplifies to

$$f\zeta = f\zeta_g = -\frac{1}{\varrho}\left(p_{xx} + p_{yy}\right), \quad (44)$$

which simply expresses the geostrophic relation.

For the sake of interest we conclude this section by relating the Rossby parameter to the Richardson number. Using (27), we namely have

$$Ri \equiv \frac{g\sigma}{v_z^2} \sim \frac{f^2S^2}{H^2} \Big/ \frac{V^2}{H^2} = \left(\frac{fS}{V}\right)^2 \quad (45)$$

Therefore (34) implies

$$Ri >> 1 \quad (46)$$

which is the condition used by Eady (1949) instead of the geostrophic approximation. We note that, in the present context, (46) is a less restrictive condition than (34), since the Rossby number occurs squared in (45).

5. Application to planetary waves

Turning now to the case where

$$\frac{V}{fS} \lesssim \frac{S}{a} \quad (47)$$

we note that (22) becomes

$$\frac{W}{H} \sim \frac{V}{a} \quad (48)$$

which, substituted in (13), yields

$$\sigma H \sim \frac{fVa}{gH} \quad (49)$$

instead of the relations (25) and (27) of the complementary case. Thus the Prandtl relation (26) is no longer valid, and both σ and W increase linearly with V but are independent of S. Again (49) is consistent with (14) for $V \lesssim 100$ m/sec.

Focussing attention on the planetary waves, for which

$$\frac{S}{a} \sim 1 \quad (50)$$

we note that (since $V \lesssim 100$ m/sec) the Rossby parameter is small:

$$\frac{V}{fS} << 1 \quad (51)$$

so that the geostrophic approximation is well satisfied. This also means

$$\frac{V}{fS} << \frac{S}{a} \tag{52}$$

so that

$$\frac{V^2}{S^2} << \frac{fV}{a} \tag{53}$$

which implies that the horizontal time-derivative of vorticity is negligible against the β-term. This leads to the important conclusion that, *on the planetary scale, even the vorticity equation displays a quasi-stationary character.*

We proceed to establish the approximate form of the vorticity equation in this case. Combination of (48) with (50) yields

$$\frac{W}{H} \sim \frac{V}{S} \tag{54}$$

in contrast to (35) which applies in Charney's case. From (18) and (48) we see that

$$\beta v \sim fD \tag{55}$$

By (5), (51), (53), and (54), all other terms on the left-hand side of (19) vanish against the two terms occurring in (55). As for the right-hand side, the solenoidal terms $\left(\sim\frac{f^2V^2}{gH}\right)$ predominate over the vorticity advection terms:

$$\frac{f^2V^2}{gH} >> \frac{V^2}{a^2} \sim \frac{V^2}{S^2}, \tag{56}$$

while (5) shows that they are never more important than the terms of (55):

$$\frac{f^2V^2}{gH} \lesssim \frac{fV}{a} \tag{57}$$

If we assume, as in Charney's case, that $V \sim 10$ m/sec (i.e. $V << 100$ m/sec), the symbol $\lesssim$ becomes $<<$, but (56) is independent of the value of V. This leads to the result that, for the planetary scale and $V \sim 10$ m/sec, the vorticity equation becomes

$$\beta v + fD = 0 \tag{58}$$

By (40) this equation is evidently simply equivalent to the geostrophic approximation, and it indicates that the very fast retrogression which would be expected from the theory of Rossby waves, does not in fact occur.

For larger V the solenoidal terms become increasingly important, and should therefore eventually be inserted on the right-hand side of (58). However, in the "p-system", in which the pressure p is used as vertical coordinate, the solenoidal terms do not occur at all. We therefore refer, at this point, to the connection between our coordinate system and the p-system. This connection is characterized by noting that the derivative u_x transforms as follows:

$$\left.\begin{aligned}(u_x)_{p\text{-system}} = u_x + u_z(z_x)_{p\text{-system}} = \\ = u_x + u_z\frac{fv_g}{g} \\ \sim \frac{V}{S} + \frac{fV^2}{gH}\end{aligned}\right\} \tag{59}$$

Thus u_x has approximately the same value in the two systems if the second term of (59) is negligible compared to the first, i.e. if

$$\frac{fV}{g} << \frac{H}{S} \tag{60}$$

We know that this second term of (59) is never predominant, since, by (5),

$$\frac{fV}{g} \lesssim \frac{H}{a} \lesssim \frac{H}{S}$$

and it is negligible if

$$VS << \frac{gH}{f} \sim 10^9 \text{ m}^2 \text{ sec}^{-1}$$

In the case where $S \sim 1{,}000$ km this is satisfied for all permissible values of V, whereas in the present case where $S \sim 10{,}000$ km, we have to require V to be ~ 10 m/sec. If both V and S approach their upper limits, the two terms of (59) are of the same order, and the value of v_x is no longer even approximately the same in the two systems (though the order of magnitude will generally be unaltered). This, as is to be expected, is exactly the case in which the solenoidal terms in the z-system become of the same order as the terms of (58). It should be noted that here the relation be-

tween the vertical speed w and the corresponding quantity in the p-system, $\omega \equiv \frac{dp}{dt}$, also becomes more complicated. We namely have

$$\left.\begin{aligned} \frac{\omega}{\varrho g} &= -w + \left(\frac{d_h z}{dt}\right)_{p\text{-system}} \\ &\sim W + \frac{fV^2}{g} \end{aligned}\right\} \qquad (61)$$

which, by (22) may be written as

$$\begin{aligned} \frac{\omega}{\varrho g} &\sim \frac{HV}{S}\left(\frac{V}{fS} + \frac{S}{a}\right) + \frac{fV^2}{g} \\ &\sim \frac{HV}{S}\left(\frac{V}{fS} + \frac{S}{a} + \frac{fVS}{gH}\right) \end{aligned}$$

and we note that, for $S \sim a$, the condition that the second term on the right-hand side of (61) is negligible against the first, is identical to (60). In summary, we may say that our results, obtained in the z-system, are easily transferable to the p-system, excepting that some care is needed in the cases when (60) is violated.

Returning, now, to the vorticity equation, it can be argued that, since the observational errors are reasonably small on the planetary scale, due to the goodness of the geostrophic approximation, such errors need not mask the time-derivative of vorticity. However, the very relation (51) which validates the geostrophic approximation, also implies (53), so that the more geostrophic the flow is, the more quasi-stationary is the character of the vorticity equation. If in spite of this, the time-derivative is retained, all other terms of comparable magnitude should of course also be retained in order to yield sensible prognostic information. We note that (54) implies that the horizontal advection of vorticity is equalled in order of magnitude by the vertical advection and twisting terms, and therefore we obtain in this case:

$$\left.\begin{aligned} \frac{d\zeta}{dt} + \beta v + fD + w_x v_z - w_y u_z &= \\ = -\left(\frac{1}{\varrho}\right)_x p_y + \left(\frac{1}{\varrho}\right)_y p_x & \end{aligned}\right\} \qquad (62)$$

which is not essentially simpler than the full vorticity equation. This points to the fact that it is very difficult to get specific information on the planetary scale beyond expressing its quasi-stationary character.

Furthermore, it should be remembered that, due to (50) the metrical terms do not drop out from the expressions (17) and (20) for D and ζ, though, of course, r may be replaced by a. As for the geostrophic divergence, this contains no metrical terms, as is evident from its vectorial form:

$$D_g = \boldsymbol{k} \cdot \nabla p \times \nabla \frac{1}{f\varrho}$$

where $\boldsymbol{k}$ is the vertical unit vector, and ∇ the gradient operator. The geostrophic vorticity is, in vector notation,

$$\zeta_g = \frac{1}{f\varrho} \nabla_h^2 p + \nabla_h p \cdot \nabla_h \frac{1}{f\varrho} \qquad (63)$$

where ∇_h denotes the gradient operator in a horizontal surface. Here the Laplacian generally does contain metrical terms. However, this is not the case with cartesian coordinates on a conformal plane projection of the earth's surface, as is customarily used in numerical prediction. Here, if X and Y denote the cartesian coordinates on the map, and m is the mapping factor (ratio of an arc increment on the map to that on the earth's surface), we namely have

$$\nabla_h^2 = m^2 \left(\frac{\partial^2}{\partial X^2} + \frac{\partial^2}{\partial Y^2}\right)$$

Thus two circumstances, viz. firstly, the use of geostrophic values, and, secondly, the use of cartesian coordinates on a conformal map, combine rather fortuitously to render a discussion of the relative importance of metrical terms in ζ and D irrelevant.

Proceeding, now, from the vorticity equation to the other equations for the planetary scale, not much is changed compared to the previous section. The equations of motion are evidently very well represented by the geostrophic and hydrostatic equations, the adiabatic equation remains unaltered, and, (if we again assume $V \sim 10$ m/sec), the continuity equation still has the form (37). If V increases, i.e. if (60) ceases to hold, (54) and (10) show that the horizontal time-derivaitve of density becomes less negligible (for large S) in the

continuity equation. In the divergence equation (41), evidently βu on the left-hand side should now be included, being of the same order of magnitude as $f\zeta$. On the right-hand side, the last two terms of (43) may be omitted for $V \sim 10$ m/sec; for larger V they should be retained, as with the solenoidal terms belonging with (58). Therefore (for $V \sim 10$ m/sec) we have

$$\left.\begin{aligned} -f\zeta + \beta u = & -f\zeta_g + \beta u_g = \\ = & -\frac{1}{\varrho}\left(p_{xx} + p_{yy} - \frac{\tan\phi}{a} p_y\right) \end{aligned}\right\}, \quad (64)$$

again simply expressing the geostrophic approximation. In fact, we could more conveniently replace this equation by directly writing down the relevant geostrophic formula for any quantity as required. Thus, for instance, the spherical coordinate form of (63) is

$$\zeta_g = \frac{1}{f\varrho}\left(p_{xx} + p_{yy} - \frac{\tan\phi}{a} p_y\right) - \\ - \frac{\beta p_y}{f^2\varrho} + \frac{1}{f} p_y \left(\frac{1}{\varrho}\right)_y + \frac{1}{f} p_x \left(\frac{1}{\varrho}\right)_x$$

and, if the last two terms are omitted, as they were in (64), this becomes

$$\zeta_g = \frac{1}{f\varrho}\left(p_{xx} + p_{yy} - \frac{\tan\phi}{a} p_y\right) - \frac{\beta p_y}{f^2\varrho} \quad (65)$$

which is exactly the value of ζ obtained from (64) by replacing βu on the left-hand side by its geostrophic value.

If we attempt to retain some of the non-linear terms of the divergence equation in (64), the position is similar to that in (62), where also terms in w as well as the density derivatives should be retained.

Finally, we note that in the present case the relation between the Richardson and Rossby numbers differs from that of the previous section. Here we have

$$Ri = \frac{g\sigma}{v_z^2} \sim \frac{fVa}{H^2} \Big/ \frac{V^2}{H^2} = \frac{fa}{V}$$

and if attention is restricted to the case (50), this becomes

$$Ri \sim \frac{fS}{V} \quad (66)$$

Evidently, therefore, $Ri >> 1$ is on the whole a less restrictive condition than $\frac{V}{fS} << 1$, over the range of values considered.

6. Conclusion

Based on the above results, the position may be summarized as follows:

(a) The simplified form (39) of the vorticity equation, geostrophically approximated, is a useful tool in forecasting on the moderately large scale of motion.

(b) The same equation applied to waves of planetary size, should fail in the details of its prognosis of their motion.

(c) If both the scales of a and b are present, the planetary waves will contribute only a small part to the forecast change. This means that the major part of the change is well handled, so that the overall performance should still be good.

(d) The fact that the changes are of lower order of magnitude on the planetary scale, is caused by a balance between the divergence and β-terms in the vorticity equation. Therefore, a divergence term has to be present in order to express this balanced state. This confirms the proposed addition of a divergence term to the barotropic model by Bolin (1955, 1956). Further since the geostrophic approximation is here well satisfied, while also on this scale the separate terms in the divergence do not tend to cancel, the divergence term may, as far as the requirements of the planetary scale are concerned, be geostrophically approximated.

(e) Any attempt beyond expressing the state of quasibalance on the planetary scale, is hampered, not only by the masking effect of errors on different scales, but also by the fact that a number of extra terms, normally considered negligible, seem not to be negligible for this purpose. However, merely adding such extra terms will increase the number of degrees of freedom of the system, also on the scales where these terms are in fact negligible, and the overall effect will probably not be satisfactory. If, for the planetary scale, an adequate representation of the quasi-stationary character only is sought, a

possible amended form of the barotropic vorticity equation for use over different scales, is therefore (38), with a geostrophically approximated divergence term. However, the moderate scales will probably be adversely affected by the geostrophic approximation in the divergence term.

(f) As with the divergence term in the vorticity equation, the β-term in the divergence equation is of prime importance on the planetary scale. Using the divergence equation (or balance equation) in the form (64), or, equivalently, using the value (65) for ζ, should therefore considerably improve the representation on this scale. Here the presence of metrical terms $\left(\text{containing } \frac{1}{a}\right)$ is important in spherical coordinates; however, as has been shown above, the use of a square grid on a conformal plane map of the earth's surface, which is customary in numerical prediction, automatically allows for the metrical terms. It should be noted that (64) is still entirely equivalent to the geostrophic approximation, and that inclusion of the β-term in the balance equation is not a step towards nongeostrophic representation.

(g) As far as the moderate scales are concerned, the condition of smallness of the Rossby number, which justifies the geostrophic approximation, is not too well satisfied for the higher wind-speeds. In considerations aimed at proceeding towards nongeostrophic effects the condition of largeness of the Richardson number may be regarded as a next approximation, being less stringent and better satisfied than smallness of the Rossby number.

(h) The Prandtl relation (26), expressing the ratio of horizontal and vertical scales, ceases to be valid on the planetary scale.

In conclusion the author wishes to thank Dr T. E. W. Schumann, Director of the South African Weather Bureau, for his stimulating interest in the work, and for permission to publish this article. It is published with the permission also of the Council for Scientific and Industrial Research, Pretoria.

REFERENCES

Bolin, B., 1955: Numerical forecasting with the barotropic model. *Tellus* **7**, 1, pp. 27—49.

— 1956: An improved barotropic model and some aspects of using the balance equation for three-dimensional flow. *Tellus* **8**, 1, pp. 1—15.

Charney, J. G., 1948: On the scale of atmospheric motions. *Geof. Publ.* **17**, 2, 17 pp.

Charney, J. G., and Eliassen, A., 1949: A numerical method for predicting the perturbations of the middle latitude westerlies. *Tellus* **1**, 2, pp. 38—54.

Eady, E. T., 1949: Long waves and cyclone waves. *Tellus* **1**, 3, pp. 33—52.

Landers, H., 1955: A three-dimensional study of the horizontal velocity divergence. *Journ. of Met.* **12**, 5, pp. 415—427.

Prandtl, L., 1936: Beiträge zur Mechanik der Atmosphäre. U.G.G.I. (Edinburgh) Assoc. Mét., Mém. et discussions, pp. 171—202.

Stümke, H., 1953: Differentialgleichungen der quasigeostrophischen Wetterentwicklung von Druckfeldern... *Ber. D. Wetterd.* **3**, 19 pp.

White, R. M., and Cooley, D. S., 1956: Kinetic energy spectrum of meridional motion in the midtroposphere. *Journ. of Met.* **13**, 1, pp. 67—69.

A Study of the Long Atmospheric Waves on the Basis of Zonal Harmonic Analysis

By E. ELIASEN, University of Copenhagen

(Manuscript received June 17, 1957)

Abstract

Characteristic features of the long atmospheric waves at middle latitudes are discussed on the basis of zonal harmonic analyses of hemispherical weather charts. In the first section mean values of the amplitudes of the waves with wavenumbers from 1 to 10 are presented for the 500-mb and the 1000-mb levels. Spectral distributions of the kinetic energy for the eastward and the northward components of the geostrophic wind at the 500-mb level are computed. In section 2 the semi-permanence of the waves with wavenumbers from 1 to 4 is illustrated. The meridional variation of the waves is investigated in relation to the question about the meridional transport of momentum. On the basis of the vertical variations of the waves of the January and July normal charts the causes of the semi-permanent waves are discussed. The travelling waves with wavenumbers 5, 6, and 7 are treated in section 3. Mean speeds of the waves are considered in relation to the mean velocity of the zonal flow. The vertical structure of the waves is investigated by means of the heights of the 1000-mb and 500-mb levels and the temperature field at the 500-mb level. Finally the speed and vertical structure of the waves are determined theoretically from the solutions of the linear equations in a two-level approximation.

Introduction

The atmospheric motion as it presents itself on hemispherical weather charts can be considered immediately as a zonal flow upon which are superimposed more or less marked disturbances. The disturbances, however, represent again a superposition of components with horizontal scales in a very wide range. The most simple, quantitative analysis of the components with the largest scales (wavelengths larger than about 3,000 km) seems to be performed by a decomposition into waves with different wavelengths in the zonal direction.

In the following the results of a series of such analyses of actual weather charts are presented in order to outline certain characteristic features related to the different wavelengths, especially the distribution of kinetic energy, the types of motion and the meridional and vertical structure of the waves in the lower and middle troposphere. The analyses have been carried out once a day for the period 21 October to 30 November 1950 on the basis of the 1,000-mb and 500-mb charts from "Daily Series Synoptic Weather Maps" published by U.S. Weather Bureau. Furthermore the investigation includes certain normal charts from "Normal Weather Charts for the Northern Hemisphere", U.S. Weather Bureau, 1952.

1. The spectral distribution of kinetic energy

By a zonal harmonic analysis the height z of a pressure surface as function of the longitude ϑ and the latitude φ can be written

$$z(\varphi, \vartheta) = \bar{z}(\varphi) + \\ + \sum_m \{a_m(\varphi) \cos m\vartheta + b_m(\varphi) \sin m\vartheta\}, \\ m = 1, 2, - - \qquad (1)$$

with

$$\bar{z}(\varphi) = \frac{1}{2\pi} \int_0^{2\pi} z(\varphi, \vartheta)\, d\vartheta$$

$$a_m(\varphi) = \frac{1}{\pi} \int_0^{2\pi} z(\varphi, \vartheta) \cos m\vartheta\, d\vartheta,$$

$$b_m(\varphi) = \frac{1}{\pi} \int_0^{2\pi} z(\varphi, \vartheta) \sin m\vartheta\, d\vartheta$$

The values of a_m and b_m have been computed by approximating the integrals round the latitude circles by the corresponding sums of the values for each five degrees of longitude.

Table 1. Mean values of A_m in m.

m	500 mb			1,000 mb
	40° N	50° N	60° N	50° N
1	49	86	111	72
2	46	76	109	54
3	43	96	92	53
4	57	58	58	36
5	58	68	54	35
6	38	45	30	31
7	37	39	29	23
8	21	25	14	17
9	19	22	14	15
10	10	16	13	13

Table 1 shows the mean values over the period 21 October to 30 November of the amplitudes $A_m = \sqrt{a_m^2 + b_m^2}$ for the wavenumbers from 1 to 10. For the 500-mb level the values are given at the latitudes 40, 50 and 60° N, and for the 1.000-mb level at 50° N. Generally the amplitudes are small to the south of 30° N and for $m > 3$ also to the north of 70° N. For $m \leqq 3$ the amplitudes have their maximum values to the north of 50° N, while for $m \geqq 5$ they have their maxima between 45 and 50° N. The ratio between the amplitude at the 1,000-mb level and the amplitude at the 500-mb level has at 50° N the largest values for $m = 1$ (0.84) and $m = 10$ (0.81) and the smallest value for $m = 5$ (0.52).

From the height of the pressure surface we get the following components of the geostrophic wind in the eastward and in the northward direction.

$$u = -\frac{g}{2\Omega \sin\varphi} \frac{\partial z}{r\partial\varphi}, \qquad v = \frac{g}{2\Omega \sin\varphi} \frac{\partial z}{r \cos\varphi \partial\vartheta} \qquad (2)$$

where g is the acceleration of gravity, r the radius and Ω the angular velocity of the earth. The decomposition of u and v corresponding to (1) becomes

$$\left.\begin{aligned} u(\varphi, \vartheta) &= \bar{u}(\varphi) + \\ &+ \sum_m \{a_m^{(u)}(\varphi) \cos m\vartheta + b_m^{(u)}(\varphi) \sin m\vartheta\} \\ v(\varphi, \vartheta) &= \\ &= \sum_m \{a_m^{(v)}(\varphi) \cos m\vartheta + b_m^{(v)}(\varphi) \sin m\vartheta\} \end{aligned}\right\} \qquad (3)$$

where the mean zonal velocity $\bar{u}(\varphi)$ is given by

$$\bar{u}(\varphi) = \frac{1}{2\pi} \int_0^{2\pi} u(\varphi, \vartheta)\, d\vartheta = -\frac{g}{2\Omega r \sin\varphi} \frac{\partial \bar{z}}{\partial\varphi} \qquad (4)$$

and where

$$\left.\begin{aligned} a_m^{(u)} &= -\frac{g}{2\Omega r \sin\varphi} \frac{\partial a_m}{\partial\varphi}, \\ b_m^{(u)} &= -\frac{g}{2\Omega r \sin\vartheta} \frac{\partial b_m}{\partial\varphi} \\ a_m^{(v)} &= +\frac{g}{2\Omega r \sin\varphi \cos\varphi} m b_m, \\ b_m^{(v)} &= -\frac{g}{2\Omega r \sin\varphi \cos\varphi} m a_m \end{aligned}\right\} \qquad (5)$$

The relative importance of the different wavenumbers can perhaps best be expressed by the spectral distribution of the kinetic energy or of the density of $\frac{1}{2}(u^2 + v^2)$ (cf. the discussion of the energy spectrum of the meridional motion for the period December 1949—February 1950 by White and Cooley, 1956). From (3) we get

$$\frac{1}{2\pi} \int_0^{2\pi} \frac{1}{2} (u^2 + v^2)\, d\vartheta = e_0^{(u)} + \sum_m \{e_m^{(u)} + e_m^{(v)}\} \qquad (6)$$

with

$$\left.\begin{aligned} e_0^{(u)} &= \frac{1}{2} \bar{u}^2 \\ e_m^{(u)} &= \frac{1}{4} \{a_m^{(u)2} + b_m^{(u)2}\}, \quad e_m^{(v)} = \frac{1}{4} \{a_m^{(v)2} + b_m^{(v)2}\} \end{aligned}\right\} \qquad (7)$$

These quantities have been computed at the latitudes 37 ½, 47 ½ and 57 ½° N using

$$\left.\begin{aligned} a_m(\varphi) &= \frac{1}{2}\left\{a_m\left(\varphi+\frac{\pi}{72}\right)+a_m\left(\varphi-\frac{\pi}{72}\right)\right\} \\ \frac{\partial a_m}{\partial \varphi} &= \frac{36}{\pi}\left\{a_m\left(\varphi+\frac{\pi}{72}\right)-a_m\left(\varphi-\frac{\pi}{72}\right)\right\} \end{aligned}\right\} \quad (8)$$

and the corresponding expressions for $b_m(\varphi)$ and $\frac{\partial b_m}{\partial \varphi}$. The mean values for the 14 days 21 October, 24 October, — — —, 29 November 1950 are shown in Fig. 1, where the lower part of the columns represents the values of $e_m^{(u)}$ and the upper part the values of $e_m^{(v)}$. It is seen that $e_m = e_m^{(u)} + e_m^{(v)}$ has a maximum for $m = 5$, which at 47 ½° N corresponds nearly to the wavelength 5.400 km. For $m > 5$ e_m decreases rather rapidly with increasing m, whereas for $m < 5$ the variation is different at the three latitudes. Table 2 gives a comparison between the kinetic energy contained in the zonal flow, the waves with m from 1 to 4 and the waves with m from 5 to 10. For each of the two groups of waves the energy is of the same order of magnitude. To the south of about 50° N the kinetic energy of the zonal flow is larger than the total kinetic energy of the waves, whereas to the north it becomes essentially smaller.

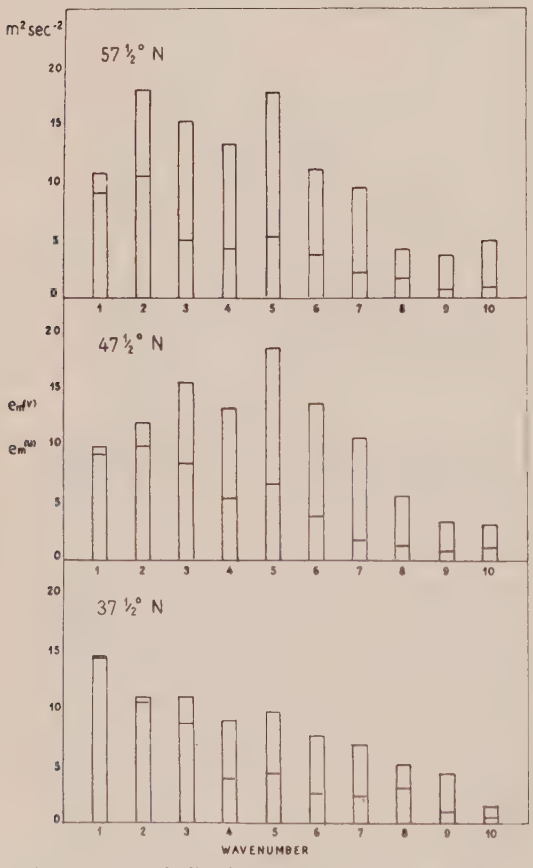

Fig. 1. Spectral distribution of kinetic energy at the 500-mb level during the period 21 October—30 November 1950. The lower part of the columns, $e_m^{(u)}$, represents the contributions from the eastward and the upper part of the columns, $e_m^{(v)}$, the contributions from the northward component of the geostrophic wind.

Table 2. Mean values of e_m in m² sec⁻² (500-mb level).

	37 ½° N	47 ½° N	57 ½° N
e_0	112	172	37
$\sum_{m=1}^{4} e_m$	44	50	57
$\sum_{m=5}^{10} e_m$	35	56	51

From Fig. 1 it is further seen that for $m = 1$ and 2 essentially more energy is contained in the u-component than it the v-component of the velocity, whereas for $m \geqq 4$ most of the energy is contained in the v-component. This indicates that the scale in the south-north direction, expressed by a "characteristic wavelength", will be smaller than the wavelength in the west-east direction for $m = 1$ and 2, whereas it will be larger for $m \geq 4$.

2. The long semi-permanent waves

In order to examine the day-to-day variations of the different waves we write

$$a_m(\varphi, t)\cos m\vartheta + b_m(\varphi, t)\sin m\vartheta = \\ = A_m(\varphi, t)\cos m\{\vartheta - \delta_m(\varphi, t)\} \quad (9)$$

where the phase angle $\delta_m(\varphi, t)$ states the position of a ridge. The motion at the 500-mb level of the longest waves, $m = 1, 2, 3$ and 4, is illustrated in Fig. 2, showing δ_m as function of time at the latitude 50° N. It is seen that each of the waves fluctuates about a certain mean position, and only in some few cases the deviation from the mean position becomes larger than a quarter of the wavelength. Oc-

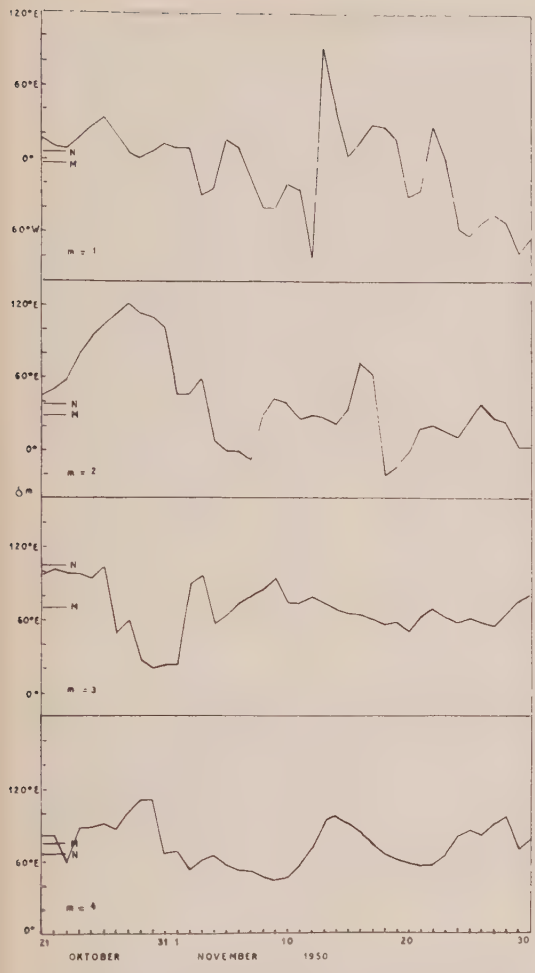

Fig. 2. The positions, δ_m, of a ridge for the waves $m=1$, 2, 3, and 4 at the 500-mb level and 50° N. *M* indicates the positions of the mean waves and *N* the positions of the waves on the normal chart of November.

casionally the displacement during one day is relatively large, but this always coincides with a small value of the amplitude. The character of the variations of the amplitudes is illustrated in Fig. 3, which shows the values of the amplitude for $m = 3$ as function of time. The standard deviations of the amplitudes are for $m = 1$: 31, for $m = 2$: 41, for $m = 3$: 37 and for $m = 4$: 25 meters.

As a consequence of the semi-permanence these long waves are maintained on the monthly mean charts. They are also present on the normal charts for the individual months, which indicates that the mean positions of the waves are nearly the same from year to year.

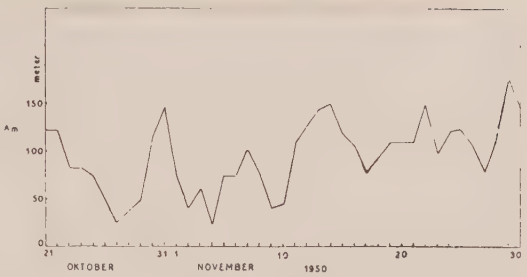

Fig. 3. The values of the amplitude A_m for $m=3$ at the 500-mb level and 50° N.

For the mean over the period 21 October—30 November 1950 the amplitudes and phase angles of the waves with *m* from 1 to 5 are shown in Table 3 for the 500-mb and 1,000-mb levels at the latitude 50° N. For $m = 1$ the amplitude of the mean wave is about 3/4 times the mean of the amplitudes (Table 1), else the amplitudes of the mean waves are about the half of the mean values of the amplitudes. This is also seen to be the case for $m = 5$ (cf. the next section), whereas the waves with $m \geq 6$ almost vanish in the mean. For comparison Table 4 contains the result of the corresponding harmonic analysis of the normal charts for the month of November. In Fig. 2 the positions of the mean waves (Table 3) are marked by *M* and the positions of the normal waves (Table 4) by *N*.

Table 3. The mean waves at 50° N. A_m in m and δ_m in degrees of longitude.

m	500 mb		1,000 mb	
	A_m	δ_m	A_m	δ_m
1	72	356	63	84
2	41	29	40	92
3	54	70	22	73
4	24	76	14	85
5	37	32	18	0

Table 4. The waves of the normal charts of November at 50°N. A_m in m and δ_m in degrees of longitude.

m	500 mb		1,000 mb	
	A_m	δ_m	A_m	δ_m
1	98	6	60	62
2	53	38	59	84
3	41	105	12	120
4	20	67	4	74
5	15	30	8	33

Table 5. Harmonic analysis of normal charts. A_m in m and δ_m in degrees of longitude.

Latitude	m	January				July			
		500 mb		1,000 mb		500 mb		1,000 mb	
		A_m	δ_m	A_m	δ_m	A_m	δ_m	A_m	δ_m
30° N	1	59	292	16	351	41	312	79	256
	2	10	145	16	110	16	175	53	165
	3	28	83	17	102	4	17	21	77
40° N	1	84	326	39	46	38	332	66	262
	2	34	42	48	89	12	77	48	179
	3	64	98	32	108	12	79	22	83
50° N	1	84	6	76	66	32	22	38	271
	2	79	43	83	85	43	73	32	14
	3	80	106	33	2	22	111	12	93
60° N	1	62	40	71	114	35	73	17	259
	2	100	33	64	79	42	58	19	30
	3	63	108	43	12	24	114	6	104
70° N	1	50	84	87	163	39	116	3	274
	2	98	21	19	71	40	40	12	23
	3	40	108	18	3	14	101	2	110

The motion of the waves has also been investigated at the latitudes 40 and 60° N, and it parallels rather closely the motion at 50° N, with a certain tilt of the trough- and ridge-lines. The meridional variation of the waves $m = 1$, 2 and 3 on the normal charts of January and July can be seen from Table 5, giving the values of A_m and δ_m at the latitudes 30, 40, 50, 60 and 70° N for the 500-mb and 1,000-mb levels. The tilt of the trough- and ridge-lines is decisive for the meridional transport of momentum in the way that the waves with SW—NE orientation of the axes give a northward transport whereas the waves with SE—NW orientation give a southward transport. With the decomposition (3) we get

$$\left.\begin{aligned} \tau &= \frac{1}{2\pi}\int_0^{2\pi} u\,v\,d\vartheta = \sum_m \tau_m \\ \tau_m &= \frac{1}{2}\{a_m^{(u)}\,a_m^{(v)} + b_m^{(u)} b_m^{(v)}\} \end{aligned}\right\} \qquad (10)$$

Using (5) and (8) τ_m has been computed from the 500-mb and 1,000-mb normal charts for January and July. The values for $m = 1$, 2 and 3 at the latitudes 27 ½, 37 ½, 47 ½ and 57 ½° N are listed in Table 6. The values for $m \geqq 4$ are quite insignificant.

A comparison with the total mean transport τ computed for instance for January 1949 by MINTZ (1951) indicates that the transport connected with the long semi-permanent waves is by no means negligible (cf. STARR and WHITE, 1952). For January 1949 the mean of τ has at the 500-mb level the maximum value

Table 6. τ_m for the normal charts in $m^2\,sec^{-2}$.

Latitude	m	January		July	
		500 mb	1000 mb	500 mb	1000 mb
27 ½° N	1	0.9	0.3	— 0.1	0.3
	2	0.2	— 0.6	0.1	2.0
	3	4.1	0.6	— 0.2	0.7
37 ½° N	1	5.0	0.6	0.6	0.5
	2	0.5	— 1.7	— 0.1	2.9
	3	5.5	0.8	0.1	0.5
47 ½° N	1	4.2	1.2	1.1	0.3
	2	— 0.5	— 0.6	0.0	1.1
	3	5.2	2.4	0.2	0.4
57 ½° N	1	2.3	4.4	0.8	— 0.1
	2	— 4.8	— 2.2	— 1.8	0.5
	3	1.5	1.2	— 0.3	0.1
67 ½° N	1	1.7	4.3	0.6	0.0
	2	— 9.6	— 0.3	— 2.4	— 0.3
	3	— 0.5	— 1.7	— 0.2	0.0

36 $m^2 sec^{-2}$ at about 40° N, and the corresponding total value for the long waves on the normal chart becomes 12 $m^2 sec^{-2}$.

The existence of the long semi-permanent waves is presumably explained as the combined effect of the large-scale distribution of heat sources and the large mountain barriers (the Rocky Mountains and the mountains in the interior of Asia). Largely the continents act as cold sources and the oceans as warm sources in winter and inversely in summer. This should indicate a phase shift for the corresponding waves during the year. The normal positions in the lower and middle troposphere of the waves m = 1, 2 and 3 in the months of January and July are therefore placed together in Fig. 4 for the latitude 50° N on

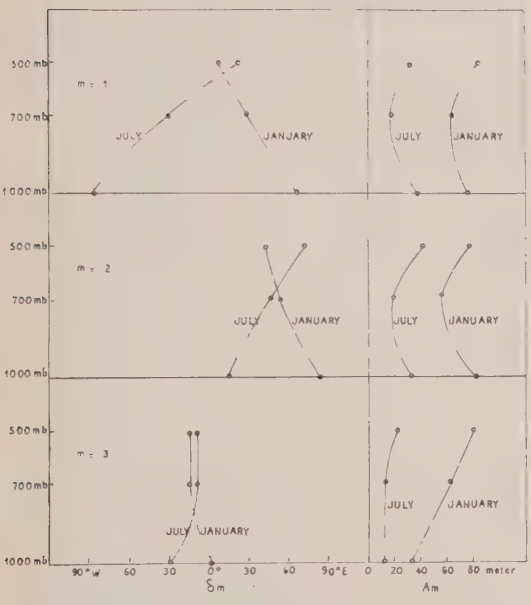

Fig. 4. Harmonic analysis of the normal charts of January and July at 50° N. The positions, δ_m, of a ridge and the values, A, of the amplitude for the waves m=1, 2, and 3 at the 1,000-mb, 700-mb and 500-mb levels.

the basis of the harmonic analysis of the normal charts for the 500-mb, 700-mb and 1,000-mb levels. The figure also shows the corresponding values of the amplitudes. In the lowest layer of the troposphere the phase differences between January and July are considerably, namely for m = 1: 0.43, for m = 2: 0.39 and for m = 3: 0.24 times the wavelength. This is at least qualitatively in agreement with the phase shift of the heat sources. However, in the layer from 700 mb to 500 mb the phase differences become much smaller, which constitutes an essential argument (Charney and Eliassen, 1949) for ascribing the large mountain barriers an essential role.

The effect of the heat sources has been studied by Smagorinsky (1953) on the basis of the linear equations, and it seems likely that the amplitudes of the waves caused by the heat sources will be rather constant or even decrease with height. The perturbations caused by the mountain barriers have been investigated for the equivalent-barotropic level by Charney and Eliassen (1949) and Bolin (1950) and a considerable agreement with the real perturbations at the 500-mb level has been demonstrated. Extending the computations to a baroclinic atmosphere, utilizing the confluent hypergeometric functions tabulated by Charney (1947), it turns out that the amplitudes of the orographically induced waves increase essentially with height, the amplitudes at the 500-mb level being between 2 and 3 times the amplitudes at the 1,000-mb level. So it seems that the large-scale distribution of heat sources plays an important role in the formation of the long waves in the lowest part of the troposphere, whereas the effect of the large mountain barriers becomes predominant in the middle and upper troposphere.

3. The travelling waves

The day-to-day variations of the wave with wavenumber 5 at the 500-mb level and at 50° N are shown in Fig. 5. In the periods 21—27 October and 5—20 November the wave moves towards the east with a speed of about 9 degrees of longitude per day. On the other hand, from 27 October to 5 November and from 20 to 30 November the wave is quasi-stationary in a position coinciding very nearly with the position of the wave on the normal chart of November, marked N (Table 4). The values of the amplitude are shown in the upper part of the figure, but (as for the other m) there seems to be no, at least no simple, relation between the motion of the wave and its amplitude.

The waves with wavenumber larger than 5 seem to move consistently towards the east.

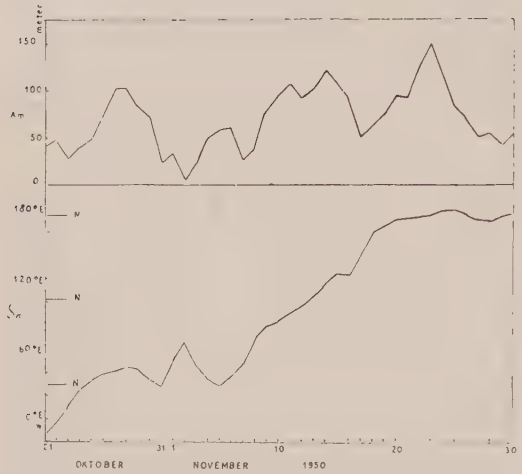

Fig. 5. The positions, δ_m, of a ridge and the values, A_m, of the amplitude for the wave $m=5$ at the 500-mb level and 50° N. *N* indicates the position of the wave on the normal chart of November.

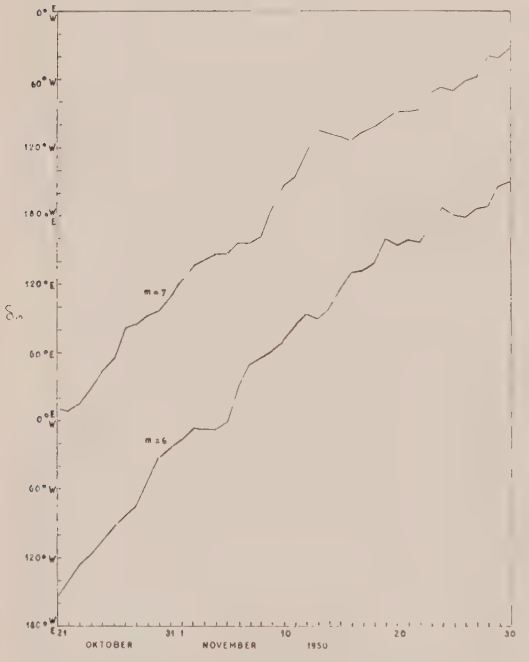

Fig. 6. The positions, δ_m, of a ridge for the waves $m=6$ and 7 at the 500-mb level and 50° N.

The motion for $m = 6$ and 7 is shown in Fig. 6, still for the 500-mb level and at 50° N. It is seen that there is no essential difference between the motion of the two waves. During the period from 23 October to 15 November they move with the same mean speed of

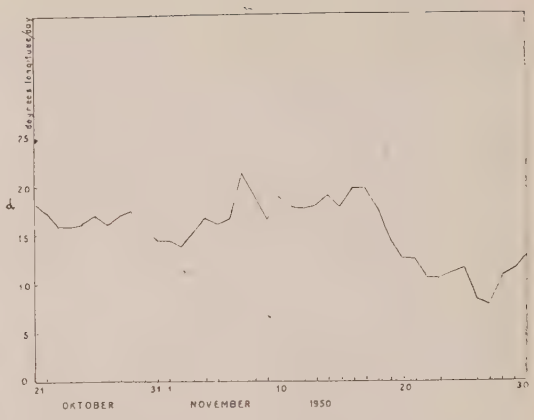

Fig. 7. The mean angular velocity, α, of the zonal flow in the belt from 40 to 60° N at the 500-mb level.

nearly 10 degrees of longitude per day, whereas from 18 to 30 November the common mean speed is only about 6 degrees of longitude per day. This decrease in the speed of the waves seems to be related to a corresponding decrease of the angular velocity α of the zonal flow, which can be seen from Fig. 7. The values of α are computed as the geostrophic values at 50° N, using the mean gradients of $\bar{z}(\varphi)$ between 40 and 60° N. The mean value of α for the period 23 October to 15 November is 16.7 and for the period 18 to 30 November 11.7 degrees of longitude per day.

The standard deviations of the amplitudes (500 mb, 50° N) become for $m = 5$: 33, for $m = 6$: 21 and for $m = 7$: 20 meters, i.e. in all three cases nearly 0.5 times the mean value of the amplitude.

The motion of the wave $m = 8$ shows a very similar picture. However, with decreasing wavelength the displacements of the waves during one day often become of the same magnitude as half of the wavelength, leading to ambiguities in the fixing of the motion.

The motion of the waves $m = 5$, 6 and 7 at the latitudes 40 and 60° N follows largely the motion at 50° N. In nearly 50 per cent of the cases the phase difference between 40 and 50° N as well as between 50 and 60° N is smaller than 5 degrees of longitude and in about 75 per cent of the cases it is smaller than 10 degrees. For both $m = 5$ and 6 there is from 40 to 60° N a SW—NE tilt of the trough- and ridge-lines in nearly 60 per cent of the

cases, but for $m = 7$ in only 40 per cent. However, for all three values of m the mean values of the phase differences between 40, 50 and 60° N become quite insignificant.

The relation between the mean of the amplitudes for the wave at the 500-mb and the 1,000-mb levels has been shown for 50° N in Table 1. For $m = 5$, 6 and 7 the correlation coefficients of the amplitudes at the two levels are about 0.50. The distribution during the 41 days of the phase differences, $\triangle_1$, from the waves at the 500-mb level to the waves at the 1,000-mb level is shown for 50° N in Table 7. It is seen that in the mean the waves

Table 7. Distribution of $\triangle_1$. Number of cases.

	$m = 5$	$m = 6$	$m = 7$
$-27 \leqq \triangle_1 \leqq -23$	1	0	0
$-22 \leqq \triangle_1 \leqq -18$	0	1	1
$-17 \leqq \triangle_1 \leqq -13$	1	0	1
$-12 \leqq \triangle_1 \leqq -8$	3	2	0
$-7 \leqq \triangle_1 \leqq -3$	2	2	2
$-2 \leqq \triangle_1 \leqq +2$	3	7	9
$3 \leqq \triangle_1 \leqq 7$	11	11	17
$8 \leqq \triangle_1 \leqq 12$	13	10	9
$13 \leqq \triangle_1 \leqq 17$	4	6	2
$18 \leqq \triangle_1 \leqq 22$	1	1	0
$23 \leqq \triangle_1 \leqq 27$	2	1	0

are displaced somewhat to the west at the 500-mb level in relation to the 1,000-mb level. The mean of the phase differences decreases with increasing wavenumber, being approximately 1/10 of the wavelength. For the waves in the thickness field from 1,000 to 500 mb the mean values of the amplitudes become for $m = 5$: 0.84, for $m = 6$: 0.82 and for $m = 7$: 0.74 times the corresponding mean amplitudes of the waves at the 500-mb level. In about 80 per cent of the cases the waves $m = 5$, 6 and 7 in the thickness field are displaced towards the west in relation to the waves at the 500-mb level, the mean displacements amounting to about 5 degrees of longitude. The distribution of the displacements (towards the west), $\triangle_2$, is shown in Table 8.

The vertical structure of the waves can be further investigated by harmonic analysis of the temperature field T at the 500-mb level. The positions of the waves $m = 5$, 6 and 7 in this temperature field correspond in the mean very nearly with the positions in the

Table 8. Distribution of $\triangle_2$. Number of cases.

	$m = 5$	$m = 6$	$m = 7$
$-27 \leqq \triangle_2 \leqq -23$	0	0	0
$-22 \leqq \triangle_2 \leqq -18$	0	1	0
$-17 \leqq \triangle_2 \leqq -13$	0	1	0
$-12 \leqq \triangle_2 \leqq -8$	0	2	1
$-7 \leqq \triangle_2 \leqq -3$	4	2	2
$-2 \leqq \triangle_2 \leqq +2$	6	7	9
$3 \leqq \triangle_2 \leqq 7$	22	17	20
$8 \leqq \triangle_2 \leqq 12$	6	6	5
$13 \leqq \triangle_2 \leqq 17$	2	2	3
$18 \leqq \triangle_2 \leqq 22$	0	1	1
$23 \leqq \triangle_2 \leqq 27$	1	2	0

thickness field from 1,000 to 500 mb, the westward displacements relatively to the positions at the 500-mb level being slightly smaller. Writing

$$T(\varphi, \vartheta) = \overline{T}(\varphi) + \sum_m \{a_m^{(T)}(\varphi) \cos m\vartheta + b_m^{(T)} \sin m\vartheta\} \quad (11)$$

we get from the hydrostatic equation

$$\frac{\partial a_m}{\partial p} = -\frac{R}{gp} a_m^{(T)}, \quad \frac{\partial b_m}{\partial p} = -\frac{R}{gp} b_m^{(T)} \quad (12)$$

where R is the gas constant of air. Introducing the thickness field

$$h = -\frac{\partial z}{\partial p} \triangle p = \overline{h} + \sum \{a_m^{(h)} \cos m\vartheta + b_m^{(h)} \sin m\vartheta\} \quad (13)$$

with $\triangle p = 100$ mb, we get

$$a_m^{(h)} = \frac{R \triangle p}{gp} a_m^{(T)}, \quad b_m^{(h)} = \frac{R \triangle p}{gp} b_m^{(T)} \quad (14)$$

The mean value of the amplitudes in this thickness field becomes at 50° N for $m = 5$: 0.24, for $m = 6$: 0.29 and for $m = 7$: 0.26 times the corresponding mean amplitudes of the waves at the 500-mb level.

Theoretical investigations (Charney, 1947; Eady, 1949 and Fjørtoft, 1950) based upon solutions of the linear equations for wave motions in a baroclinic zonal current have demonstrated the possible development of long waves transforming potential and internal energy into kinetic energy. Certainly the interactions between the different waves play

an important role in the actual atmospheric developments, but owing to the relatively large velocity of the zonal flow and the steadiness of its effect it seems reasonable to suppose that the mean conditions of the waves are decisively influenced by the interaction with the zonal flow. So it may be of some interest to compare the solutions of the linear equations with the mean conditions of the actual waves.

In order to avoid mathematical troubles approximations concerning the vertical variations may be introduced, cf. for instance Eliassen (1952) and Thompson (1953). Following the method of finite differences by Charney and Phillips (1953) we have for the quasi-geostrophic motion at the two levels p_1 and p_2

$$\left.\begin{aligned}&\left(\frac{\partial}{\partial t}+\mathbf{v}_1\cdot\nabla\right)\left(\xi_1+2\Omega\sin\varphi\right)-\\&-\varkappa\frac{g}{2\Omega\sin\varphi}\left(\frac{\partial}{\partial t}+\mathbf{v}_1\cdot\nabla\right)\left(z_1-z_2\right)=0\\&\left(\frac{\partial}{\partial t}+\mathbf{v}_2\cdot\triangle\right)\left(\xi_2+2\Omega\sin\varphi\right)+\\&+\varkappa\frac{g}{2\Omega\sin\varphi}\left(\frac{\partial}{\partial t}+\mathbf{v}_2\cdot\nabla\right)\left(z_1-z_2\right)=0\end{aligned}\right\}\quad(15)$$

with the vector $\mathbf{v}$ given by (2),

$$\xi=\frac{g}{2\Omega\sin\varphi}\nabla^2 z$$

and

$$\varkappa=-\frac{4\Omega^2\sin^2\varphi}{(p_2-p_1)^2}\left\{\frac{1}{\varrho}\frac{\partial\log\Theta}{\partial p}\right\}^{-1}_{p=\frac{p_1+p_2}{2}}$$

where ϱ is the density and Θ the potential temperature. ∇ denote the spherical del-operator. Approximating the stabilizing influence of the stratosphere on the tropospheric motion by a rigid top placed a little higher than the tropopause, the levels p_1 and p_2 become nearly the 400-mb and the 800-mb levels (cf. Bolin, 1953). Corresponding to normal conditions $\varkappa$ then has a value equal to or somewhat smaller than $3\cdot10^{-12}\ m^{-2}$ and is treated as a constant.

We now consider a zonal flow with the angular velocity α upon which is superimposed the wave motion

$$z'(\varphi,\vartheta,p,t)=k(p)\,P_n^m(\sin\varphi)\,e^{im(\vartheta-\gamma t)}\quad(16)$$

where $P_n^m(\sin\varphi)$ denotes the associated Legendre functions of order m and degree n. Neglecting the meridional variation of α we get from (15) the following linear equations

$$\left.\begin{aligned}\{\alpha_1-\gamma-\gamma^\star+q(\alpha_2-\gamma)\}\,z_1'-q(\alpha_1-\gamma)\,z_2'=0\\\{\alpha_2-\gamma-\gamma^\star+q(\alpha_1-\gamma)\}\,z_2'-q(\alpha_2-\gamma)\,z_2'=0\end{aligned}\right\}\quad(17)$$

where

$$\gamma^\star=\frac{2\Omega}{n(n+1)}\approx\frac{2\Omega+\alpha}{n(n+1)}$$

and

$$q=\frac{\varkappa r^2}{n(n+1)}$$

These equations determine the following values of γ

$$\gamma=\frac{\alpha_1+\alpha_2}{2}-\frac{1+q}{1+2q}\gamma^\star\pm\\\pm\frac{1}{1+2q}\sqrt{q^2\gamma^{\star2}+\frac{1-4q^2}{4}(\alpha_1-\alpha_2)^2}\quad(18)$$

This expression demonstrates the existence of the amplified waves with horizontal scales fixed by the conditions

$$\left.\begin{aligned}n^2(n+1)^2>2\varkappa^2r^4\left(1-\sqrt{1-\frac{4\Omega^2}{\varkappa^2r^4(\alpha_1-\alpha_2)^2}}\right)\\n^2(n+1)^2<2\varkappa^2r^4\left(1+\sqrt{1-\frac{4\Omega^2}{\varkappa^2r^4(\alpha_1-\alpha^2)^2}}\right)\end{aligned}\right\}\quad(19)$$

which with the values of α_1—α_2 and $\varkappa$ used in the following become $7<n<15$. As we may assume that it is the energy transforming processes underlying the amplification which, in the mean, maintain the waves against frictional dissipation it seems reasonable to compare just the amplified waves with the actual waves in the atmosphere.

The accuracy of the above two-level approximation was tested by a comparison with the solutions obtained by including more levels in the description of the vertical variation. Introducing four levels we get instead of (17) four equations and consequently four solutions. For the relatively large horizontal scales here considered two of these solutions agree quite

well with the two solutions obtained from the two-level representation and the two additional solutions correspond to waves with no amplification.

In the mean the amplitudes of the waves with $m \geqq 5$ have relatively small values about 30° N, increase to a maximum value between 45 and 50° N and then decrease again to small values about 70° N. Furthermore the tilt of these waves seems to be negligible, at least in the belt from 40 to 60° N. Certainly the exact meridional variation of a wave with the wavenumber m must be described by a superposition of several Legendre functions P_n^m (sin φ), however for $5 \leqq m \leqq 7$ the above, crude variation is rather well described (in the belt 30—70° N) by the single function P_n^m (sin φ) with $n - m = 4$. In the following we consider especially the amplified solution of (17) with $n = 10$ as being representative for the wave with wavenumber 6.

Having neglected the meridional variation of the angular velocity of the zonal flow it seems reasonable to fix α as the mean value in the belt from 35 to 60° N. From the normal charts of November α then becomes at the 500-mb level: 16.4, at the 700-mb level: 10.1 and at the 1,000-mb level 2.5 degrees of longitude per day, leading to the values $\alpha_1 = 20$ and $\alpha_2 = 7.5$ degrees of longitude per day.

With these values of α and $q = \dfrac{110}{n(n+1)}$ (i.e. $\varkappa = 2.7 \cdot 10^{-12}$ m^{-2}) equation (18) becomes for $n = 10$

$\gamma = (9.4 \pm 2.9i)$ degrees of longitude per day

This value of the velocity of propagation agrees rather well with the value determined from Fig. 6 for the period 23 October to 5 November in which the mean angular velocity of the zonal flow corresponds nearly to the normal of November. Also the subsequent decrease in the velocity of propagation (18—30 November) is in accordance with the formula (18) (cf. Fig. 7).

For the amplified solution with $\gamma = 9.4 + 2.9i$ equations (17) yield

$$z_2' = (0.33 \div 0.45i) z_1'$$

Determining z' for the 500-mb level by linear interpolation we find that the amplitude of the wave in the thickness field from p_2 to p_1 becomes 0.96 times the amplitude at the 500-mb level. Further the wave in the thickness field is displaced 0.11 times the wavelength towards the west in relation to the wave at the 500-mb level. These conditions seem to be rather well in agreement with the mean conditions outlined above for the actual waves in the atmosphere.

REFERENCES

Bolin, B., 1950: On the influence of the earth's orography on the general character of the westerlies. *Tellus* **2**, pp. 184—195.

— 1953: Multiple-parameter models of the atmosphere for numerical forecasting purposes. *Tellus* **5**, pp. 207—218.

Charney, J. G., 1947: The dynamics of long waves in a baroclinic westerly current. *J. Meteor.* **4**, pp. 135—162.

— and Eliassen, A., 1949: A numerical method for predicting the perturbations of the middle latitude westerlies. *Tellus* **1**, **2**, pp. 38—54.

— and Phillips, N., 1953: Numerical integration of the quasi-geostrophic equations for barotropic and simple baroclinic flows. *J. Meteor.* **10**, pp. 71—99.

Eady, E. T., 1949: Long waves and cyclone waves. *Tellus* **1**, **3**, pp. 33—52.

Eliassen, A., 1952: Simplified models of the atmosphere, designed for the purpose of numerical weather prediction. *Tellus* **4**, pp. 145—156.

Fjørtoft, R., 1950: Application of integral theorems in deriving criteria of stability for laminar flows and for the baroclinic circular vortex. *Geof. Publ.* **17**, **6**, 52 pp.

Mintz, Y., 1951: The geostrophic poleward flux of angular momentum in the month of January 1949. *Tellus* **3**, pp. 195—200.

Smagorinsky, J., 1953: The dynamical influence of large-scale heat sources and sinks on the quasi-stationary mean motions of the atmosphere. *Quart. J. R. Meteor. Soc.* **79**, pp. 342—366.

Starr, V. P., and White, R. M., 1952: Schemes fort he study of hemispheric exchange processes. *Quart. J. R. Meteor. Soc.* **78**, pp. 407—410.

Thompson, P. D., 1953: On the theory of large-scale disturbances in a two-dimensional baroclinic equivalent of the atmosphere. *Quart. J. R. Meteor. Soc.* **79**, pp. 51—69.

White, R. M., and Cooley, D. S., 1956: Kinetic-energy spectrum of meridional motion in the mid-troposphere. *J. Meteor.* **13**, pp. 67—69.

An Empirical Correction to the Barotropic Forecast

By SCOTT WILLIAMS, Captain, United States Air Force

(Manuscript received June 5, 1957)

Abstract

An investigation of error fields in 30 consecutive barotropic forecasts for the 500 mb surface has been performed. It is found that the error fields show persistence in the time to such an extent that a correction consisting of the mean error field for a number of preceding forecasts can be applied to a barotropic forecast with advantage. The improvement of the forecast depends upon the number of preceding forecasts included in the mean error field. The greatest increase in accuracy is found when 10—15 preceding forecasts are contributing to the correction field. The 24 hour forecasts are improved to the greatest extent by the correction, but the 48 hour-forecasts also show a significant increase in accuracy. The same is true to a smaller extent for the 72 hour-forecasts.

In section 3 an investigation is made as to whether the height change obtained by making barotropic forecasts from the time-averaged map for the period investigated or from the normal 500 mb map for the corresponding month can be used with the same success as the correction used in section 2. It it found that the correction from the mean chart consistently improved the forecasts. The overall effect is, however, small. The correction obtained from the normal chart did not affect the accuracy of the forecasts appreciably.

1. Introduction

In examining barotropic forecasts made by the Royal Swedish Air Force (BOLIN, 1955; DÖÖS, 1956), it is apparent that some of the errors are persistent and show a definite pattern if averaged over a period of several days or weeks (figure 1). The question arises as to whether these errors are conservative enough to be used as empirical corrections to synoptic forecasts. To answer this question, a test was made using a series of 30 consecutive 24 hour forecasts beginning 14 November, 1955. These forecasts were made from numerical analyses on the Swedish electronic computer BESK (DÖÖS, 1956).

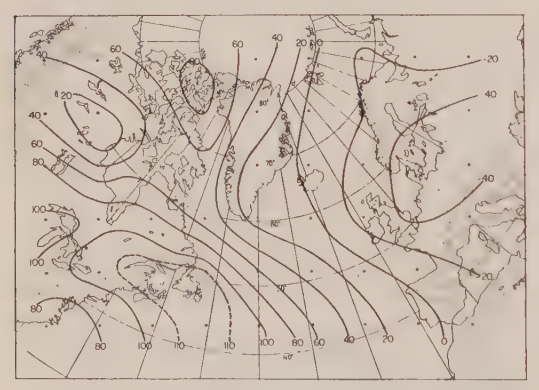

Fig. 1. Average algebraic error ($A\Phi_A$) in 24 hour forecasts, 14 November—14 December, 1955. Grid points shown.

2. Method of investigation and results

Computations were made at 54 individual grid points spaced as shown in figure 1. Numerical analyses and forecasts had been made over roughly the entire area shown in figure 1. Each forecast height change field was corrected by subtracting from it the mean error field of several immediately preceding forecasts. Comparisons were then made of correlation coefficients between observed and forecast height changes and of root-mean-square errors of forecast height change. The results are given in table 1 where: N denotes the number of previous forecasts used in correcting a given forecast, r_0 denotes the

Table 1

Date	r_0	ε_0	$N = 2$		$N = 5$		$N = 10$		$N = 15$	
			r_1	ε_1	r_1	ε_1	r_1	ε_1	r_1	ε_1
16—17/11/55...	0.35	114	0.48	86						
17—18.....	69	96	78	58						
18—19.....	62	93	71	60						
19—20.....	65	110	70	77	0.73	72				
20—21.....	54	104	50	78	68	59				
21—22.....	79	77	75	61	80	57				
22—23.....	67	99	75	55	81	51				
23—24.....	64	103	80	55	79	61				
24—25.....	45	107	86	43	83	47	0.80	52		
25—26.....	63	72	73	62	78	53	79	54		
26—27.....	58	61	74	54	71	55	68	58		
27—28.....	66	69	66	64	52	84	51	83		
28—29.....	79	60	70	70	79	62	83	60		
29—30.....	73	96	82	75	86	66	83	68	0.82	69
30— 1.....	91	56	90	46	92	42	85	55	85	56
1— 2/12/55...	79	77	69	68	81	60	79	65	76	65
2— 3.....	73	81	74	51	77	55	73	59	73	57
3— 4.....	57	93	55	73	64	66	73	56	77	50
4— 5.....	42	80	65	51	51	59	63	51	73	44
5— 6.....	61	82	72	59	73	56	69	61	74	57
6— 7.....	68	81	70	72	75	71	75	64	75	62
7— 8.....	78	73	86	56	89	54	90	49	89	46
8— 9.....	51	83	53	74	53	72	64	64	66	61
9—10.....	83	64	71	71	74	78	78	85	79	80
10—11.....	62	70	86	44	75	61	75	68	75	68
11—12.....	62	71	81	58	68	69	66	73	66	73
12—13.....	63	75	35	91	37	93	39	96	45	89
13—14.....	53	93	69	74	58	90	46	88	51	80
Average.....	0.64	84	0.71	64	0.72	64	0.71	66	0.72	64
$\bar{r}_0$, $\bar{\varepsilon}_0$			0.64	84	0.65	81	0.65	77	0.66	78
W_r, W_ε.....			29	11	12	16	25	20	33	20

Results of correcting 24 hour forecasts by subtracting the mean error field for N previous forecasts.

correlation coefficient between observed and forecast height changes, r_1 is the same as r_0 except that it is for corrected forecasts, ε_0 stands for the root-mean-square error in forecast height changes (in whole meters) of the original forecasts and ε_1 denotes the same quantity for corrected forecasts.

An examination of table 1 shows that most of the forecasts are improved by the correction. The average figures at the bottom of each column show that, overall, the corrected forecasts are significantly better than the uncorrected forecasts. Of course, some of the forecasts are made worse by the correction. The percentage of forecasts for which r_1 is smaller than r_0 is given at the bottom of each r_1-column and is denoted by W_r. The percentage of forecasts for which ε_1 is larger than ε_0 is given at the bottom of each ε_1-column and is denoted by W_ε. Values of $\bar{r}_0$ and $\bar{\varepsilon}_0$ are averaged over the same time period as the adjacent average r_1 and ε_1 values.

Altogether the results looked so good that the test was extended to include all available forecasts based on numerical analyses and which could be verified by numerical analyses. Forecast procedure was the same for all forecasts. Small differences in the numerical analysis procedure between the different series of forecasts were probably not important for the purposes of this test. A summary of the results is given in table 2. Forecasts

Table 2

Summary of Results. 24 Hour Forecasts

	N	D	r_0	r_1	W_r	ε_0	ε_1	W_ε
Autumn 1955	2	2	0.66	0.71	33	78	64	13
29 Nov.—								
14 Dec.	5	5	0.66	0.70	13	78	66	13
15 forecasts	10	10	0.66	0.71	20	78	67	20
	15	15	0.66	0.72	33	78	64	20
Winter 1956	2	4	0.65	0.73	18	87	71	6
8 Febr.—								
15 March	5	10	0.65	0.71	0	87	69	0
17 forecasts	10	21	0.65	0.71	18	87	65	0
	15	31	0.65	0.72	18	87	65	0
Spring 1956	2	4	0.68	0.60	79	76	63	21
19 March—								
24 April	5	10	0.68	0.70	21	76	62	0
19 forecasts	10	21	0.68	0.65	68	76	59	16
	15	31	0.68	0.64	84	76	60	16
	20	42	0.68	0.64	63	76	59	16
	30	62	0.68	0.64	79	76	59	5
Autumn 1956	2	3	0.71	0.74	36	75	63	19
21 Oct.—								
14 Dec.	5	7	0.71	0.76	28	75	60	14
36 forecasts	10	15	0.71	0.77	17	75	59	14
	15	22	0.71	0.78	6	75	58	11
	[1]15	22	0.764	0.765	39	66	64	39
Autumn 1956	2	3	0.68	0.71	38	81	67	19
12 Nov.—								
14 Dec.	5	7	0.68	0.73	29	81	63	10
21 forecasts	10	15	0.68	0.75	14	81	60	10
	15	22	0.68	0.75	10	81	60	0
	20	29	0.68	0.75	10	81	60	5
	30	44	0.68	0.75	10	81	60	5

[1] Three easternmost columns of grid points only (18 grid points), see figure 1.

Table 3

Summary of Results. 48 Hour Forecasts

	N	D	r_0	r_1	W_r	ε_0	ε_1	W_ε
Autumn 1955	2	3	0.61	0.62	36	151	140	21
29 Nov.—								
22 Dec.	5	8	0.61	0.62	43	151	146	29
14 forecasts[1]	10	16	0.61	0.64	29	151	133	14
Autumn 1956	2	3	0.60	0.63	36	132	114	21
22 Oct.—								
14 Dec.	5	8	0.60	0.63	40	132	112	12
33 forecasts[2]	10	15	0.60	0.64	33	132	112	15
	15	23	0.60	0.68	27	132	105	15
Autumn 1956	2	3	0.51	0.56	39	149	126	22
14 Nov.—								
14 Dec.	5	8	0.51	0.56	33	149	116	6
18 forecasts[2]	10	15	0.51	0.62	28	149	108	6
	15	23	0.51	0.62	28	149	115	6
	20	31	0.51	0.62	28	149	111	6
	30	46	0.51	0.62	22	149	111	6

[1] 48 grid points, westernmost column omitted, see figure 1.

[2] 42 grid points, two westernmost columns omitted, see figure 1.

Table 4

Summary of Results. 72 Hour Forecasts

	N	D	r_0	r_1	W_r	ε_0	ε_1	W_ε
Autumn 1956								
6 Nov.—	2	3	0.44	0.42	52	184	178	39
14 Dec.	5	9	0.44	0.39	43	184	174	43
23 forecasts[1]	10	17	0.44	0.43	35	184	162	26
	15	26	0.44	0.45	30	184	158	13
	20	35	0.44	0.45	30	184	157	9

[1] 42 grid points, two westernmost columns omitted.

in the additional series were not all on consecutive days and the symbol D denotes the average number of 24 hour periods included by N forecasts.

An examination of table 2 shows that the autumn and winter forecasts were significantly improved by the correction. Best results were obtained with D equal to ten or more but there appears to be no justification for using a D of more than 20.

The test on the spring data was not as conclusive as the other two. The root-mean-square errors were reduced about the same as in the other tests but the correlation coefficients between observed and forecast height changes were generally made worse by the correction.

One test was made using only the three easternmost columns of grid points (18 grid points in Europe and the Eastern North Atlantic). The result is marked by "1" in table 2. There was no significant change in either correlation coefficient or root-mean-square error. The average algebraic error in this region was generally between — 30 and + 40 meters. This seems to indicate that the correction has no value in regions where the absolute value of the mean error is less than about 40 meters. Also, one would expect that more improvement would have been shown in the other tests if these easternmost columns of grid points had been omitted.

Tests were made on two sets of 48 hour forecasts and one set of 72 hour forecasts with the results shown in tables 3—4. Improvement in the 48 hour forecasts was somewhat less than for 24 hour forecasts but still significant. The correction also gave an overall improve-

Table 5

Comparison of Different Methods of Correcting 48 Hour Forecast 29 Nov.—1 Dec. 1955

Method[1]	r_0	r_1	ε_0	ε_1
a	0.68	0.71	133	115
b	0.68	0.71	133	117

[1] a. Forecast corrected at end of 48 hour time step by subtracting mean error field for previous 10 48-hour forecasts.
b. Forecast corrected at ends of 24 and 48 hour time steps by subtracting mean error field for previous 15 24-hour forecasts. (This mean error field covers about the same time period as that used in method a.)

ment in the 72 hour forecasts; however, the improvement was smaller than for the other forecasts and a large proportion of individual forecasts were made worse.

One would expect that a better way to correct 48 and 72 hour forecasts would be to use a 24 hour forecast correction after the 24, 48, and 72 hour time steps. This procedure was used for one 48 hour forecast, the one for 29 November—1 December, 1955. The correction used was the mean error field for the previous fifteen 24 hour forecasts. The result is shown in table 5. There was very little difference in the results of the two methods of correction. This is particularly surprising in view of the large improvement the correction gave in the 24 hour forecast (see table 1, 29—30

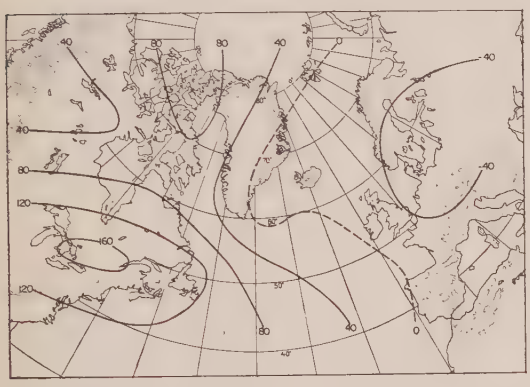

Fig. 2. $\Delta\Phi_A$, Average error field, 24 hour forecasts, (in whole meters) 14 November—29 November, 1955, 15 forecasts.

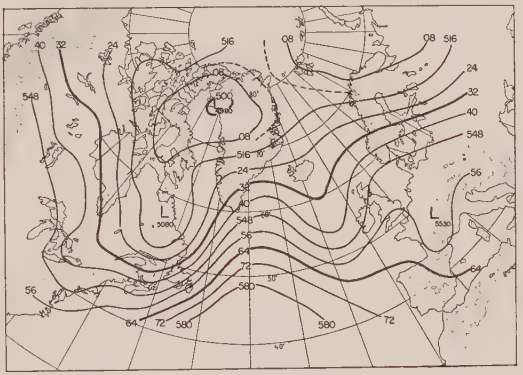

Fig. 4. 500 mb, 29 November, 1955, 1500 Z + 24 hr $r_0 = 0.73$, $\varepsilon_0 = 96$ meters.

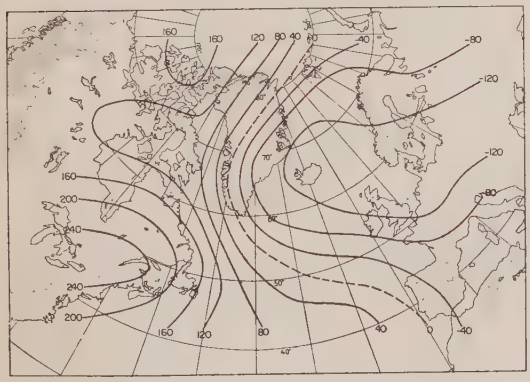

Fig. 3. $\Delta\Phi_A$, Average error field, 48 hour forecasts, (in whole meters) 14 November—30 November, 1955, 10 forecasts.

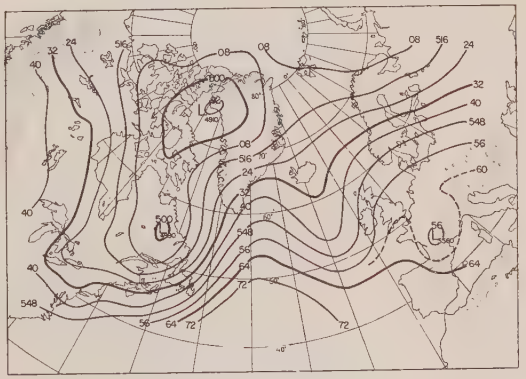

Fig. 5. 500 mb, 29 November, 1955, 1500 Z + 24 hr. $-\Delta\Phi_A \cdot N = D = 15 \cdot r_1 = 0.82$, $\varepsilon_1 = 69$ meters.

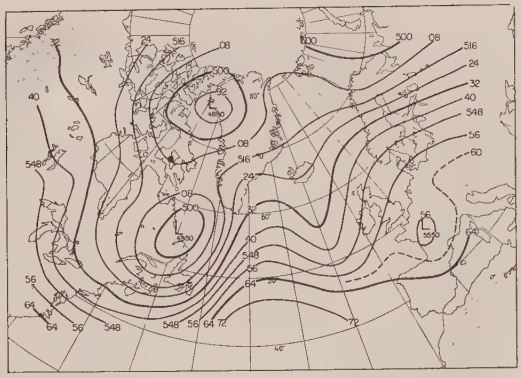

Fig. 6. 500 mb, 30 November, 1955, 1500 Z, Objective Analysis.

November, $N = 15$). The two error fields used as corrections are given in figures 2 and 3.

A check of any of the tables of results will show that some forecasts in nearly every test were made worse by the correction. Generally the decrease in accuracy was small but, if the correction is to be used in routine forecasting, it would be good to know when not to use it. Unfortunately, it has not been possible to find any criterion which will tell when or when not to use the correction. It can be shown that:

a. Bad forecasts are helped more than good forecasts,

b. The correlation coefficients between observed and forecast height changes tend to be largest when the root-mean-square height change is largest,

c. There are different flow patterns for good forecasts, bad forecasts, forecasts which are improved by the correction, and forecasts which are made worse by the correction.

However, these results are statistical only; there are too many exceptions for them to be used as rules.

A comparison of a corrected and an uncorrected forecast is given by figures 4 and 5. The corresponding objective analysis is given by figure 6. Probably the most noticeable difference is in the improved accuracy of height values in the corrected forecast. The corrected forecast also gives somewhat better wind directions in the Newfoundland area as well as better configuration of the trough near the British Isles.

3. Normal charts or time-averaged charts as corrections

A physical explanation for the persistence of errors in barotropic forecasts is suggested by several writers (Berson, 1953; Bolin, 1955; Clapp, 1953). The chief reason given is that barotropic forecasts do not take into account the effect of irregularities of the earth's surface. Clapp suggests that this effect may be allowed for in barotropic forecasts from mean charts by subtracting, at each time step, the change called for by a barotropic forecast from a normal chart.

In view of the slight difference between the final results obtained by applying a correction, in one case, every 24 hours, in another case at the end of the 48^h forecast, one might apply the correction suggested by Clapp at the end of the forecast period instead of at every time step. Thus, if $\Delta\Phi_F$ is a height change obtained by a barotropic forecast from a synoptic chart and $\Delta\Phi_N$ is the height change obtained by a forecast from a normal chart, we arrive at a corrected forecast of height change by using

$$\Delta\Phi_{FN} = \Delta\Phi_F - \Delta\Phi_N.$$

The above idea was tested on the series of 30 forecasts beginning 14 November, 1955. Further, since the baroclinic effect of the North American East Coast is largely due to thermal contrast between land and sea, an effect which can be expected to vary from year to year at a given season, it was considered advisable to compare forecasts from both the normal and mean charts for the period with the actual error field of the 24 hour barotropic forecasts. An additional test was to use each of these three fields to correct the synoptic forecasts and see which one gave the most improvement. Obviously, one would expect that subtracting the actual time averaged errors from the forecasts would give more improvement than the use of any other constant correction field.

Neither the normal chart nor the mean chart for the test period was available and it was necessary to prepare them before starting on the main problem. Since there is little difference between the normal charts for November and December, it was considered sufficiently accurate to average these two

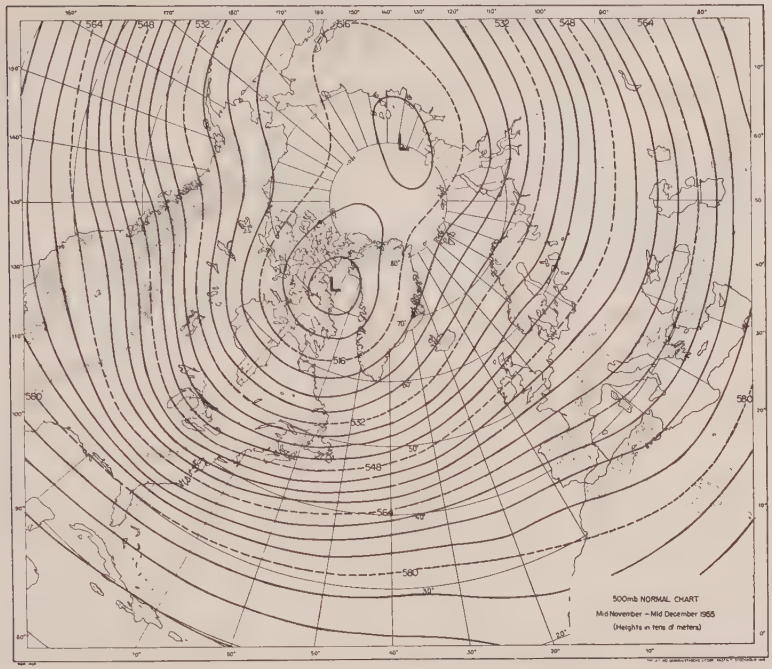

Fig. 7. 500 mb normal chart, November – December.

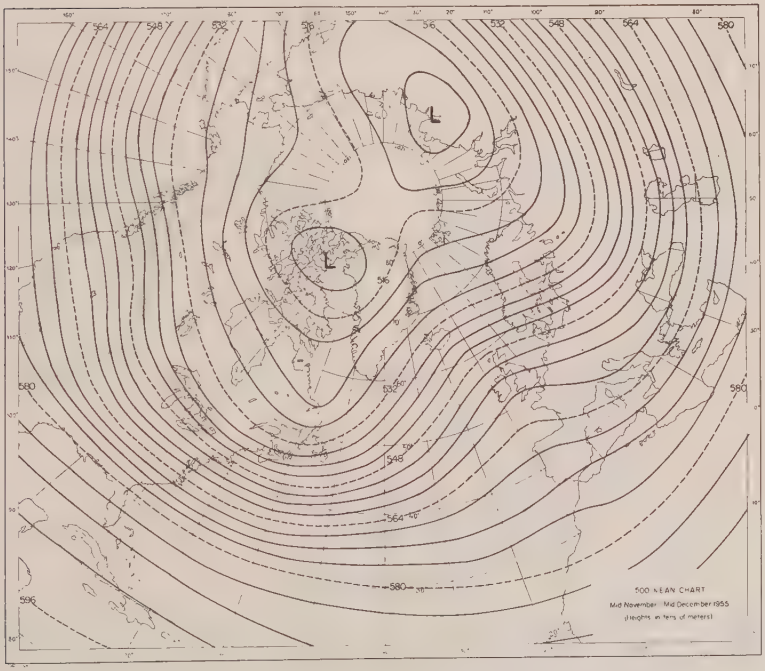

Fig. 8. 500 mb mean chart, mid November – mid December, 1955.

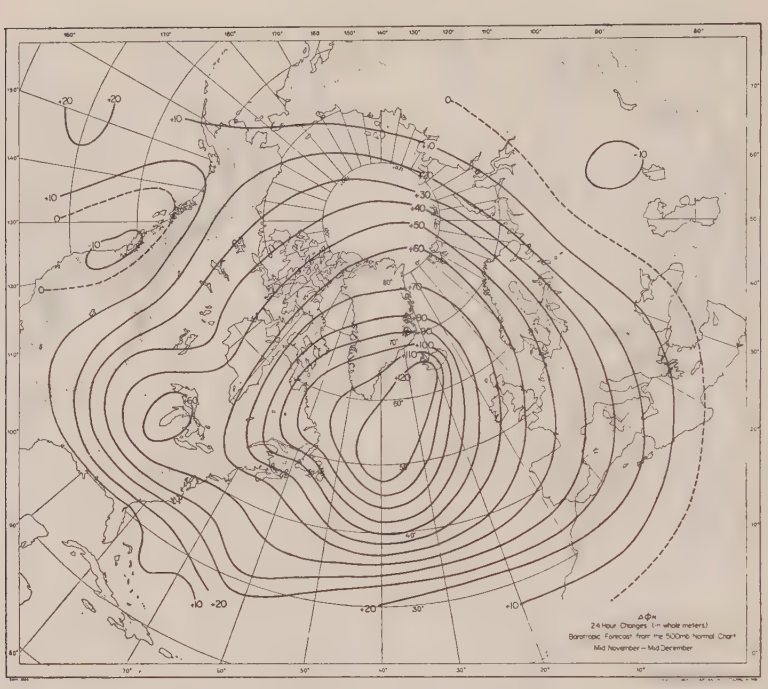

Fig. 9. 24 hour barotropic forecast from the normal chart ($\Delta\Phi_N$), November – December, 1955.

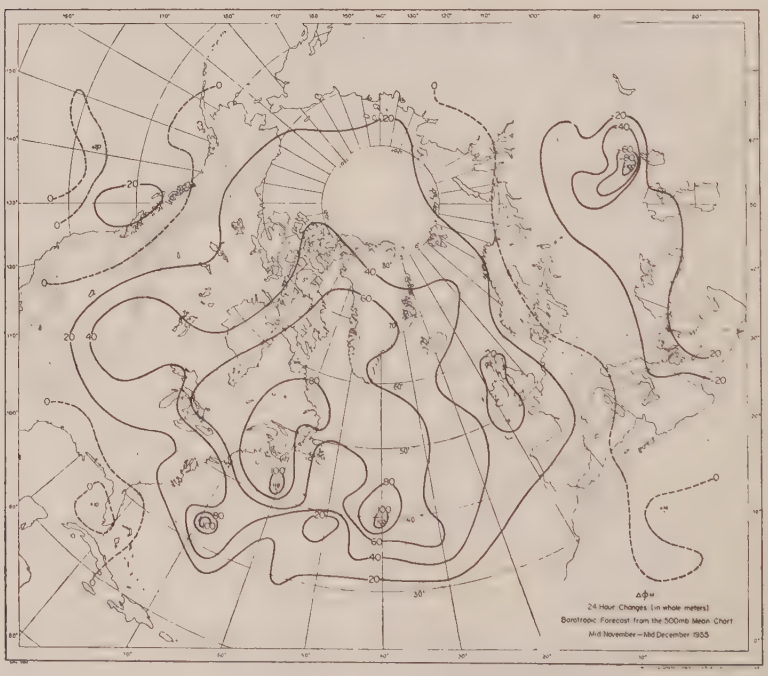

Fig. 10. 24 hour barotropic forecast from the mean chart ($\Delta\Phi_M$), mid November – mid December, 1955.

Table 6

Date	r_0	r_N	r_M	r_A
14—15 11/55.	0.69	0.67	0.72	0.82
15—16.....	60	63	64	78
16—17.....	35	34	42	62
17—18.....	69	67	75	87
18—19.....	62	54	57	70
19—20.....	65	61	66	74
20—21.....	54	51	57	70
21—22.....	79	81	83	89
22—23.....	67	66	66	80
23—24.....	64	63	66	76
24—25.....	45	50	56	74
25—26.....	63	69	74	86
26—27.....	58	71	77	82
27—28.....	66	75	70	64
28—29.....	79	74	81	90
29—30.....	73	79	83	85
30— 1.....	91	92	93	91
1— 2 12/55.	79	81	82	81
2— 3.....	73	77	79	75
3— 4.....	57	53	58	79
4— 5.....	42	39	51	75
5— 6.....	61	53	61	74
6— 7.....	68	65	68	74
7— 8.....	78	78	81	89
8— 9.....	51	55	55	67
9—10.....	83	83	86	81
10—11.....	62	67	71	75
11—12.....	62	60	62	64
12—13.....	63	59	57	47
13—14.....	53	60	57	48
Average.....	0.64	0.65	0.68	0.76

Results of correcting 24 hour forecasts by adding a constant correction field.

r_0 is the correlation coefficient between observed and forecast height changes.

r_N is the same as r_0 except that the forecast height changes were corrected by subtracting the forecast changes from a normal chart.

r_M is the same as r_N except that the correction was obtained from a mean chart.

r_A is the same as r_N except that the correction was the actual mean error field of the uncorrected forecasts.

charts. This was done using the tables in "Normal Weather Charts for the Northern Hemisphere". The resulting normal chart is shown in figure 7.

The 500 mb mean chart was obtained with sufficient accuracy by extrapolating from a United States Weather Bureau mean 700 mb chart for mid-November to mid-December, 1955 (figure 8).

Barotropic forecasts were made from both the normal and mean charts and the corresponding height change charts prepared, see figures 9 and 10. These two charts were compared with the mean error chart for the period (figure 1). These three charts at least show great similarity. All have a positive maximum of about 120 meters per 24 hours. The maximum for the forecast from the normal chart, $\Delta\Phi_N$, is in the area south of Greenland and northeast of Newfoundland. Maxima for the mean chart, $\Delta\Phi_M$, and the mean error chart, $\Delta\Phi_A$, are both in the area immediately south of Newfoundland. The correlation coefficient between $\Delta\Phi_M$ and $\Delta\Phi_A$ is 0.64, that between $\Delta\Phi_N$ and $\Delta\Phi_A$ is 0.28. Thus the forecast from the mean chart comes much nearer to explaining the actual errors than does the forecast from the normal chart.

The next step was to use the above height change fields and error field to correct the synoptic forecast height changes. This was done by obtaining at each grid point:

$$\Delta\Phi_{FN} = \Delta\Phi_F - \Delta\Phi_N$$
$$\Delta\Phi_{FM} = \Delta\Phi_F - \Delta\Phi_M$$
$$\Delta\Phi_{FA} = \Delta\Phi_F - \Delta\Phi_A$$

($\Delta\Phi_F$ is the barotropic forecast of height change from a synoptic chart.)

Correlation coefficients were then obtained between observed and forecast height changes with the results shown in table 6. It can be seen that the correction obtained from the normal chart did not affect the accuracy of the forecasts appreciably. The correction obtained from the mean chart consistently improved the forecasts; it gave lower correlation coefficients in only three cases as opposed to fifteen for the correction from the normal chart. However, the overall effect of the second correction was also small. The average algebraic error for the month, used as a correction, gave improvements which in some cases were spectacular; see 16—17 November, 24—25 November, and 4—5 December.

It was concluded from the above test that it is not worth while to try to use $\Delta\Phi_N$ or $\Delta\Phi_M$ to correct short range barotropic forecasts. However, the test indicated that the actual error field is relatively stable from day to day and that a correction like $\Delta\Phi_A$ might be

useful in routine forecasting. This test furnished the immediate basis for the tests discussed at the beginning of this paper. It should be noted that Berson used a similar method to correct forecast 5-day mean heights.

A comparison of $\Delta\Phi_M$ (and $\Delta\Phi_N$) values at the 12 and 24 hour time steps shows that the rate of height change is essentially linear. This probably accounts for the fact that no difference was observed in the results, previously mentioned of correcting a 48 hour forecast by two different methods (table 5).

Conclusions:

The close correspondence observed between forecast changes from a mean map and the average errors in 24 hour barotropic forecasts for the same period indicate that the baroclinic effect of irregularities of the earth's surface may be an important source of error in short range barotropic forecasts.

The test results presented here on correcting the barotropic forecast must be regarded as incomplete. More tests need to be made, for example, with spring and summer data, 48 and 72 hour data, and in correcting only those areas of the forecast where the mean error is usually large. However, it is suggested that such a simple empirical correction is a very practical means of securing an immediate improvement in the accuracy of barotropic forecasts. Although these tests were all made on forecasts using the geostrophic assumption, good results could also be expected from forecasts made by use of the balance equation.

Acknowledgements:

This project was begun as a joint effort with Major Lloyd W. Vanderman, United States Air Force, and was continued by myself after he was transferred to the Joint Numerical Weather Prediction Unit at Suitland, Maryland. Much of the work with normal, mean, and error charts was done by Major Vanderman.

Dr. Bert Bolin suggested the project and gave much helpful advice and encouragement. Mr. Aksel Wiin-Nielsen checked the manuscript and suggested a number of important changes. In addition, several members of the Institute of Meteorology and of the staff at BESK helped in the preparation of maps and tapes and in making computations; in particular, I should like to thank Mr. and Mrs. Axel Bring and Mrs. Heinz Kreis.

REFERENCES

Berson, F. A., 1953: A Quantitative Analysis of the Evolution of Large-Scale Flow with Regard to the Effect of Eddy Motion. Quarterly Journal of the Royal Meteorological Society, **79**, 340, pp. 210—223.

Bolin, B., 1955: Numerical Forecasting with the Barotropic Model. Tellus, **8**, 1, pp. 27—49.

Clapp, P. F., 1953: Application of Barotropic Tendency Equation to Medium-Range Forecasting. Tellus, **5**, 1, pp. 80—94.

Döös, B. R., 1956: Automation of 500 mb Forecasts through Successive Numerical Map Analyses. Tellus, **8**, 1, pp. 76—81.

Staff, Weather Bureau, U. S. Dept. of Commerce, 1952: Technical Paper no. 21, Normal Weather Charts for the Northern Hemisphere.

The Strong Index Change Period from January 1 to January 7, 1956

By FR. DEFANT and H. TABA, International Meteorological Institute in Stockholm

(Manuscript received April 14, 1957)

Abstract

In continuation of a recent paper (DEFANT, TABA, 1957) a seven days period (January 1—7, 1956) has been investigated on a hemispheric scale. During this period strong world wide changes in the circulation type occurred. Such a circulation change from a meridional into a zonal type* has been studied for the first time by means of hemispheric tropopause maps and by using a special technique of dividing the total available material of atmospheric sound ings into three different groups as described in the previous paper. The following points summarize the results:

1. The hemispheric tropopause maps are most suitable for obtaining a clear picture of three dimensional structure of the atmosphere. The distribution of cold and warm air masses can easily be seen. Breaks in tropopause heights give an immediate impression of the location and the form of the two principal westwind maxima of the westerlies (polarfront jet and subtropical jet). The concentrations in the temperature field of the tropopause level are a further guide for the location of the main wind belts. This temperature field makes it possible to picture the meandering structure of the wind belts and shows the interaction of tropical and mid-latitude circulation. Clear distinction has to be made between subtropical and polar jet.

2. By the use of this method strong northward displacements of the tropical atmosphere have been shown. At the same time a strong meandering behaviour of the subtropical jet appears. These tropical impulses play a dominating role in producing pronounced changes in mid-latitude circulation and for the generation of large blocking anticyclones.

3. During the seven days period the character of soundings in the three selected groups (north of the polar jet, between the two jets and south of the subtropical jet) remained nearly unchanged.

4. Whenever the tropical atmosphere shifted northward stations inside deep troughs having a polar isothermal structure in the stratosphere showed a strong cooling in the higher stratosphere and at the end of the period even the polar stations showed the same feature. It is thought that this cooling is mainly due to advection from the tropical regions, but outgoing radiation and vertical motion may contribute.

5. A possible cyclic change and three dimensional interaction of the three different parts of the atmosphere is outlined at the end of the paper.

Introduction

In a recent paper (DEFANT, TABA, 1957) an attempt was made by the authors to show an essential three-fold difference in the complete vertical structure of atmospheric soundings for January 1, 1956. This three-fold distinction in the structure was obtained as a result of a special selection of soundings with respect to the location of the main hemispheric west wind maxima of the westerlies (polar front jet and subtropical jet). South of the subtropical jet a typical temperature structure with a high tropopause (about 90 mbs) was observed. In the

* meridional and zonal with respect to the form of polarfront jet.

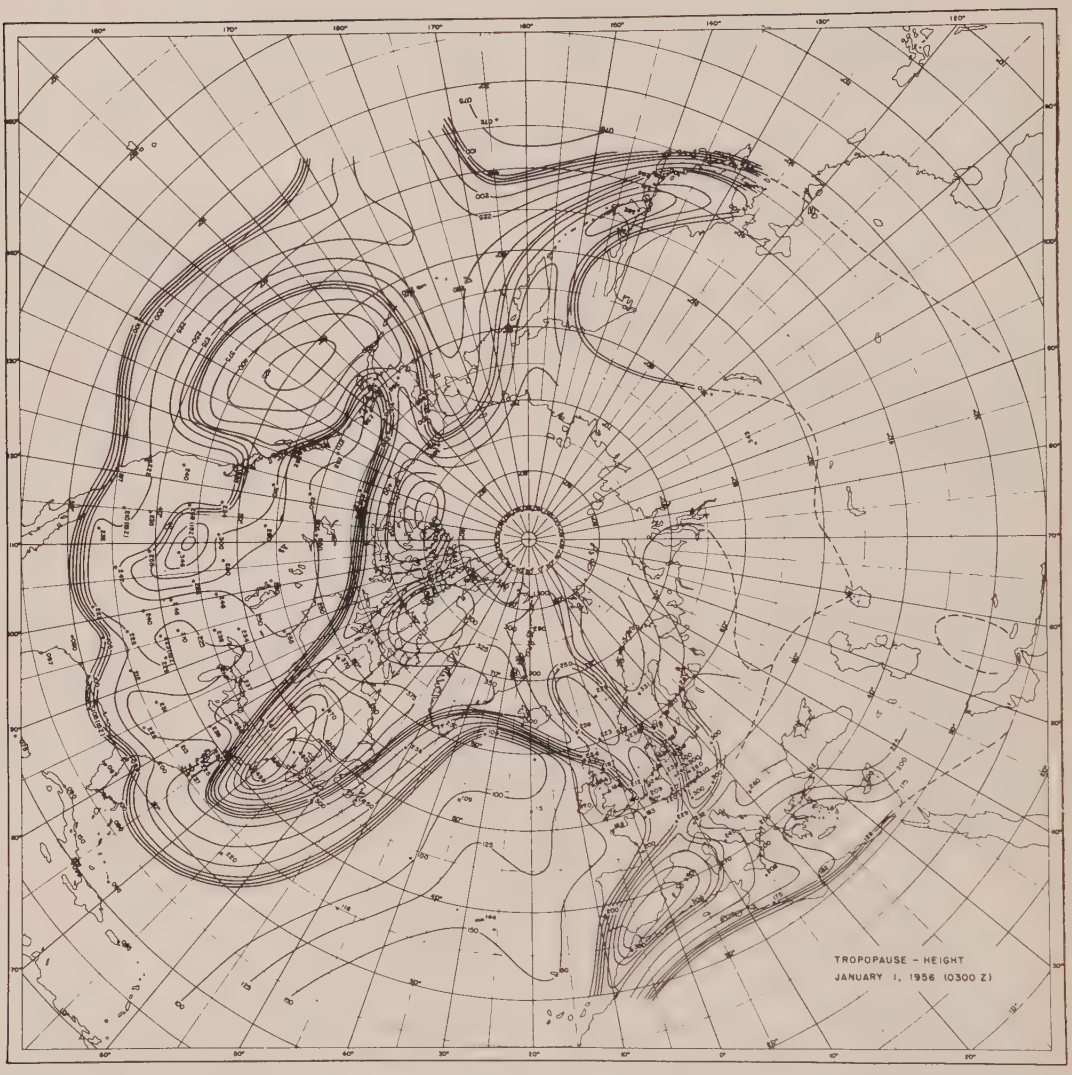

Fig. 1. Hemispheric tropopause map January 1, 1956 (0300 Z). For each station tropopause height in mb (3 figures) and tropopause temperature in °C (2 figures, minus sign omitted). In case of double tropopause levels both values are plotted. When the tropopause was not well defined no values are given. The breaklines in tropopause height are indicated by the concentration of the isolines.

area between the two jets the type of sounding was different, having a characteristic tropopause height near the 240 mb level. North of the polar front jet a third type of sounding could be distinguished by a rather low tropopause level (always lower than 300 mb, in rare cases even as low as 500 mb). It was further shown by presenting a hemispheric map of the tropopause height that the main west wind belts were closely related to the so called "breaklines" in the tropopause height which could be used as a guide in selecting stations of the different types mentioned above. Special discussion was devoted to soundings either close to the polar front or the subtropical jet. It was stated at the end of the paper, that an extension of this more or less formal discussion to a longer period (January 1 to January 7, 1956) was planned. It is the purpose of this paper to carry out such a study for this period, selected because strong changes in the world wide pattern of hemispheric circulation oc-

Fig. 2. Hemispheric tropopause map January 2, 1956 (0300 Z). For each station tropopause height im mb (3 figures) and tropopause temperature in °C (2 figures, minus sign omitted). In case of double tropopause levels both values are plotted. When the tropopause was not well defined no values are given. The breaklines in tropopause height are indicated by the concentration of the isolines.

curred and which offered certain advantages for studying their nature and the mechanism of such index changes.

For each day of this period (7 days) tropopause maps similar to those in our previous paper have been prepared and a similar grouping of soundings according to their location was made. For each day and each group of soundings mean values have been computed. The number of soundings in each area changes from day to day according to the fluctuation of the breaklines north and southward or according to the meandering of the two west wind belts. We have been well aware of the fact that for instance a southward movement of the polarfront jet over the continent with a denser coverage of soundings meant the inclusion of more soundings of the cold type. This did not effect the correctness of the averaging process as inside each part, the latitudinal change effects only the lower tropospheric layers and does not change appreciably

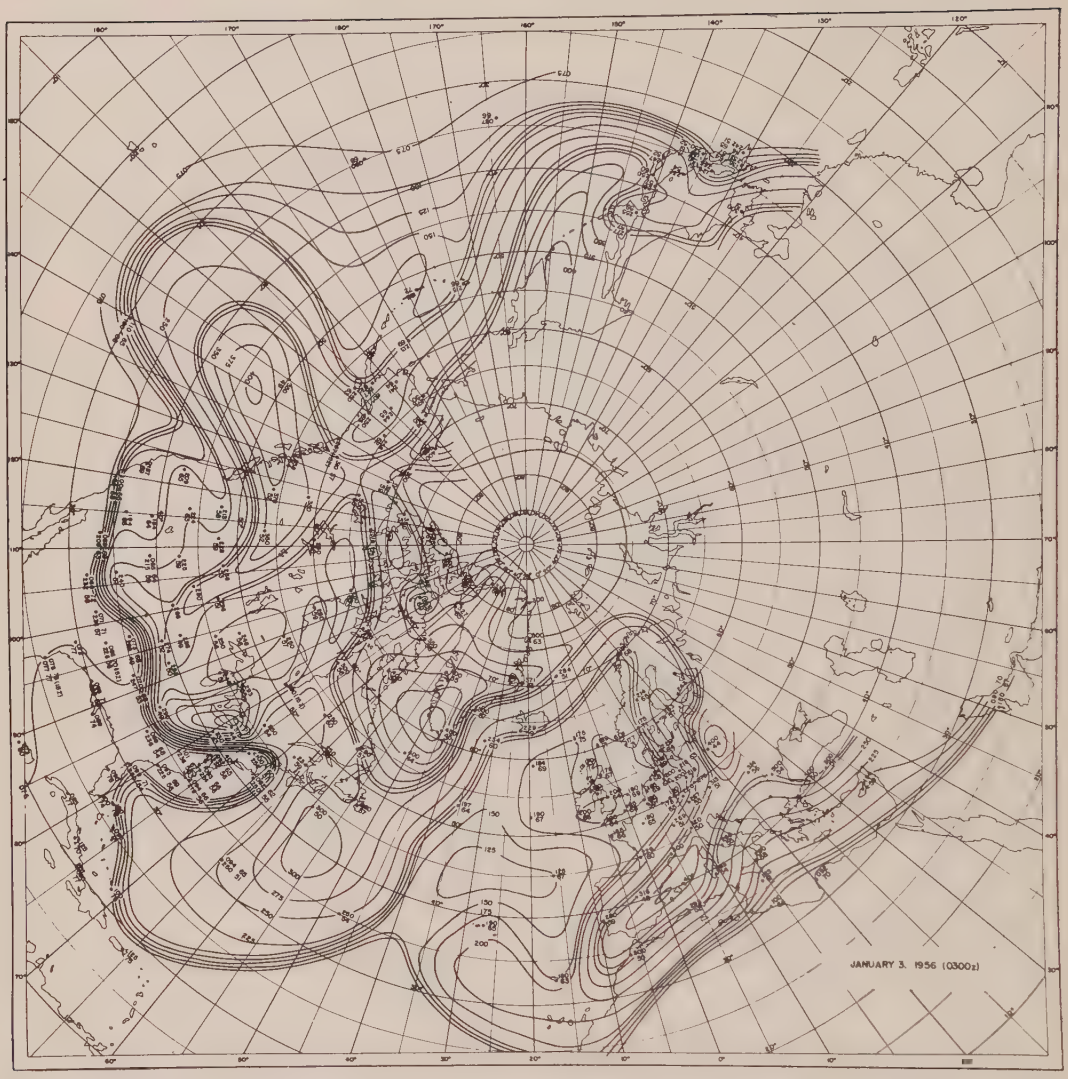

Fig. 3. Hemispheric tropopause map January 3, 1956 (0300 Z). For each station tropopause height in mb (3 figure) and tropopause temperature in °C (2 figures, minus sign omitted). In case of double tropopause levels both values are plotted. When the tropopause was not well defined no values are given. The breaklines in tropopause height are indicated by the concentration of the isolines.

the characteristic features in the upper troposphere, the height of the tropopause or the typical temperature distribution in the stratosphere.This is precisely the reason why such a selection is possible and just this feature characterises the different types in the total vertical structure of atmospheric soundings. In the lower tropospheric levels the vertical temperature distribution of the mean sounding for each separate day may differ somewhat from the means of other days. However, this change disappears completely when taking the mean for seven days, as the number of soundings in each area becomes great (about 250 in each area).

I. Tropopause maps for the period January 1 to January 7, 1956

Fig. 1 to 7 present a hemispheric analysis of the tropopause height for each day of the period January 1 to 7, 1956, 0300 Z. In all these analyses a rather marked distinction can

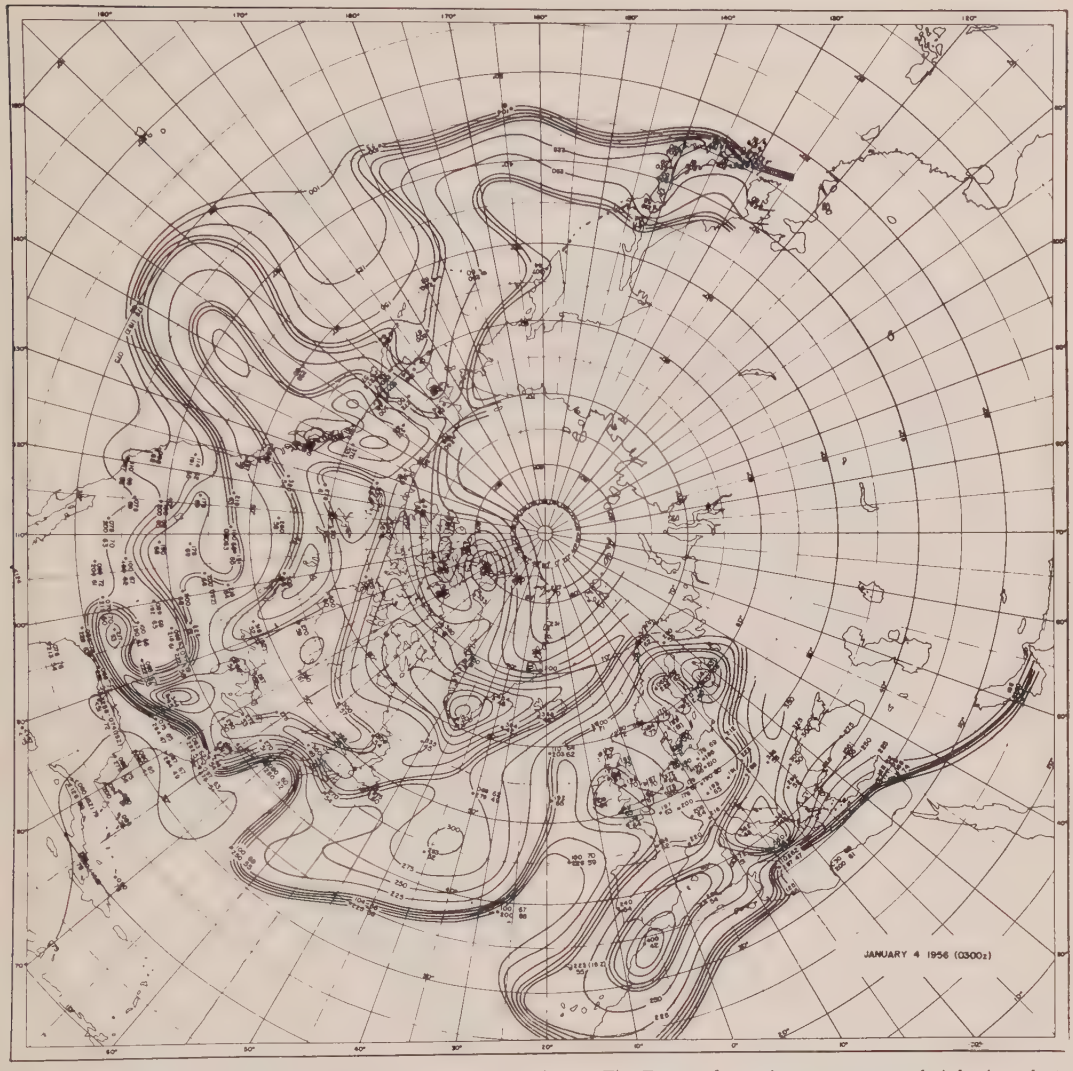

Fig. 4. Hemispheric tropopause map Januar 4, 1956 (0300 Z). For each station tropopause height in mb (3 figures) and tropopause temperature in °C (2 figures, minus sign omitted). In case of double tropopause levels both values are plotted. When the tropopause was not well defined no values are given. The breaklines in tropopause height are indicated by the concentration of the isolines.

be made between the tropopause breakline connected with the polar front jet and the one connected with the subtropical jet.

a) *Subtropical impulses in the Atlantic and European sector.*

We will first discuss the southern breakline. On January 1 (Fig. 1) this breakline situated near the latitude 30° N, shows a more zonal distribution in most parts of the northern hemisphere. This is true for the whole Pacific and the North American continent as well as North Africa. But over the North Atlantic it is displaced northward and crosses even the 60° parallel in the region south of Iceland. From there on it can be followed across England and France and down to the western part of North Africa. There seems to be no possibility of placing this breakline over the North Atlantic along 30° N. This rather surprising fact that the subtropical jet meanders so far

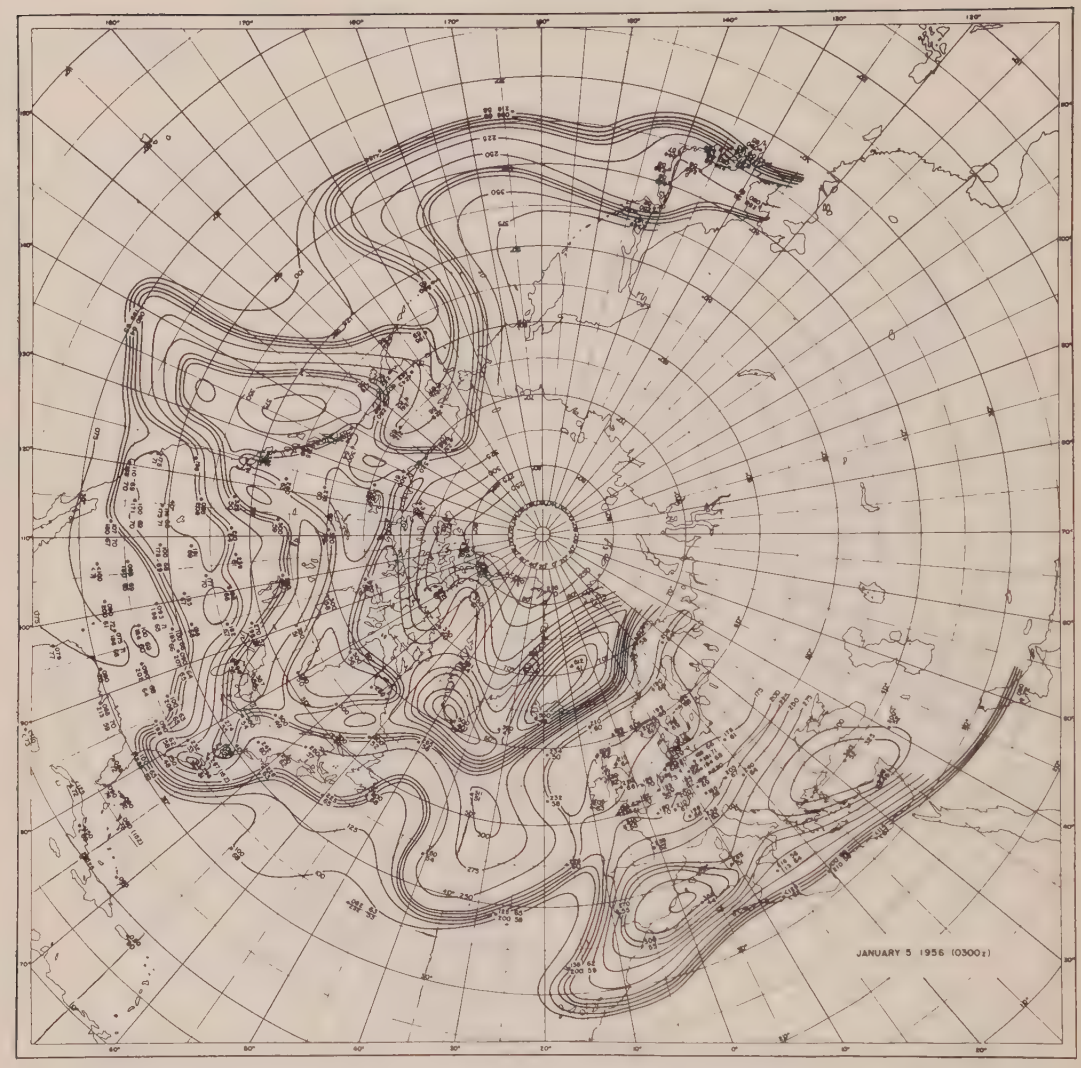

Fig. 5. Hemispheric tropopause map January 5, 1956 (0300 Z). For each station tropopause height in mb (3 figure) and tropopause temperature in °C (2 figures, minus sign omitted). In case of double tropopause levels both values are plotted. When the tropopause was not well defined no values are given. The breaklines in tropopause height are indicated by the concentration of the isolines.

to the north has not been mentioned to our knowledge in literature before. In a later paper (DEFANT, TABA, 1957) we shall present a definite proof that in this case a double jet exists over the British Isles and a sharp distinction must be made between the polarfront jet and the subtropical one. The northern breakline connected with the polarfront jet is well separated from the one discussed before.

Strong trough formation can be seen over the American East Coast. On its eastern side the two breaklines come closer together and in the region of Southern Greenland and Iceland no clear distinction between them can be made.

The surface cyclone situated just to the east of Iceland, on January 1 developed rather rapidly and an outflow of cold polar air occurred during the following night. It is worthwhile to mention that the approach of the two breaklines of the tropopause height seems to be closely related to this rapid out-

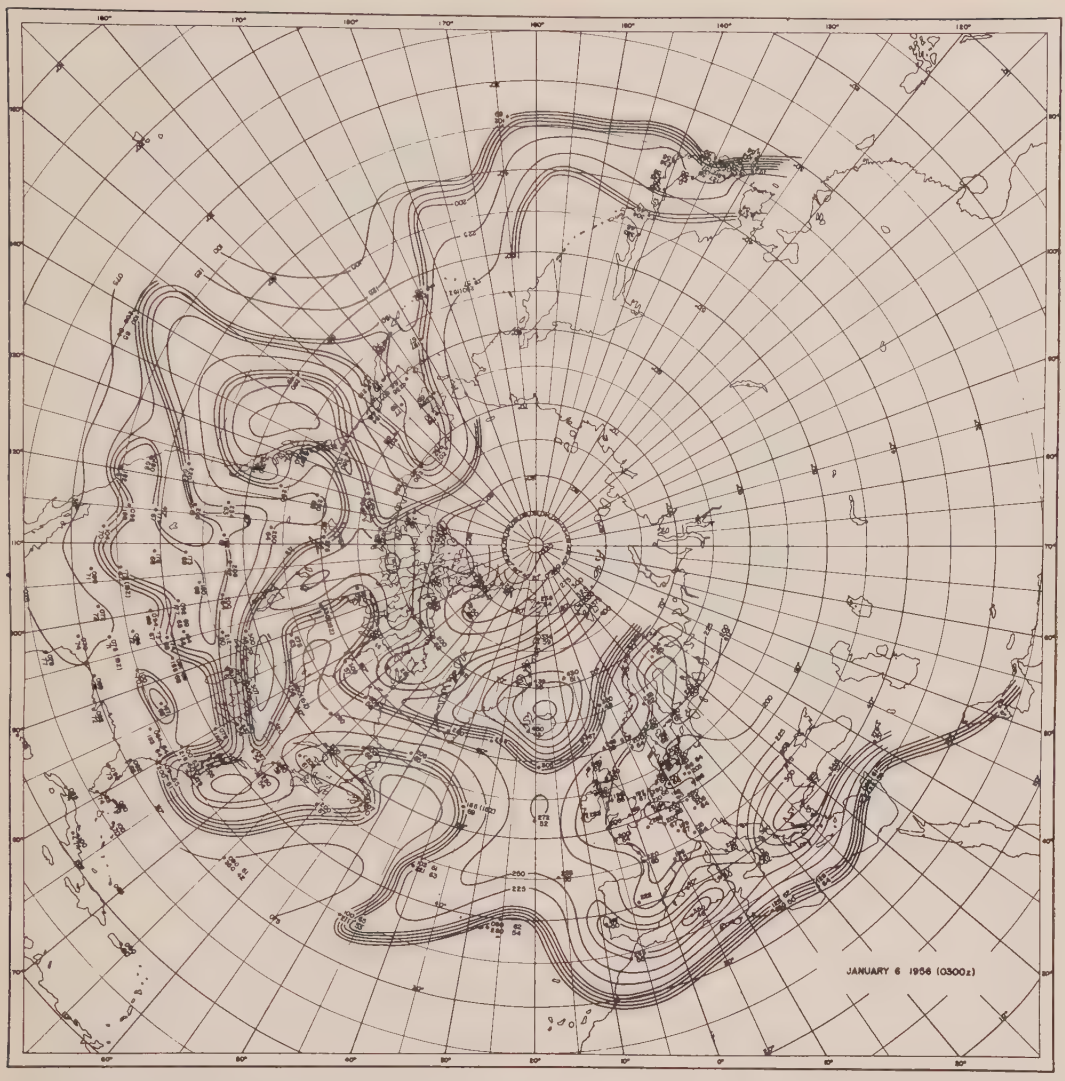

Fig. 6. Hemispheric tropopause map January 6, 1956 (0300 Z). For each station tropopause height in mb (3 figures) and tropopause temperature in °C (2 figures, minus sign omitted). In case of double tropopause levels both values are plotted. When the tropopause was not well defined no values are given. The breaklines in tropopause height are indicated by the concentration of the isolines.

break of polar air directed towards Central Europe.

The tropopause map of January 2 (Fig. 2) shows over Central Europe an area of low tropopause height connected with this cold outbreak of polar air. The more interesting feature is that the southern breakline still continued its movement towards the northeast and even approached Southern Scandinavia. The strong trough formation over the East Coast of North America is still present, but especially over its southern part the height of the tropopause rises.

On January 3 (Fig. 3) the development over Europe continues and it can be seen that this subtropical intrusion covered all of Western and Northern Europe. A branch of the subtropical jet surrounds this large area, inside of which the soundings have typical subtropical temperature structure. The tropopause is everywhere above the 200 mb level (mostly near 175 mb) with a tropopause temperature

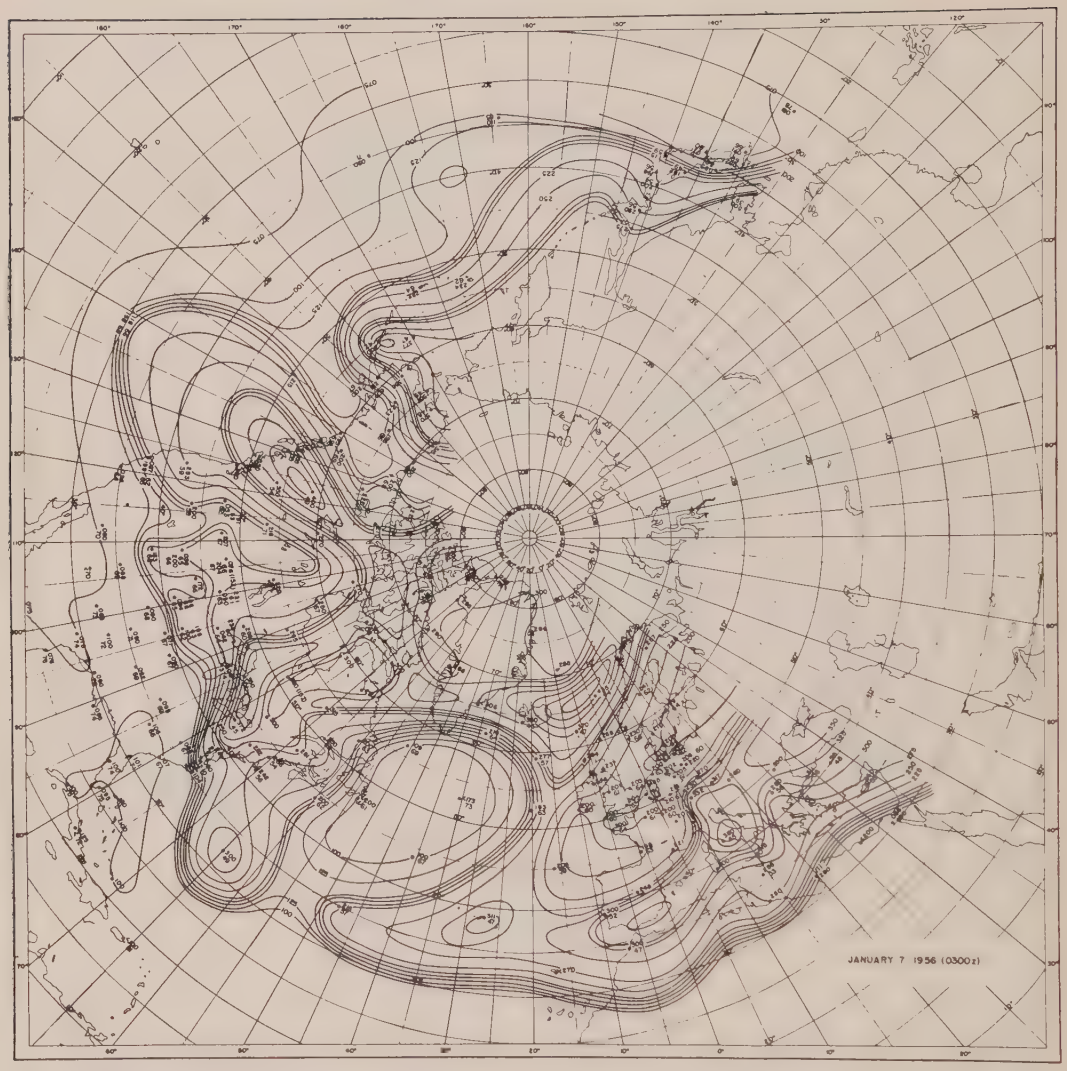

Fig. 7. Hemispheric tropopause map January 7, 1956 (0300 Z). For each station tropopause height in mb (3 figures) and tropopause temperature in °C (2 figures, minus sign omitted). In case of double tropopause levels both values are plotted. When the tropopause was not well defined no values are given. The breaklines in tropopause height are indicated by the concentration of the isolines.

between — 65 and — 72° C. This northward progression of a large part of the subtropical atmosphere over the Atlantic causes an extremely strong pressure rise at the surface and a formation of the well known blocking anticyclone takes place. One would expect that the advection of subtropical warm air should cause a pressure fall but as in the higher tropospheric layers and in the lower stratosphere extremely cold air is advected northward, a strong pressure rise at the surface is created. It is a well known rule in synoptic meteorology (ERTEL, 1930), (ERTEL, SJAN-ZSI-LI, 1935), (HAURWITZ, 1927), (ROSSBY, 1928), (SCHEDLER, 1917), (STEINER, 1926), (THOMAS, 1935), that advection of warm air in the lower troposphere in combination with strong pressure rise at the surface always tends towards the establishment of very persistent anticyclonic conditions. The over-compensating effect of cold

advection in the very high troposphere and lower stratosphere was studied several years ago by H. THOMAS (1935).

We may further observe that after a separate high pressure cell has formed in northern latitudes the subtropical jet forms again along latitude 30° N. The trough over the Western Atlantic Ocean has weakened considerably and the northern tropopause breakline connected with the polarfront jet and the polar front appears in rather northerly latitudes over Southern Greenland and Northeastern Canada.

In the area north of Florida one can observe the start of a development similar to that just described. The subtropical breakline in that region shifts northward again and on January 4 (Fig. 4) it becomes quite obvious that a second intrusion from the subtropical region takes place which builds up more and more east of the American East Coast (Fig. 5, Fig. 6, and Fig. 7 on the 5th, 6th, and 7th). By this process the development of a second large anticyclonic block was expected on January 7 west of Newfoundland surrounded in the higher tropospheric layers by a branch of the subtropical jet. It is of the same type as that over Europe which extended in the meantime its influence far into the North Asiatic continent. This cannot be seen from the tropopause maps presented here as no data are available in Asia but the lower level charts point in this direction.

From the 4th to the 7th the rather high tropopause over Europe (considerably higher than 200 mb) remains unchanged. The subtropical structure of the soundings inside this first subtropical intrusion was conserved during four days and did not alter appreciably. In spite of the northward movement from 30° N to Central and Northern Europe and the four days time taken, the soundings in Central and Northern Europe do not indicate a temperature structure characteristic of soundings taken between the two breaklines (with a tropopause height around 240 mb). Therefore no doubt remains to which category they belong. This characteristic temperature persistence inside such a blocking anticyclone is well known.

b) *Subtropical impulses over Southern America and Pacific.*

Thus far only developments over the Atlantic and European sector of the maps have been discussed. We now proceed to explain the features of atmospheric developments in the North American sector and the Pacific. On January 1 the two tropopause breaklines in this part of the world are well separated. The polar line is located at rather high latitudes. Over the Japanese Islands, south of Alaska, over the Southern Rocky mountains and along the American East Coast trough formations can be noticed with low tropopause heights. This separation of the two breaklines continues on January 2. On the 3rd the subtropical jet starts to move northward over Southern California, similar to its behaviour over the Atlantic and European sectors. On January 3 and 4 the two breaklines of tropopause height come close together and a cold outbreak takes place over the Northern Rockies. This progresses rapidly southeastward towards Florida. The source region for this cold outbreak was the cold air mass south of Alaska. This outbreak of polar air was followed by a second one on the January 5 and 6 which even entered the Southern Atlantic Ocean. This can be seen from the tropopause maps of January 6 and 7 by a tongue of low tropopause height extending from Canada in south-easterly direction to the Atlantic area between Florida and Bermuda. This cold outbreak, directed towards the southwestern part of the Atlantic, has a close connection with the second subtropical impulse northward in the western Atlantic area described before. It suggests that such an outbreak of cold air directed from the continent across the American East Coast, moving out over the rather warm Gulf stream part of the Atlantic, may contribute to a northward displacement of the subtropical system farther to the east. Although this may not be the only cause of the development at the northern border of the tropical circulation cell (at about latitude 30° N), but it may favour its formation. Over Southern California a second impulse follows the first one on January 6 and advances very far northward towards Central Canada by January 7. Each of these intrusions caused cyclogenesis followed by outbreaks of polar cold air. A similar development can be noticed in the middle of the Pacific Ocean. Here the subtropical system even approached Alaska on the 5th and tropopause heights higher than

200 mb can be noticed over Alaska on January 6 and 7.

c) *Summary of the above discussion.*

In summarizing the above discussion of large scale atmospheric developments which become very noticeable in the changes of the tropopause height, resp. in the latitudinal changes of the analysed tropopause breaklines, one may state that during the period January 1 to 7 the subtropical part of the atmosphere has been active. This was in the sense that the subtropical breakline of tropopause height in many parts of the earth shifted northward and part of the subtropical atmosphere seems to be displaced to rather northern latitudes. In the higher troposphere a deep inflow of extremely cold air occurs on top of rather warm air. By overcompensation large anticyclones are generated (blocking highs) over Europe and Northern Asia, over the Western North Atlantic, over the whole USA and Alaska. These large areas contain subtropical warm air and the structure of the soundings inside these intrusions was found to be typical for the subtropical group. They all possess a tropopause unusually high for these latitudes. The temperature at the tropopause is always between — 65° and — 72° C which are typical temperatures of the subtropical tropopause for stations south of 30° N. The northward shift of large parts of the subtropical atmosphere starts from preferred regions (mostly southwestern parts of oceans). However, this is not true in all cases. Such a development goes parallel with a strong meandering behaviour of the subtropical jet. The subtropical jet surrounds these large anticyclonic eddies. Finally a complete separation from the source region may be observed. The subtropical jet then forms again along latitude 30° N.

II. The principal distinction between meridional and zonal circulation type[1] at different levels

Fig. 8 presents in a schematic way the fundamental difference in atmospheric circulation patterns at the beginning (January 1) and the end (January 7) for surface, 500 and 200 mb. On the surface map of January 1 tracks of cyclones (cyclone families) are oriented in a more meridional direction separated by individual high pressure cells. No continuous subtropical high pressure belt exists. In 500 mb a meandering polar front jet with a number of long waves separates the polar air inside the jet (northern side) from the warmer air on its southern side. In this warm air the temperature increases gradually towards south. South of about 30° N we only observe 500 mb temperatures characteristic for real subtropical air. A clear distinction between the two types of warm air mentioned before is rather difficult at this level. However, in studying the complete vertical structure of the soundings and the height difference of the tropopause this difference will stand out clearly. Evidently the phenomenon of the subtropical jet is not visible at this level. It was already pointed out clearly by PALMÉN and BRADBURY (1953), when discussing the features of 500 mb analysis, that in addition to the temperature concentration of the polar front another but very much weaker temperature concentration could be noticed farther south. This is due to the difference between the middle and subtropical group of soundings discussed before and is closely related to the existence of a continuous hemispheric west wind belt in higher elevations (the subtropical jet). For the sake of clearness one should point out that the 500 mb analysis deals therefore only with the polarfront jet and the strong tropospheric temperature concentration related to the polar front. When the subtropical jet near the 200 mb level is well developed, one might observe some indications of high wind velocities at 500 mb which are in magnitude comparable with those of the polar front jet, but are widely different in latitude. One should be rather careful not to speak about a double polar front jet in these

[1]) Meridional and zonal with respect to a more meridional and zonal form of the polar front jet stream.

Fig. 8. *Principal differences in surface, 500 and 200 mb charts.* Upper pictures: Jan. 1, 1956; surface, 500 and 200 mb. *Meridional circulation type* (meridional type of polarfront jetstream, see 500 mb) (approximately zonal subtropical jetstream with exception of Atlantic Ocean, see 200 mb). Lower pictures: Jan. 7, 1956; surface, 500 and 200 mb. *Zonal circulation type* (zonal type of polarfront jetstream, see 500 mb; note its rather northern position, with exception of more permanent trough over Eastern Asia;) see 500 mb) (rather strongly meandering subtropical jetstream; see 200 mb).

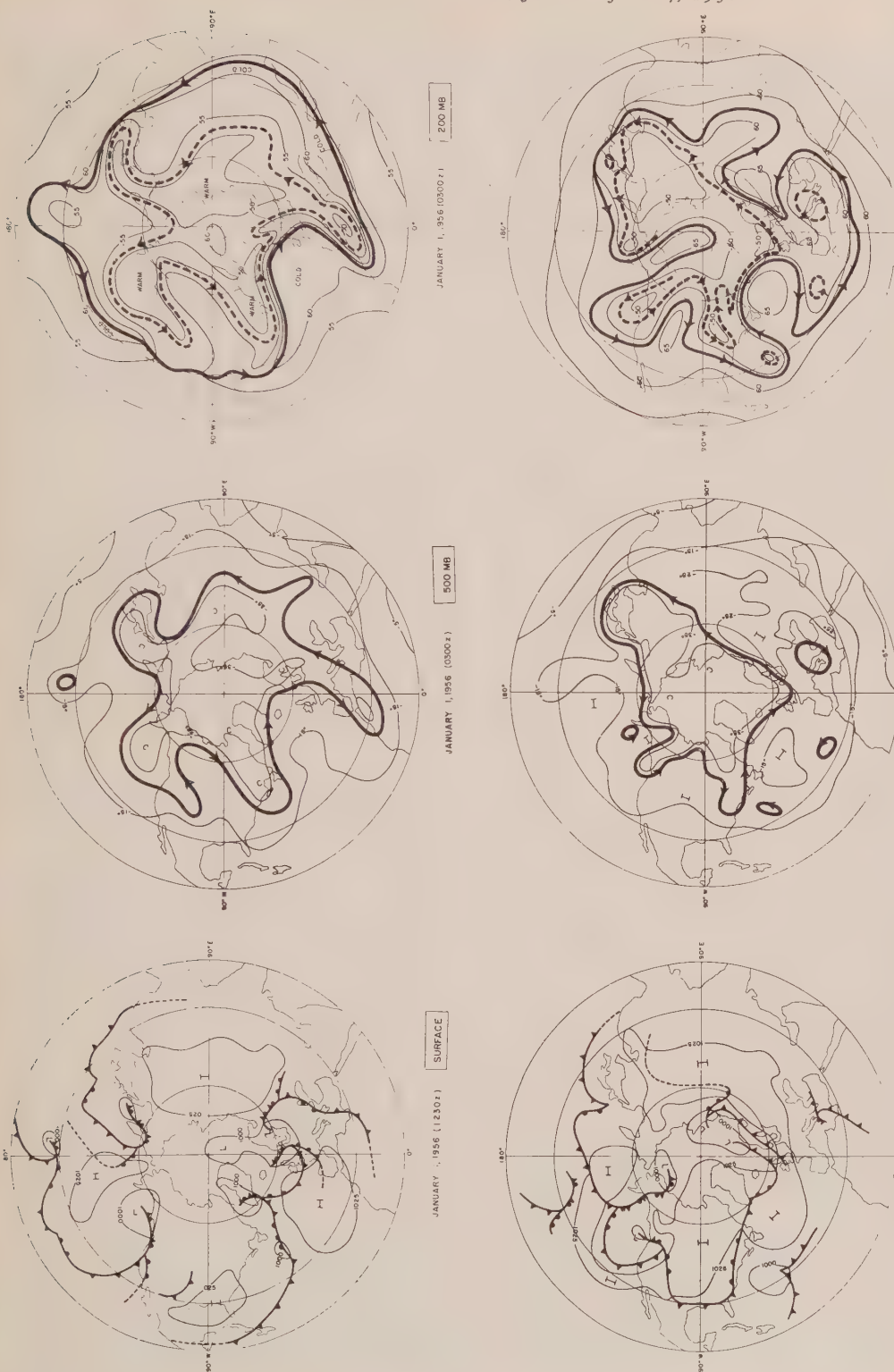
JANUARY 1, 1956 (0300 Z)
200 MB
JANUARY 7, 1956 (0300 Z)
200 MB
JANUARY 1, 1956 (0300 Z)
500 MB
JANUARY 7, 1956 (0300 Z)
500 MB
JANUARY 1, 1956 (1230 Z)
SURFACE
JANUARY 7, 1956 (1230 Z)
SURFACE

occasions (ALAKA ET AL., 1953). The analysis of moving jet maxima and minima along the jet axis on one and the same isobaric surface is quite erroneous due to the fact that the jets do not follow isobaric surfaces. Such deviations may be relatively smaller at 500 mb, but at 200 mb where the wind speed decreases sometimes rather rapidly with height when entering the stratosphere, winds at that level may widely differ in speed from one region of the map to the next although the jet may still be present very close to this level (ALAKA ET AL., 1953).

At the 200 mb level inside the area surrounded by the upper part of polar front jet relatively warm stratospheric air is present. The subtropical jet on January 1, with the exception of the Atlantic area, appears near latitude circle 30° N. In most of the northern hemisphere its location is widely different in latitude from the polar jet. In the belt between the two jets the temperatures belong also to the stratosphere. But south of the subtropical jet they belong to the high subtropical troposphere. Here mostly very low temperatures are present in a band, where the tropopause intersects the 200 mb level (ALAKA ET AL., 1953). A strong temperature gradient appears to the north of the subtropical jet. This different vertical structure in surface, 500 mb and 200 mb, characterises the meridional type of circulation on January 1. The 300 mb analysis is the most difficult one with respect to the separation of the two jets. The polar front jet is strongest close to that level but also high wind speeds appear at 300 mb below the subtropical jet. A further difficulty is the weak temperature gradient in meridional direction.

Contrary to this state the zonal circulation of January 7 has quite another character. At the surface a more or less continuous high pressure belt is present quite north of latitude 30° N. The main polar front appears in the very northern latitudes. One should not mix up weak frontal systems connected with low pressure centres south of the main high pressure belt with the main polar front. These are minor frontal systems. At 500 mb a rather concentrated circulation appears and the polar front jet is present in very northern latitudes, specially over the Atlantic, Northern Europe and Northern Asia. One can observe strong anticyclonic cells over the Northern Atlantic, over Asia and in the Mid-Pacific as well as over the Southern United States. Inside these anticyclonic cells the temperature is usually high which indicates strongly that they belong principally to subtropical air. No subtropical jet phenomenon can be seen on January 7 in 500 mb, but in 200 mb the subtropical jet meanders extremely far to the north in many parts of the earth. Therefore the vertical temperature structure of such a subtropical intrusion is so that above the centers of the high pressure belt in the surface, rather warm anticyclonic cells are present at 500 mb. However, in the upper troposphere and lower stratosphere a deep cold layer near to the high tropopause exists. One gets the impression that the polar jet in principle has a zonal form and the subtropical jet meanders strongly. The large area between the two jets, present on January 1, has diminished, and in special regions of the map in very northern latitudes, polar front- and subtropical jet nearly superimpose each other.

The six schematic pictures of Fig. 8 contain therefore the essential differences between meridional and zonal circulation, with respect to the behaviour of the main west wind belts and with respect to the temperature field in different altitudes.

III. Interpretation of vertical temperature field and their means during the whole period January 1—7, 1956

The computation described in the previous paper (DEFANT, TABA, 1957) was carried out for the seven days period along the same lines. Stations were again selected according to their location with respect to the tropopause breaklines. For each day the mean vertical temperature for each of the three groups (polar, middle and subtropical group) has been computed. Fig. 9 shows the mean soundings for each group and for each separate day. The mean soundings in each group look rather similar. Only minor changes are present within each group. Therefore it is quite justified to state that the atmosphere in this seven days period can be divided in three typical parts each of which having a characteristic vertical temperature distribution in the upper troposphere and in the stratosphere, as well as a rather different tropopause height. We may clearly state that each of these means

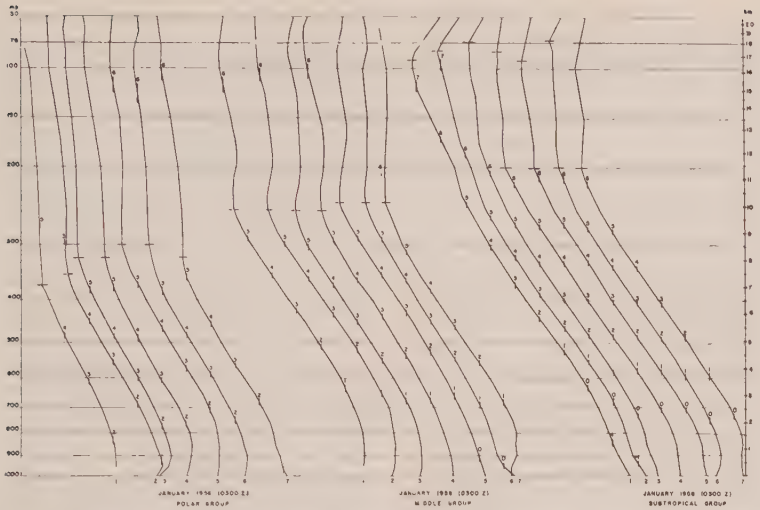

Fig. 9. Mean vertical temperature distribution for each day of the period January 1 to January 7, 1956 (0300 Z) and for the three different groups (polar, middle and subtropical group). The — 10, — 20, — 30° C a.s.o. are indicated by 1, 2, 3 etc.).

is made out of soundings distributed in widely different latitudes. It is therefore not the latitudinal location which characterises the type of sounding, but its position with respect to the main west wind belts. In looking at the temperature distribution in the upper troposphere in each of the three groups one can notice that the heights in which f.i. — 20°, — 30°, — 40°, — 50° C appear are almost constant during the whole period. So the temperature structure of the upper troposphere is almost conserved *in each group* with time, but it changes markedly from group to group. The temperature discontinuity in the troposphere between the polar and the middle group is more pronounced than that between the middle and subtropical group. The height of the tropopause seems to be the best indication to distinguish one type from the other. In the polar group the mean tropopause height remains between 300 and 370 mb. In this group the tropopause of each individual sounding is rather changeable, within the range 300—500 mb, but mostly between 300 and 400 mb. In the middle group the mean tropopause keeps almost a constant height (240—250 mb). Under no condition can these tropopause heights be mixed up with those of the polar group. The third group shows the very high subtropical tropopause (little above the 100 mb level). Only in the last four days there is a tendency for formation of a lower tropopause level at about 200 mb. This is due to the fact that all the soundings inside the strong latitudinal displacements of the subtropical atmosphere described above have been included in the subtropical group for making the mean. They really belong to this group. This, however, does not alter principle features of the subtropical group. If one would only select soundings south of 30° N and exclude those inside the subtropical northward displacements, one would certainly obtain means which would have the same vertical construction as the means for January 1, 2 and 3.

On January 1 three different areas with a markedly different character represented by the three means are present and therefore the polarfront jet and subtropical jet are far apart in most of the northern hemisphere, as was shown in Fig. 8. But on January 1 the approach of the two jets in most parts of the map has caused the middle part to disappear so that the temperature structure of polar mean has come side by side with the subtropical mean. The mean of the middle group on January 7 consists of very few soundings and its temperature structure is very similar to that of the subtropical group although there is no difficulty in identifying it.

The layers lower than 750 mb in all different groups are greatly affected in the individual soundings by different kinds of influences, so

that the means show a rather weak temperature decrease with height, isothermal conditions or slight inversion. They should not be looked upon as representative means. After all in this study we are not very much interested in the behaviour of these layers. Therefore the above discussion refers to the levels from 700 mb upwards.

There is still another interesting feature to be seen in Fig. 9. Looking at the polar means one can observe in the higher stratospheric layers deviations from a purely isothermal temperature distribution. On January 1 the temperature remains constant with height from the tropopause level up to about 175 mb. Going further up, a slight temperature decrease with height occurs which becomes stronger in the very high levels (above 100 mb). It seems that these high stratospheric deviations from an isothermal structure become stronger and stronger in time. On January 7 only a very shallow layer with constant temperature may be seen immediately above the polar tropopause and from there on a pronounced decrease of temperature continues upward. Therefore the upper stratosphere is cooled in very high altitudes at first and later on the lower stratospheric layers seem to be affected. It is remarkable that in these higher layers negative deviations of 10° to 12° C from the isothermal structure can be seen in the mean soundings. In the individual soundings this influence in the high stratospheric polar layers can amount to as much as 15 to 20° C. The magnitude of these temperature deviations suggests that they are not only due to outgoing radiation and this factor cannot be the sole reason although it might contribute. Furthermore cooling due to upward motion can hardly be the cause as pronounced vertical motions in these layers are unlikely to exist. Therefore it is justifiable to attribute this stratospheric cooling which becomes stronger and stronger during the time interval in question mainly to an advective inflow of cold air from the subtropical regions. This idea is supported by the fact that not only soundings situated in the very high latitudes show this kind of high level stratospheric cooling, but also soundings inside deep troughs situated over more southern latitudes. They also show this phenomenon whenever the subtropical system shifts northward and the trough is approached by the subtropical jet. This subject will be referred to in section IV.

The middle group shows in almost all soundings a similar further temperature decrease with height in the higher stratospheric layers. Only on rare occasions (strong northward shifting of the subtropical system) are the polar soundings affected. This points again in the direction that this upper cooling is mainly due to horizontal advection from southern latitudes.

For each of the three groups a total mean sounding for all the seven days has been computed. These means are shown in Fig. 10. Each of these means is made out of approximately 250 soundings. The three-fold difference is again very obvious. In the troposphere a strong baroclinicity can be seen between polar and middle group which amounts to about

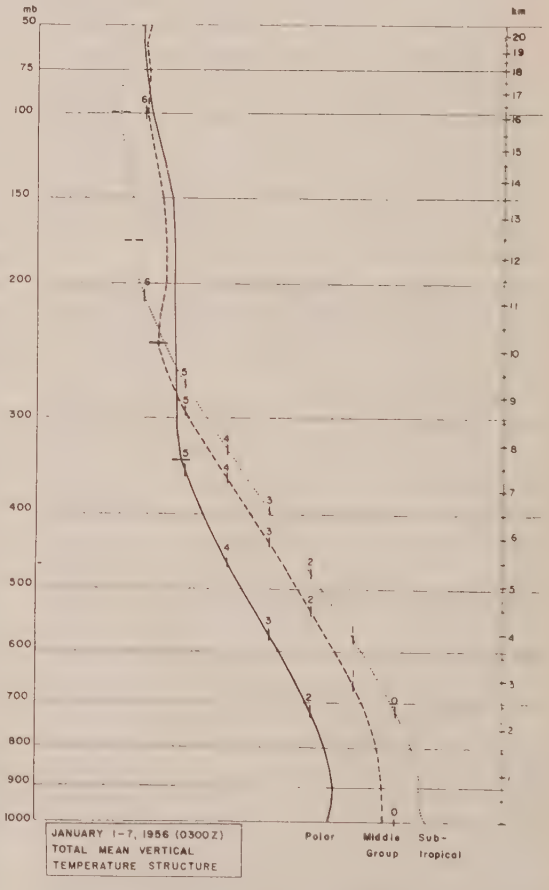

Fig. 10. The total mean vertical temperature distribution for the period January 1 to January 7, 1956 and for each different group (polar, middle and subtropical).

12° C between 700 and 400 mb. It is strongest near 500 mb (14° C). It becomes less between 400 and 280 mb and at 280 mb no meridional temperature difference is present. One could already see from Fig. 9 that inside each of both groups (polar and middle) the vertical temperature structure in all tropospheric layers above 700 mb was very much conservative, otherwise the temperatures — 20°, — 30° C, — 40° C would not appear in all the means at nearly the same height. So in both of these groups a quasi-barotropic state is present which is a well known feature in all synoptic meridional cross sections where the horizontal levels have to be drawn quasi-horizontally. This quasi-barotropic behaviour of upper troposphere in each of the two different groups of soundings which most of the time are separated by the polarfront is of special interest. It is this feature which allows us to treat the atmosphere in the mid- and upper troposphere as a quasi-barotropic one in numerical forecasting. As we deal most of the time only with these two groups of soundings and from 280 mb upward relatively little change can be seen in the stratospheric vertical temperature structure, very little influence or contribution may be expected from the stratosphere. Essentially only the baroclinicity at the polar front has to be dealt with. Fig. 10 shows furthermore that comparably little temperature contrast between middle and subtropical group appears in the troposphere from 700 to 230 mb. This contrast is strongest in the layers between 700 and 500 mb and gradually decreases upwards. But in the stratosphere between 230 up to 50 mb a marked reversed temperature contrast appears. In case of a strong northward displacement of the subtropical system and in cases where the middle soundings cover only a small part of the northern hemisphere (decrease in area) not only a stronger baroclinicity will be present in the troposphere and concentrated at the polar front surface (difference between polar and subtropical soundings), but in the stratosphere above the reversed temperature contrast between the two systems under consideration will be of great importance. Under these circumstances one might expect the presence of a state in which drastic changes in the general circulation might occur. In this case the underestimation of stratospheric contributions on tropospheric developments may be serious and may lead to severe failures in applying barotropic assumptions. In numerical forecasting the application of quasi-barotropic models not taking into account the stratospheric changes during such time intervals, may lead to failures. Under such conditions we observe extremely strong and rather surprising cyclone developments just in such locations where the above described interaction of tropo- and stratospheric temperature conditions were present. It will be left for a later investigation to show definitely that from these locations the rapid breakdown of the zonal circulation type of January 7 occurred, resulting in a meridional circulation type later on (DEFANT, 1957).

IV. A general outline of a possible mechanism of index change

The foregoing discussion dealing with a characteristic behaviour of the whole general circulation during a time interval of several days, during which the main features drastically changed, gives some clues which might possibly be tied together to a more orderly mechanism which acts in such a period of circulation change. According to the foregoing discussion it seems only possible to get some insight in this complicated process by considering the whole space of the atmosphere up to the very top (about 25 km). Such a possible mechanism we attempt to present here and we clearly state that it is not a definite and final presentation. We further must point out that this mechanism may only operate in such time intervals in which large interactions between the more permanent tropical-subtropical circulation cell and the mid-latitude circulation takes place (DEFANT, 1954), (DEFANT, 1954).

In the beginning one can think of a cyclic change where one can start at any instant and return later to the starting state. One mostly deals in the mid-latitude circulation with a meandering circulation type as we have described in Fig. 8. This type of circulation is characterised in the surface layers by individual cyclone tracks which are oriented more in a meridional direction and the subtropical high pressure belt is divided up in separate anticyclonic cells. In the middle troposphere a meandering polar jet with a certain number of

long waves (mostly 5 or 6) around the northern hemisphere is present. The tropical circulation cell is restricted to about the latitude range between the equator and the 30° parallel, so that the subtropical jet near the 200 mb level is more zonal. The whole atmospheric temperature field can be divided up into three quite different parts. Each part has its typical tropopause height as well as its tropospheric and stratospheric temperature structure. Under these conditions one might expect in the region between two successive cyclone families a low level shallow outflow of polar air which penetrates even across latitude 30° N into the trade wind regions. (Breaks in a continuous polar front surface.) In addition one might expect cut-off processes of cold vortices towards the south due to instability in the long-wave pattern whereby cold vortices are excluded from their polar source region and penetrate into the tropical circulation. This doublefold process intensifies the tropical circulation. By these interactions not only the mean meridional circulation of the tropical cell, but also the turbulent transfer of angular momentum may increase. From the more recent works of the mean angular momentum balance of the tropical circulation PALMÉN (1955), PALMÉN and ALAKA (1952), RIEHL and YEH (1950), RIEHL (1954), a.o. it becomes likely that a stronger output of angular momentum northward in the high levels along the northern border of the tropical circulation may occur, because the angular momentum balance of the tropical circulation gets disturbed. In special regions along lat. 30° N in which in addition to the zonal components strong meridional northward components develop, the subtropical jet tends to take on a meandering form and shifts towards northern latitudes. These special preferred regions are mostly observed over the western parts of the Atlantic and the Pacific Ocean. The very favourable trough formations over Eastern Asia and over Eastern North America may favour such northward shifts of the tropical system over the western parts of the Oceans. Cold polar air flows out over the warm ocean areas (Gulf stream and Kuroshio) and strong heat will be given off to favour the displacement of the subtropical jet.

As a result of these processes the subtropical jet moves in several places far northward and therefore subtropical air is advected with it. This advection does not only take place in the lower and middle tropospheric layers (warm air advection), but especially in the higher troposphere and in the stratosphere (cold air advection). The advection of very cold high level subtropical air is even more pronounced due to the presence of higher wind velocities at these levels. Strong blocking highs develop in rather northern latitudes and the meandering polar front jet takes on a more zonal form. In certain areas polar front- and subtropical jet come very close together and form an extremely strong jet of a complicated vertical structure (double wind maxima or a single maximum of a broad vertical extent). On the surface a continuous high pressure belt forms around the earth which has on top in the high layers near the tropopause the very cold subtropical air. This situation we call then a zonal circulation type. This is characterized in the mid-troposphere by a more zonal polar front jet in northern latitudes. The polar front now separates the polar air north of it from the purely subtropical air to its south. But in the stratosphere the relatively warm stratospheric polar air stands next to the extreme cold high tropospheric tropical air separated by a tropopause with a very steep front-like slope.

Kinetic energy from the tropics has been transported into mid-latitude circulation by this process. A strong source of potential energy has been created in the vicinity of the polar front. Strong baroclinicity is present in the troposphere at the polar front, but a reverse strong baroclinicity appears in the higher levels of the atmosphere above the polar front. In this stage in our opinion half of the cycle has been performed. We need now to look for mechanisms to offset this critical stage.

There are several factors, which act simultaneously in this occasion. We have discussed before the apparent cooling of the very upper layers of polar stations just before we arrived at the critical stage. We have seen that this influence started at the very high stratospheric layers and could be noticed later on effecting the lower polar stratosphere. We also pointed out that this cooling of the polar stratospheric layers may be mainly due to an advection process of the subtropical air which slowly

approached the polar cap from the south in very high stratospheric layers during the time interval before the zonal circulation was formed. Parallel with this process we noticed an increase of surface pressure in the polar cap which gradually increased from a value of 995 on January 1 to 1035 mb on January 8. By the establishment of a meridional pressure gradient (north—south) in the lower layers of the troposphere the conditions become favourable for easterly or northeasterly winds in the polar area. The air tends to break out towards more southern latitudes because of surface friction, especially in regions where the surface friction becomes large due to the topography of the earth's surface (east of Greenland, east of the Northern Rocky mountains and North-Eastern Siberia). This may be one factor to offset the critical stage. A second powerful factor may be instability of different kinds occurring in the regions,where the polar front has a steep slope and above a frontlike inclined tropopause with a counter slope exists. The upper wind field due to the superposition of the polar front jet and the subtropical jet branches becomes strong and there exists strong baroclinicity (strong positive vertical wind shear) in the inclined polarfront below the jet, but also an additional strong baroclinicity at the tropopause (strong negative vertical wind shear). In the upper parts of the polarfront and in the region between the jet core and the tropopause hydrodynamic instability may occur. This instability may destroy the equilibrium of the polar front. Strong cyclogenesis occurs and a new adjustment of mass distribution has to be made. The energy for such rapid cyclogenesis cannot be taken only from the horizontal temperature differences on both sides of the polar front within the troposphere but the very cold layers on top of the warm subtropical anticyclonic cells may act as a source in such a case. So not only the cold air tends to break out horizontally towards southern latitudes but it may get a continuous support from the upper cold air. Even if the upper cold air (with temp. of — 65 to — 70° C) has to descend during this process to the layers 300 or 400 mb and warm adiabatically, it will still be cold enough for these levels (— 40 to 45°). We may mention that a study of an extremely strong cyclogenesis of this type which took place south of Iceland on January 8 has guided us to these ideas. The result of an investigation of this cyclogenesis will be presented in a later paper (DEFANT, 1957). When this break-down has happened (and this does not necessarily happen only in one place of the northern hemisphere) the behaviour of the whole circulation changes drastically into a meridional type characterised by a meandering polar jet. There will be a strong outflow of polar cold air in different parts of the earth. The air inside such polar outbreaks gradually sinks and spreads out over a large area. This phenomenon has been clearly described by PALMÉN (1953, 1951). The blocking anticyclonic cells gradually shift westwards as a result of the strong polar outbreaks on their eastern sides. The cold layer on top of these anticyclones gradually disappears and the subtropical structure of the soundings gets destroyed. The soundings obtain a vertical temperature structure similar to the middle group in the sense of the foregoing discussion. In our opinion the cycle is completed and a meridional circulation pattern is being formed. Mid-latitude circulation only deals with polar and middle systems separated by the polar front. The subtropical system remains south of latitude of about 30° N and the subtropical jet takes on its normal zonal character near this latitude circle. We may clearly state that this life cycle during which a large index change happens is not always in action. Only when the subtropical system takes part in mid-latitude circulation, such remarkable index changes occur. There are cases when strong subtropical impulses of an unusual type develop and an extremely large blocking anticyclone is formed in high latitudes which remains stationary for a long time. A series of strong polar outbreaks may occur which are supported by the cold high tropospheric air on top of the large blocking anticyclone. We refer in this connection to the unusually long cold February 1956 in Europe, when such a development occurred.

REFERENCES

Alaka, M. A., Jordan, C. L., Renard, J. R., 1953: The jet stream, Chief Bureau of Aeronautics, *Techn. Report*, see p. 16.

Cressman, G. P., 1948: On the forecasting of long waves in the upper westerlies, *J. Meteor.*, **5**, p. 44.

Defant, Fr., 1954: Über den Mechanismus der unperiodischen Schwankungen der allgemeinen Zirkulation der Nordhalbkugel, *Arch. Met., Geophys. und Bioklim.*, **6**, Heft 3—4, 254—279.

Defant, Fr., 1954: Über charakteristische Meridionalabschnitte der Temperatur für High- und Low Index-Typen der allgemeinen Zirkulation und über die Temperaturänderungen während ihrer Umwandlungsperioden, *Arch. Met., Geophys. und Bioklim.*, **6**, Heft 3—4.

Defant, Fr., 1957: On hydrodynamic instability caused by an approach of subtropical and polarfront jet stream in northern latitudes before the onset of strong cyclogenesis, *Rossby Memorial Volume*, in press.

Defant, Fr., and Taba, H., 1957: The threefold structure of the atmosphere and the characteristics of the tropopause, *Tellus* **9**, p. 259—274.

Defant, Fr., and Taba, H., 1957: Details of wind- and temperature field and generation of the blocking situation over Europe (Jan. 1 to 4, 1956), *Beitr. Phys. d. Atmos.*, in press.

Ertel, H., 1930: Zur Dynamik der atmosphärischen Druckschwankungen, Gerlands Beitr. *Geophys.* **25**, 59—73.

Ertel, H., and Sjan-zsi-Li, L., 1935: Der Advektionsmechanismus der atmosphärischen Druckschwankungen, *Z. Phys.*, **94**, 662.

Haurwitz, B., 1927: Beziehungen zwischen Luftdruck und Temperaturänderungen. Ein Beitrag zur Frage des „Sitzes" der Luftdruckschwankungen, *Veröff. Geophys. Inst. Univ. Leipzig*, 2. Ser., **3**, Heft 5, 267—335.

Palmén, E., 1951: Aerology of extratropical disturbances, Comped., *Americ. Meteor. Soc.*, Boston, Mass., 599—620.

Palmén, E., 1955: On the mean meridional circulation in low latitudes of the Northern Hemisphere in winter and the associated meridional and vertical flux of angular momentum, *Soc. Sci. Fennica Phys. Math.* **17**, 1—33.

Palmén, E., 1953: On the dynamics of cold air outbreaks in the westerlies, Univ. Chicago, Dept. Meteor., Off. of Naval Res., *Final Rep. General Circ. Project.*

Palmén, E., and Alaka, M. A., 1952: On the budget of angular momentum in the zone between equator and 30° N., *Tellus*, **4**, 324—331.

Palmén, E., and Bradbury, D. L., 1953: On the existence of polar front zone at the 500 mb level, *Bull. Amer. Met. Soc.*, **34**, no. 2, 56—62.

Riehl, H., 1954: Tropical Meteorology, Mc.Graw Hill Book Comp. Inc., New York, Toronto, London, p. 371 a.f.

Riehl, H., and Yeh, T. C., 1950: The intensity of the net meridional circulation, *Quart., J. Roy. Meteor. Soc.*, **76**, 182—188.

Riehl, H., and Jenista, C. O., 1952: A quantitative method for 24 hour jet stream prognosis, *J. Meteor.*, **9**, p. 159, see also The jet stream, p. 6—10.

Rossby, C. G., 1928: Studies on the dynamics of the stratosphere, *Beitr. Phys. fr. Atmos.*, **14**, 240—265.

Schedler, A., 1917: Über den Einfluss der Lufttemperatur in verschiedenen Höhen auf die Luftdruckschwankungen am Erdboden, *Beitr. Phys. fr. Atmos.*, **7**, 88—101.

Steiner, L., 1926: Druck- und Temperaturänderungen in der Atmosphäre, *Meteor. Z.*, **43**, 271—276.

Thomas, H., 1935: Zum Mechanismus stratosphärisch bedingter Druckänderungen, *Meteor. Z.*, **52**, p. 41—48.

On the Amount of Carbon Dioxide in the Atmosphere

By G. S. CALLENDAR

A. R. D. E. Ministry of Supply, London

(Manuscript recieived June 17, 1957)

Abstract

Of late years there has been much interest in the effect of human activities on the natural circulation of carbon. This demands a knowledge of the amount of CO_2 in atmosphere both now and in the immediate past. Here the average amount obtained by 30 of the most extensive series of observations between 1866 and 1956 is presented, and the reliability of the 19th century measurements discussed. A base value of 290 p.p.m. is proposed for the year 1900. Since then the observations show a rising trend which is similar in amount to the addition from fuel combustion. This result is not in accordance with recent radio carbon data, but the reasons for the discrepancy are obscure, and it is concluded that much further observational data is required to clarify this problem. Some old values, showing a remarkable fall of CO_2 in high southern latitudes, are assembled for comparison with the anticipated new measurements, to be taken in this zone during the Geophysical Year.

Introduction

During the last few years there has been much interest in problems associated with atmospheric carbon dioxide, and new methods have been brought to bear on some of them. Examples of the latter include the exchange of this gas between atmosphere, oceans and biosphere (Craig 1957, Arnold & Anderson 1957), its influence on climate (Callendar 1949, Plass, 1956), and the effect of human activities on the amount in circulation. The significance of man's activities for all these problems has been emphasised by Revelle and Suess (1957 P. 19) who say —"Thus human beings are now carrying out a large scale geophysical experiment of a kind which could not have happened in the past nor be reproduced in the future. Within a few centuries we are returning to the air and oceans the concentrated organic carbon stored over hundreds of millions of years."

In order to follow the course of this "experiment" it is important to know as accurately as possible how much CO_2 the atmosphere contained before the use of fossil fuel began to add a significant amount. Fortunately there was a lot of interest in the CO_2 problem towards the end of last centry, and a number of measurements of its amount in the atmosphere were made at a time when the contribution from fossil fuel was relatively small, certainly less than 2 % of the total already there.

These early measurements are scattered through the literature of many countries and the original papers are often difficult to find, or absent from central libraries. For this reason it has been thought worth while to include a summary, with references in appendix tables, of what appear to be the most representative average CO_2 values reported during the last 90 years. Others are rejected with the aid of

simple criteria. From this summary a few 19th century averages have been selected as the most accurate, and, together with a brief discussion of the basis for selection, they should provide a reasonably accurate base line for the amount of CO_2 in the air of the north Atlantic region at the end of last century. The value proposed here for this quantity is 290 p.p.m. by volume.

Similar data for the present century is given in the Appendix, and compared with the amount of fuel CO_2 in Figure 1. Most of these recent averages appear to be quite reliable, and only a few scattered readings have had to be rejected because of the criteria mentioned above. They show a marked tendency for the amount of CO_2 to rise during the last few decades, roughly in proportion to the addition from fuel. However, the possibility of the latter causing such an increase of atmospheric CO_2 has been strongly questioned in the light of new radio-carbon measurements (Revelle & Suess l.c.) and the whole question is in a very interesting stage at the present time. Some further comments on it will be found below.

1. Rejection of inaccurate values

Because the measurement of CO_2 in the air may be, and often has been in the past, 100 % or more in error unless great care is taken in both air sampling and analysis, it is essential to use discrimination in deciding which of the old values are reliable. In some cases examination of the original papers will show that the samples used were not representative of the free air, but for others this is not so, and rejection criteria such as those given below must be used.

The following have been excluded from the tables as not representative of the free air:—
(a) Period mean values 10 % or more different from the general average of the time and region.
(b) Air samples taken in towns, because these often give 5 to 20 % more CO_2 than uncontaminated air.
(c)[1] Averages depending on only a few samples, or made within s short period, because real fluctuations may exceed 10 % in such cases.
(d) Measurements intended for special purposes, such as biological, soil air, atmospheric polution, etc.

As a result of these criteria practically all values reported before about 1870 had to be rejected. In those early days a relatively crude instrumentation seems to have been responsible for differences of 50—100 % between many of the reported averages. (See Fonselius et al. 1956. Fig. 1.) In addition to the sets which, quite obviously, do not represent free air conditions, there remain a few borderline cases where the reported value comes within 10 % of the genral average, but it has not been possible to estimate the quality of the air samples used. Either the original papers could not be found, or else the given data was insufficient for this purpose.—The latter being an all too common fault in reporting the old measurements. In some of these borderline cases the rather high average suggests that town air may have been included in the samples, these are marked + in the tables. On the other hand the rather low values reported from Dorpat suggest instrumental causes, and the overall average of the 18 sets in Appendix table A comes out only 1 % above the more certain measurements discussed in the next section.

2. The most reliable of the 19th Century observation

Although the weight of numbers in appendix table A gives what is probably a good average for the period and region, it will be appreciated that the sets used are a very mixed lot. Some of these averages are from an elaborate research, including flow rate—absorption studies, artificial sample checks, preferential surface absorption of CO_2 in sampling vessels, etc., whereas others are based on a large number of rapid determinations, or a few dozen free air samples taken in connection with some biological research.[1] In addition most of the averages include a significant proportion of local effects, such as:— Samples taken in stagnant surface air, at night, or over

[1] This criteria has been neglected in a few special cases, (Krogh, Spector, and certain of Muntz and Aubins obs.), where study of the original papers showed that it did not fully apply.

[1] Letts & Blake (Appx. A) in particular, made a study of the instrumental errors which arise in the CO_2 measurement.

water in which photosynthesis is active, in air which has recently traversed large urban areas, and so on. Hence some further selection is very desirable.

This has been attempted as far as the published data allow, with the asistance of the daily weater maps for west Europe, and the result is summarized in Table 1. It is, of course, a subjective estimate, but the writer is fairly confident that a completely independent assessment of the data for this period would find an average within about 1 % of that given. These sets are amongst several examined in relation to the weather maps of the period, and the results of this analysis have been discussed in an earlier paper (CALLENDAR 1940), which should be consulted for further details of the measurements.

Table 1. Preferred 19th century CO_2 averages. (All daytime obs.)

Authority [Ref. Appx. Table A]	Location	Observations			Average CO_2	
		Date	Period	No.	p.p.m.	Ref. Fig. 1
J. Reiset	N. Coast of France	1872—73	12 months	56	291.1	a
J. Reiset	» » nr. Dieppe	1879—80	9 »	67	288.7	a
Muntz & Aubin	France. Country	1881	9 »	64	287.0	b
Letts & Blake	Nr. Belfast	1897	5 »	67	289.4	c
Brown & Escombe	Kew. Nr. London	1898—1901	20 »	54	286.1	d
5 Sets average	W. Europe	1872—1901	55 »	305	288.5	

Apart from the probable accuracy of the measurements themselves, other reasons for selecting the particular averages assembled in Table 1, include the following:— (a) Reiset. The average of all air samples taken at night was 4 % higher than for the day samples as given here. On calm foggy nights it was 10 % higher. (b) Muntz and Aubin: The free air quality of their average is supported by the fact that they obtained the same value from 14 samples taken at the summit of the Pic du Midi, 2,900 m, on very windy days. The dispersion of single reading was only half as great for the latter series. (c) From time to time Letts and Blake standardized their analysis with artificial air samples of exactly known CO_2 content. (d) At Kew the easterly winds from London averaged 10 % more CO_2 than westerly winds from the country. Only the latter are included here. Apart from this set, all the reported day measurements are included in Table 1.

Neither the perferred values in Table 1, nor the many averages in Appendix table A, show a significant trend between 1870 and 1900. Together these two sets of averages give a mid-point of 290 p.p.m., hence it seems reasonable to choose this round figure as the amount of CO_2 in the free air of the north eastern Atlantic region at the turn of the century. Its probable accuracy is thought to be $\pm$ 1 %, and, without further hair splitting, it is difficult to see how a more precise base value could be obtained from the old data.

3. The 20th Century Observations

With the exception of a few measurements excluded by the criertia given in section (1) above, all the 20th century CO_2 averages known to the writer are assembled in Appendix table B. As in the case of the earlier values, very different methods were used by most of these observers. Some like Benedict, Carpenter, and Haldane, relying on large numbers of small air samples, whilst others, like Krogh and Spector, aimed at basic accuracy with a few very careful measurements.

The average values from Table B are plotted against the years of observation in Fig. 1. The full curve on this figure shows how the CO_2 from fossil fuel combustion would increase the amount in the whole atmosphere if there were no net losses to other CO_2 reservoirs. For this curve the base line is taken as 290 p.p.m. in the year 1900, and one part per million of CO_2 by volume as equal to 8.10^9 tons. By 1956 this "fuel line" is up to 325 p.p.m., or 12 %, owing to the addition of 280 thousand million tons of fuel CO_2 since 1900.

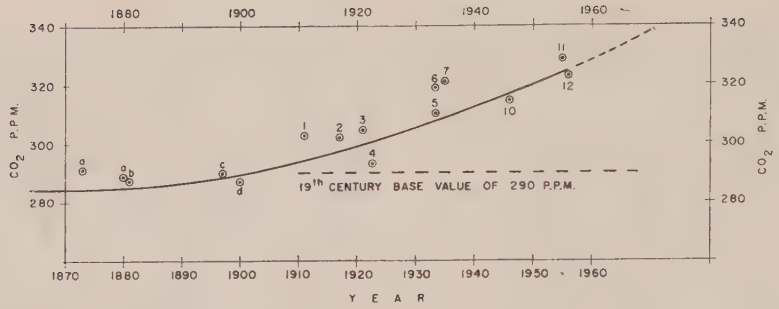

Fig. 1. Amount of CO_2 in the free air of the N. Atlantic region. 1870—1956. Full curve, amount from fossil fuel (See Appx. Table B. for numbered obs. points, and text Table 1 for the 19th century obs. points.)

4. Discussion of Figure 1

It will be seen that the observed points show a decided rising tendency in the later decades, but they appear rather scattered on the scale used for the figure. This scatter is, however, less disturbing when it is realized that both seasonal mean values, and those taken in different parts of Europe during the same season, may differ on occasion by over 5 %. This has been demonstrated by the valuable and extensive new series from Scandinavia, (Fonselius et al. 1956). Similar differences are also seen in the 19th century sets covering several seasons, and must result from the interaction of meteorological, biological, and oceanic factors. Certain of these factors have been suggested, (Callendar 1957), to account for the relatively high CO_2 values in the 1930's reported by some observers.

Coming to the present time. It happens that the average of all the new Scandinavian measurements from Dec. 1954 to Dec. 1956, (326 p.p.m. from about 1,000 readings in 25 months at 15 stations. Lat. 56°—68°N. Long. 10°—28°E), lies almost on the fuel line, 12 % above the 1900 base value of 290 p.p.m. Although such very close agreement may be a coincidene, the general upward trend of the observations since the turn of the century, and especially the manner in which most of them keep near the fuel line, seems very significant. It is, however, most difficult to account for such a large increase of atmospheric CO_2 from the fuel addition only, because radio-carbon methods have recently shown it is in active exchange with very large CO_2 reservoirs in the oceans and biosphere. (Craig, l. c. & others). Thus, if the increase shown by the measurements discussed here is even approximately representative of the whole atmosphere, it means that the oceans have not been accepting additional CO_2 on anything like the expected scale. However, this important and interesting problem awaits further observational data, in particular from the Southern hemisphere.

5. CO_2 observations in the Tropics and South

It seems probable that new measurments of atmospheric CO_2 will be made in distant parts of the world during the Geophysical Year, and therefore it may be useful to give a summary of old values taken in the Tropics and south Atlantic. The averages known to the writer are assembled in Table 2, but there may be others reported in the literature of the southern countries. Even so the most valuable is likely to be the series reported by Muntz & Aubin, (1886)[1], not only because of their wide extent, probable accuracy, etc., but also because they took many values in France, by the same elaborate technique, which are directly comparable, Table 2.

Although Thorp's values in Table 2 are possibly a few percent up for instrumental reasons, his high Belem average could well be accounted for by rapid decay of river debris from the Selvas, in the esturies and swamps

[1] Dr. C. H. Keeling, of the California Institute of Technology, who is directing the United States CO_2 program for the I. G. Y., considers that the measurements by Muntz & Aubin are probably amongst the most reliable of the 19th century CO_2 observations. (Private communication).

Table 2. CO_2 averages from the Tropics and south in the 19th Century

Authority	Region or place	Lat. Range	Observations				Diff. from Europe p.p.m.
			Date	period	No.	CO_2 p.p.m.	
Thorp	West Indies region	0—22 N	1866	2 mts	38	297	—
»	Para (Belem)	1. S.	1866	3 mts.	31	328	—
Muntz & Aubin	West Indies region	14—25 N	1882	4 »	23	282	— 5
» »	S. Atlantic & Chile	0—42 S	1882—3	4 »	13	273	— 14
» »	At Santa Cruz	50 S	1882	2 »	10	267	— 20
» »	Nr. Cape Horn	56 S	1882—3	10 »	39	256	— 31

of this hot region. Of more general significance is the regular fall of Muntz and Aubin's averages as higher latitudes were reached in the southern hemisphere. This fall is a good pointer to where the oceans withdraw atmospheric CO_2 on a large scale.

The latter phenomenon has since been confirmed, and more precisely located, by some very low readings from the Antarctic reported by MUNTZ and LANE (1911). These averaged as little as 205 p.p.m. over near freezing water in 65°—70° S. lat. Another "CO_2 sink" evidently exists near the Artic ice margin, for Prof. BUCH (1948), reports an average of only 225 p.p.m. from several samples of cold Arctic sea air. This nothern sink, however, must be relatively small compared with the southern, because the north temperature zone measurements do not show an appreciable change of CO_2 with latitude.

In conclusion, perhaps we may anticipate that the CO_2 measurements in distant parts, promised during the Geophysical Year, will resolve the discrepancy between the radio carbon data and that discussed here, although one suspects that the final answers to this problem lie in the chill darkness of the ocean abyss.

Table A. Appendix.
19th Century mean CO_2 values

Ref.	Authority	Location of observations	Date obtained	No. obs.	Mn. CO_2 p.p.m.
1.	T. E. Thorp	N. Atlantic 0—52° Lat.	1865—66	77	297
2.	F. Schulz	Nr. Rostock	1868—71	1 034	292
3.	J. A. Reiset	France N. W. Coast	1872—73	124	293
4.	— Risler	Cleves — Switzerland	1872—73	—	303 +
5.	J. Claesson	Nr. Lund	1875	31	279
6.	G. F. Armstrong	Grassmere, N. W. England	1879	53	296
7.	J. A. Reiset	Nr. Dieppe	1879—80	122	296
8.	A. Muntz & E. Aubin	France Country	1881	64	287
9.	A. Levy	Montsouris Obs. Nr. Paris	1876—87	Large	292
10.	— Blockmann	Koningsberg	1885	40	310 +
11.	— Dragendoff	Nr. Dorpat	1886	366	266
12.	T. Van Nuys & B. Adams	Nr. Bloomington U.S.A.	1887	18	282
13.	E. Von Frey	Nr. Dorpat	1887—88	932	264
14.	A. Petermann & J. Graftiau	Belgium Country	1889 –91	525	293
15.	A. Palmquist	Nr. Stockholm	1891—92	395	312 +
16.	— Libedineff	Odessa	1896—97	—	303 +
17.	E. Letts & R. Blake	Nr. Belfast	1897	67	289
18.	H. Brown & F. Escombe	Nr. London	1898—1901	92	294
		Average of 18 Sets	1865—1901		291.5

+ See text Sec. (1).

REFERENCES — Appx. Table A.

1. Thorp, T. E.: *J. Chem. Soc.* **5**, 189, 1867.
2. Schulz, F.: *Landu, Vers, Stationer* **14**, 366, 1871.
3. Reiset, J. A.: *Ann. Chim.* **26**, 145, 1882.
4. No ref. found.
5. Claesson, J.: Berichte. *Deut. Chem. Ges.* **9**, 1876.
6. Armstrong, G. F.: *Proc. Roy. Soc.* **30**, 343, 1880.
7. Reiset, J. A.: loc. cit.
8. Muntz, A and Aubin, F.: *Ann. Chim.* **26**, 1882.
9. Levy, A.: *Annu. Montsouris*, 1877—87.
10. No ref. found.
11. Dragendoff: *Chemi. Central Blatt* **3**, Fol. 18, 1367, 1887.
12. Nuys, T. and Adams B.: *Amer. Chem. J.* **9**, 1887.
13. Frey, E.: *Inarig. Diss.* Dorpat 49 p. 1889.
14. Petermann, A and Graftiau, J.: *Mem. Cour. Akad. Roy. Belg.* **47**, 87, 1892.
15. Palmquist, A.: *Sevens. Vet. Hand.* **18**, 1, 1892—3.
16. No ref. found.
17. Letts, E. and Blake, R.: *Sei. Proc. Roy. Dublin Soc.* **9**, N. S. Part 2. 107, 1900.
18. Brown, H. and Escombe, F.: *Proc. Roy. Soc. B.* **76**, 118, 1905.

Table B. Appendix

20th Century mean CO_2 values.

Ref. to Fig. 1	Authority	Location	Date obtained	No. obs or Period	CO_2 p.p.m.
1.	F. G. Benedict	Nr. Boston, Mass.	1909—12	645	303
2.	A. Krogh	Nr. Copenhagen	1917	4 mts.	302
3.	H. Lundegardh	Hallands Väderö, S. Sweden	1920—23	4 yrs.	305
4.	B. Schultz	N. Sea & Baltic	1922—23	2 yrs.	293
5.	T. M. Carpenter	New England	1930—35	1 156	310
6.	K. Buch	N. Atlantic 40—50° Lat.	1932 &35	81	319
7.	K. Buch	Petsamo — Finland	1934—35	95	321
8.	J. B. Haldane	Nr. Perth — Scotland	1935	152	324 +
9.	E. Pozzi Eskot	Lima, Peru	1937	—	323 +
10.	N. Spector & B. Dodge	Yale Uni. Conn.	1946	Few	315
11.	S. Fonselius & F. Koroleff	Scandinavia. 15 Stations. 500. Obs.	1955	12 mts	328
12.	S. Fonselius & F. Koroleff	Scandinavia. 15 Stations. 522. Obs.	1956	12 mts	322

+ See text Sec. (1)

Refs. Appx. Table B.

1. Benedict, F. G.: *Pub. Carnegie Inst.* No. 166, 1912.
2. Krogh, A.: *Dan. Videns. Sel. Math-fys. Medd.* 1. 1—19, 1919.
3. Lundegardh, H.: "Der Krieslauf der Kohlensaure in der Nature". Jena 1924.
4. Schulz, B.: *Arch. Deut. Seewarte*, 41. 6, 1923.
5. Carpenter, T. M.: *J. Amer. Chem. Soc.* 59. 232, 1937.
6. Buch, K.: *Acta Akad. Aboensis. Math. Phys.* 11. No. 12 1939.
8. Haldane, J. B.: *Nature.* 137. 573, 1936.
9. Pozzi-Escot, E.: *Revista der Cieneias*, Lima. 40, 133, 1938.
10. Spector, N. and Dodge, B.: *Anal. Chem.* 19. No. 1 55, 1947.
11—12. Fonselius, S. and Koroleff, F.: *Tellus*, **7**, **8**, and **9**, 1955 to 1957.

REFERENCES

Arnold, J. R. & Andersson, E. C., 1957: *Tellus* **9**, No. 1. pp. 28—32.

Buch, K., 1948: Geophysica (Helsinki) **3**, p. 63.

Callendar, G. S., 1940: *Quart. J. R. Met. Soc.* **66**, p. 395.

— 1949: »Weather». (London). **4**, p. 310.

— 1957: *Tellus* **9**, p. 421.

Craig, H., 1957: *Tellus* **9**, pp. 1—17.

Fonselius, S., Koroleff, F., and Wärme, K., 1956: *Tellus* **8**, pp. 176—183.

Muntz, A. and Aubin, E., 1886: »Researches sur la constitution chimique de l'atmosphere». Tome 3. Les Ministeres de la marine et de l'Instruction Publique. Paris.

Muntz, A. and Lane, E., 1911: *Compt. Rend.* **153**, p. 1116.

Plass, G. N., 1956: *Amer. J. Phys.* **24**, pp. 376—387.

Revelle, E. and Suess, H. E., 1957: *Tellus* **9**, pp. 18—27.

On the Ångström Absolute Pyrheliometric Scale

By F. LINDHOLM, Swedish Meteorological and Hydrological Institute, Stockholm

(Manuscript received April 24, 1957, revised October 10, 1957)

Abstract

A critical examination of the original Ångström pyrheliometric scale has been made from the result of recent calibration of the new modified Ångström pyrheliometer using the sun as radiation source.

The mean marginal error of the old standard pyrheliometer is found to be +2.4 per cent. The influence of the small difference in aperture of the two models is esteemed to increase the correction insignificantly.

This result is equivalent in meaning that the original scale-values added with 2.4 per cent are given in the true energy scale.

The corrected values are nearly one per cent higher than in the pyrheliometric scale recommended by the Radiation Conference at Davos 1956.

A practical pyrheliometric standard scale is a question of specification of the aperture conditions or of the amount of circumsolar sky radiation to be allowed in the standard pyrheliometer. A proposal of such a specification is given and recommended by the Conference at Davos.

1. Introduction

At the International Meteorological Conference at Innsbruck 1905 the K. Ångström electrical compensation pyrheliometer was adopted as the standard instrument for absolute measurements of solar energy.

Since that time the pyrheliometer No 70 at the Physical Institute of the University of Uppsala has served as the Standard instrument to which all outgoing compensation-pyrheliometers have been referred and the instrument constants of all outgoing pyrheliometers have thus been evaluated to this standard.

The constant determinations were made at the Physical Institute by Professor K. Ångström himself and after his decease 1910 under the supervision of his successors of the leadership of the Institute.

The constant was determined by considering:

1) the relation

$$baq = ri^2 \text{ or}$$

$$q = \frac{r}{ba} i^2 \text{ watt cm}^{-2}$$

$$q = \frac{60}{4{,}187} \frac{r}{ba} i^2 \text{ gr cal min}^{-1} \text{ cm}^{-2}$$

i is the mean intensity of the compensation-current in ampère.

r is the mean resistance of the two strips of manganin in ohm pro cm.

b is the mean width of the strips in cm.

a is the coef. of absorption.

According to the special proceeding of blackening used, the K. Ångström value $a = 0.98$ has been accepted.

The calculated $k_{calc} = \frac{60}{4.19} \frac{r}{b \cdot a}$ [1] has been determined for every pyrheliometer.

2) The constant has also been obtained by comparison with the standard No 70 or one of the substandards. The radiation (q) is given

$$q = k_{obs} \times i^2 = k_N \times i_N^2$$

$$k_{obs} = k_N \left(\frac{i_N}{i}\right)^2$$

[1]) For the comparison of results with the new instruments the old value of K. Ångström 4,19 is maintained instead of the correct 0,07 % lower value 4,187.

The average value, k_{obs} of a series of comparisons on clear days is given in a constant certificate of the instrument.

The value of $k_N = 17.48$ was given by K. Ångström and the Ångström pyrheliometric scale refers to this value of the standard pyrheliometer No 70.

The constant-determinations at Uppsala, were treated by G. Granqvist (1912), by E. Bäcklin (1924, 1925) and E. Bäcklin and G. Kellström (1930). Newly the whole Uppsala material 1910—1935 has been critically examined by Courvoisier (1957). Particular stress was thereby laid upon verification of the constancy of the standard pyrheliometer No 70. From the 185 determination during the period 1910—1935, Courvoisier found for the quotient $Q = \frac{k_{obs}}{k_{calc}}$ an average value of 1.0039 or a deviation from unity of 0.4 per cent.

The small defect in the blackening of the one of the strips of No 70, in 1928 first observed by Bäcklin (1930), could be eliminated by renewed blackening.

2. *The marginal effect of the standard pyrheliometer.* — If the strip exposed to the sun radiation is shaded at the border by the inner diaphragm in the proportion 4 mm² of the whole strip area 2 × 20 mm² i.e. of 10% and the adjoining screened strip is heated to its whole length of 20 mm by a compensation current it is evident that this current takes a little too low value with a correction factor of the instrument-constant corresponding to the unexposed part of the strip. This is the case concerning the standard pyrheliometer No 70 (length of the strips 20 mm, interior diaphragm 17.8 mm) and the pyrheliometers made on the model of this standard.

This marginal error was first mentioned and examinated by A. Ångström (1914). By teoretical considerations and from experiments on No 158 Ångström gave the probable value 1.3 per cent for the marginal error of this pyrheliometer.

In the mean time C. G. Abbot at the Smithsonian Institution Washington (see Annals Astrophys. Obs., volumes 3 to 6) has developped his silver-disk pyrheliometer, which scale-factor had been determined by comparison with the absolute water-flow and water-stir pyrheliometers. Marten (1913) made a great number of comparisons between the compensation pyrheliometer and the silver-disk pyrheliometer and found a discrepance between the Ångström and Smithsonian scales of 3.4% with lower radiation values for the Ångström instrument, though with a little greater angular aperture (greater circumsolar radiation) for the Ångström instrument.

Marten (1922) referred this discrepance owing to the marginal error after carefully investigations by series of measurements of solar intensity with alternations of the diaphragm. The experiments gave a mean value of 2.8 per cent for the correction-factor for the Potsdam pyrheliometer Å No 140 III. The Smithsonian scale of 1913 i.e. Ångström original scale + 3.5 per cent has been fairly generally accepted in U.S.A. and Central Europe. The constants of Ångström pyrheliometers were given in the Ångström original scale during 1910—1935 at Uppsala and afterwards during 1935—1956 in both Ångström and Smithsonian scales. From 1957 the constants are given in the Ångström original scale added with 1.5 % (cf. p. 253).

3. *Standardization of Ångström pyrheliometers carried out at the Swedish Meteorological and Hydrological Institute.* — Since 1940 the scale-factors of the outgoing Ångström pyrheliometers (from Albert Lindblad, Stockholm) have been evaluated at the Swedish Meteorological and Hydrological Institute. The constant values are given graphically on fig. 1—3 as continuation of the corresponding curves of the period 1910—1935.

The average mean of the pyrheliometric constants to a number of 70, obtained by comparison, to a greater part with Å 158, during 1940—1956 was $k_{obs} = 14.27 \pm 0.204$.

As seen from fig. 1 the earlier determinations 1940—48, the minor part, have given a little lower values. Some of the earlier pyrheliometers has been arranged with the one strip shielded by a fix screen. These pyrheliometers have a mean calibration-factor of 13.13.

In the year 1951 the standard pyrheliometer No 70 has been given over as loan to the Swedish Meterorological and Hydrological Institute in Stockholm by the Physical Institute at Uppsala by courtesy of Prof. A. Lindh, the Director of the Institute at that time.

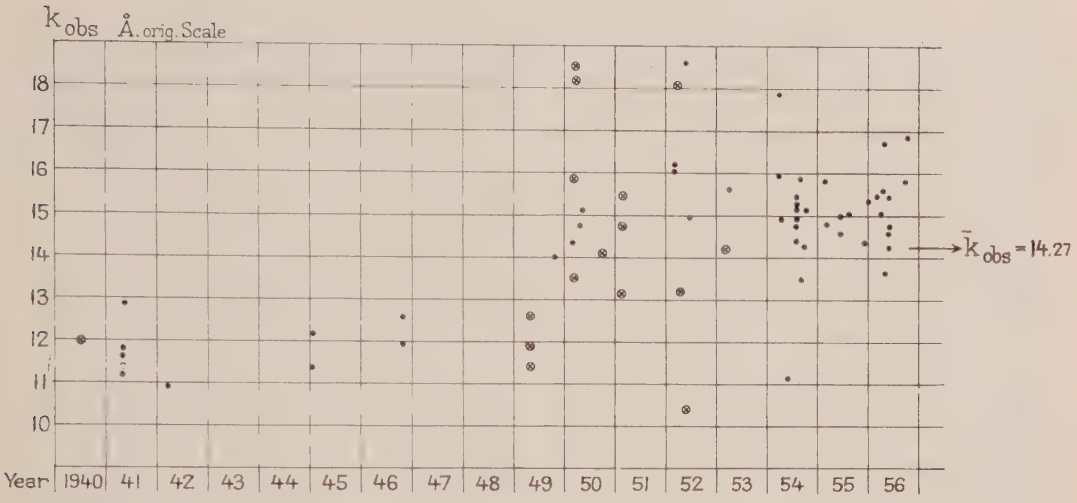

Fig. 1. The calibration factor, k_{obs}, of the individual pyrheliometers, tested 1940–1956, from the comparison with the standard Å pyrheliometer.

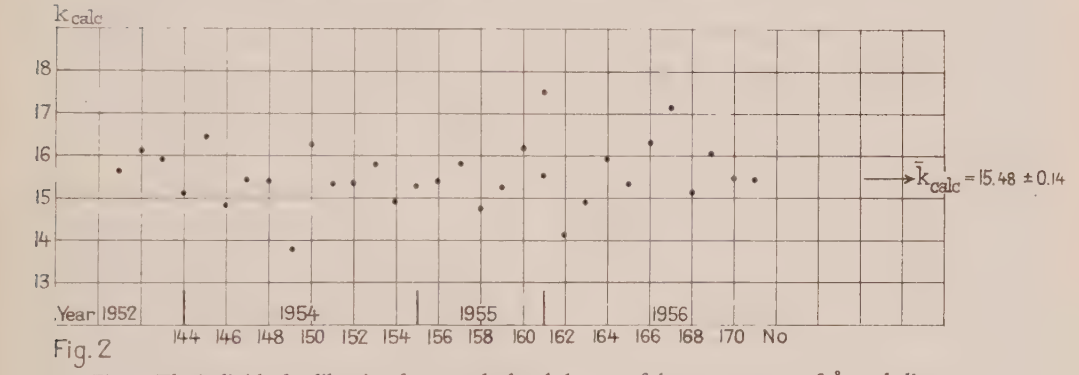

Fig. 2. The individual calibration factors calculated, k_{calc}, of the new pattern of Å pyrheliometer.

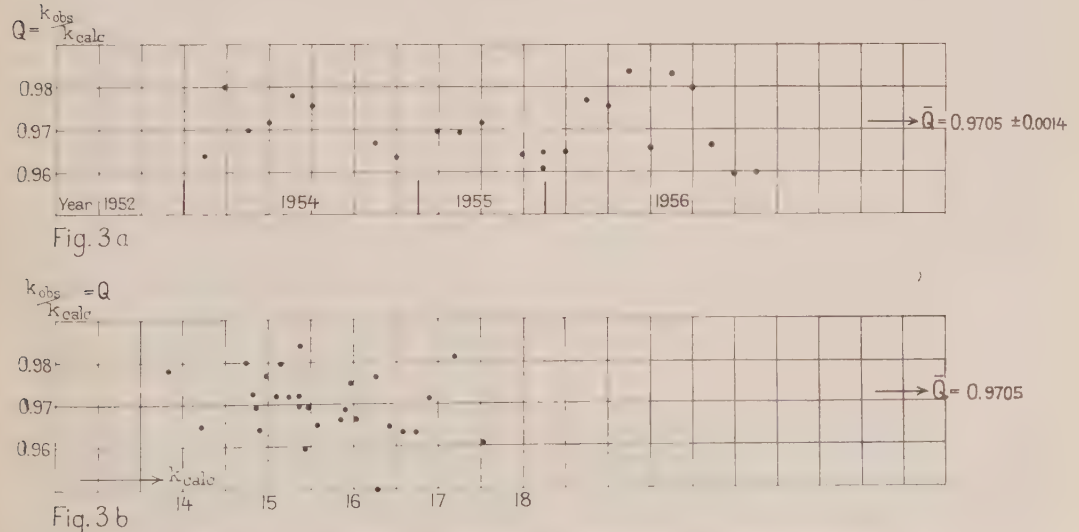

Fig. 3a, 3b. Q-values of individual pyrheliometers of the new pattern.

After repair by means of renewed blackening the standard pyrheliometer No 70 was compared with the two substandards No 158 and No 153 used at the Swedish Meteorological and Hydrological Institute for the constant determinations of outgoing pyrheliometers. The result from the measurements in July and August 1951 has given the following values for

	No 158	No 153
k_{obs}	13,765 ±0.022	14,784 ±0.031
k_{obs}/k_{calc}	1.0012	1,005

The calibration factor of the standard Å 70 differs with 0.0031 or 0.31 per cent as a mean for both these sets. Courvoisier has found this difference to 0.4 %, as a mean considering the calibrations factors of all the other Ångström pyrheliometers.

In 1952 a new pyrheliometer has been constructed at the Institute as an exact copy of the original standard pyrheliometer No 70. Particular importance was attached to confirmity concerning tube, diaphragme, length of the strips, thus concerning aperture and mariginal effect. To this pyrheliometer were made three different receivers I, II and III.

From this time the constant determinations are made by the earlier methods discribed by Bäcklin (1930), i.e. 1) by calculation from the electrical resistance and the with of the strips and 2) by comparison, generally with the substandard pyrheliometer No 158.

In tab. 1 are given the constant factors of two groups of pyrheliometers with the same marginal effect as Nos 70 and 158.

Table 1

Group 1	No	k_{calc}	k_{obs}/k_{calc}
	I	15,00	0,990
	II	16,12	1,005
	III	15,96	1,006
		Mean	1,0003
Group 2	No	k_{calc}	k_{obs}/k_{calc}
	151	15,29	0,994
	152	15,40	0,994
	155	15,26	0,995
	159	15,18	0,991
		Mean	0,9935

4. *The new pattern of the Ångström pyrheliometer.* — In the last years an alteration reffering to the internal diaphragm is made for eliminating the shielding—error in the former instruments in that sense, that the diaphragm, close in front of the strips, is opened to the whole length of the strips. An automatic coupling system of the compensation current is introduced in that manner, that the circuit is currentless with the screen being in zero-position i.e. both strips exposed to the sun radiation. The current-connection through the shaded strip is made by turning the screen. The advantage in this arrangement is that more momentary observations can be made.

In Fig. 2 are given the calculated constants for the new pyrheliometers since 1952, to a number of 32. The average value of the calculated constants is $k_{calc} = 15.48$. This value differs slightly from the Uppsala mean 1910—1935 $k_{calc} = 15.14$ ($Q = 1.0039$).

For the new pyrheliometers compared with the substandard No 158 the average quotient Q (Fig. 3) is found

$$Q = \frac{k_{obs}}{k_{calc}} = 0.9705 \pm 0.0014$$

The average deviation of individual values is 0.006 or 0.6 per cent. Referred to the original standard No 70 according to the result above

$$Q_{corr} = 0.9717.$$

In the value of k_{obs} the influence of the small aperture-difference between the older and the new pattern of pyrheliometer has not been taken into account. As the aperture of the new pattern is somewhat smaller the correction to equal aperture can bee esteemed to give only any pro mille greater value of k_{obs} and Q.

This insignificance of aperture influence is also confirmed by the Q-material from Uppsala. The mean of Q for two separate groups of instruments, the one with short, the other with long tube is found to not differ more than 0.13 per cent, the group with long tube showing the greater value. This is, contrary to the statement by Dr. Courvoisier, in agreement with what is to be expected, since the long tube with smaller aperture and thus lower value of circumsolar radiation gives the higher value of k_{obs} by the comparison with a given standard pyrheliometer than an instrument with greater aperture (Cfr Courvoisier (1957), p. 10).

This value of Q_{corr} differs from unity with 2.8 per cent as the marginal error for the original standard No 70. If we take in account

that the constant-value of the standard No 70 is 0.4 % too high in reference to the mean of the calibration-factors of all the Ångström pyrheliometers 1910—1935, we have the correction for the Ångström original scale to the true energy scale 2.4 ±0.14 per cent.

For the measurements with the earlier Ångström pyrheliometers the correction would be +2.4 per cent for the radiation values given in the Ångström original scale or —1.1 per cent for values given in the Smithsonian revised pyrheliometer scale of 1913.

From the result of a large number of comparisons 1932, 1937 and 1947 between an improved water-flow absolute pyrheliometer and the standard silverdisk-pyrheliometer ABBOT and ALDRICH (1948) concluded that the scale of Smithsonian revised pyrheliometry of 1913 is very nearly 2.4 per cent too high. The silverdisk instrument have remained unchanged. The correction to this new Smithsonian scale 1948 of the Ångström pyrheliometer readings in its original scale is thus +1.1 per cent.

In the newly adopted International Pyrheliometer Scale 1956, recommended by the International Radiation Conference Davos september 1956, the measurements may be given in the uncorrected Ångström scale increased by 1.5 per cent. This scale gives thus 0.9 per cent lower values than the above mentioned absolute scale based on calculated constants of the Ångström pyrheliometers without any marginal error and 0.4 per cent higher values than the Smithsonian scale of 1948.

5. *Accuracy of the calculated constants.* — The systematic error in the calculated constants can be evaluated from the error in the determinations of the electrical resistance and of the width of the strips.

An essential condition for the compensation principle, already pointed out by K. ÅNGSTRÖM (1893), is the similarity of the strips as receivers of the incoming sun radiation and for the watt-energy of the compensation current and great care is therefore taken by selection of the strips.

Cutting of the strips into sufficiently exactly equal width presents no great difficulty. The foregoing tests bears essentially on the equality in the electrical resistance pro unity of length; the resistance, not allowed to differ as more

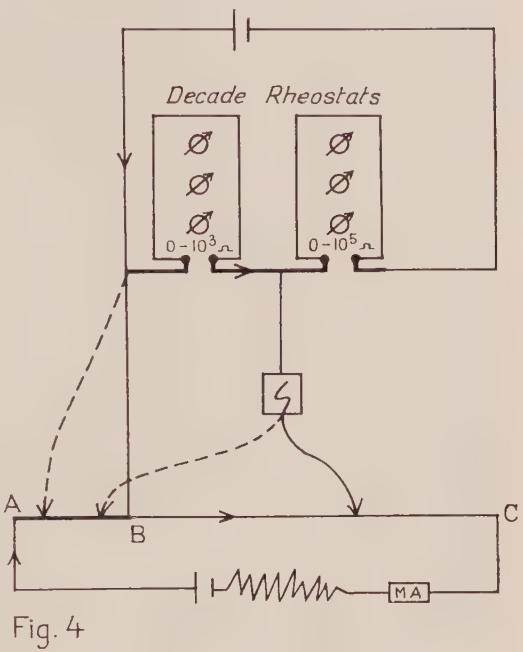

Fig. 4

Fig. 4. The potentiometric arrangement for determination of the electrical resistance of the strips.

than one or two per cent (in most cases not exceeding one per cent). The value of r and of b refers to the mean width of the two strips.

Special care is taken to give the sensitive surfaces a well defined blackening, electrolytic deposit of Pt-black covered with a layer of fine grained stearin—soot, the absorption of which K. ÅNGSTRÖM (1898) had determined the value of 0.98.

The width of the strip was measured with microscope and Leitz ocular-micrometer, which permit an accuracy of 0.1 per cent. The determination of the electrical resistance pro cm (r) was made with a potentiometer arrangement with a sensitive galvanometer in zero-coupling (Fig. 4). The strip A B is inserted in an electrical currentcircuit in series connection with a calibrated measuring-wire B C of manganin of 1 mm diameter. The potential difference between two fixed points on the strip is egalized with the potential difference between two points on the measuring wire. The resistance of the strip between the two points has thus the same value as the known resistance on the measuring-wire. The arrangement of egalization by the potentiometer and a sensitive galvanometer is shown on Fig. 4.

The distance between the two fixed points was determined with comparator to 0.976 ± 0.001 cm. The calibration of the manganin measuring-wire gave as result the resistance $\alpha = 0.0005557$ ohm per mm.

From the equation

$$k = \frac{60}{4{,}187} \frac{r}{b \cdot a}$$

we have the procentual error of k

$$\frac{dk}{k} = \frac{dr}{r} + \frac{db}{b} + \frac{da}{a}$$

In the experiments the resistance of a given length (l) of the strip is compared and measured by the resistance in mm (L) of the measuring-wire.

We have $r = \frac{\alpha L}{l}$ where α is the resistance per mm of the manganin wire and

$$\frac{dr}{r} = \frac{d\alpha}{\alpha} + \frac{dL}{L} + \frac{dl}{l}$$

For the width (b) we have $b = \beta \times B$ where β is the magnification and B is the reading on the micrometer scale.

The values of $\frac{d\alpha}{\alpha}, \frac{d\beta}{\beta}, \frac{dl}{l}$ are of order of magnitude ±0.01 % and can be neglected in proportion to $\frac{dL}{L}$ and $\frac{dB}{B}$ which are estimated to each 0.1 per cent.

Thus $\frac{dk}{K} = \pm 0.2$ %, if $\frac{da}{a}$ is neglected.

Concerning the value of a, we have accepted the value of 0.98 found by K. ÅNGSTRÖM for the blackening mentioned. This is generally supposed to be the greatest possible value. It is to be remarked that, if a lower value of a is taken, the calculated pyrheliometer constants k_{calc} would be greater and the discrepance found above would be larger.

From experience with different pyrheliometers with only deposite of platinum-black and afterwards with this platinum-black covered with a layer of the fine grained stearin-soot, I have found an average difference of the constants in this both cases to be 1.4 per cent. The Ångström value 98.0—1.4 = 96.6 % is near the value determined by RUBENS and HOFFMANN (1922) for the absorption coeff. of electrolytic deposit of platinum-black.

6. *Error from difference in aperture.* — Considering that the new pattern of the Å pyrheliometer has been given a somewhat smaller aperture than the older model, this would cause an error in the k_{obs}-values, by the comparisons, in account of the difference in amount of circumsolar sky radiation entering in the respective instruments.

The aperture conditions of the two models in the parameters of PASTIEL (1948), the opening angel Z_0, the slope angel Z_p, and the limit angel Z_l are specified in tab. 2 for the two principal sections of the rectangular aperture. R is the limiting aperture, r half of the length resp. width of the strips, l the distance between the limiting diaphragma and the receiver.

Table 2

	No 158	No 168	No 158	No 168
	Section along the strips		Section cross the strips	
	mm	mm	mm	mm
R	10,0	10,0	2,0	2,5
r	8,8	9,5	1,0	1,0
l	43,0	80,0	43,0	80,0
Z_0	12,6°	7,1°	2,6°	1,8°
Z_p	1,6°	0,4°	1,3°	1,1°
Z_l	23,1°	13,7	3,9°	2,5°

The smaller aperture angles shown in the table for the new pattern No 168 would result in a correspondent too high k_{obs} value. But in account of the steep slope of the circumsolar sky radiation the correction to equal aperture would be of the same order of magnitude as the mean error of measurements and thus insignificant in this regard.

I am indebted to Dr. L. RAAB at the Instrumental Department and Mr. L. E. HAEGGBLOM, State Hydrologist at the Ice Section of this Institute for valuable advises and assistance in the experimental part of this study.

REFERENCES

Abbot, C. G., 1913: Annals of the Astrophys. Observ. of the Smithson. *Institution*, Vol. **3**. p. 52—72.

Abbot, C. G., 1922: Annals of the Astrophys. Observ. of the Smithson. *Institution*, Vol. **4**. p. 42—97.

Aldrich, L. B., and Abbot, C. G., 1948: Smithsonian pyrheliometry and the standard scale of solar radiation. *Smiths. Misc. Coll.* Vol. **110**, No. 5.

Ångström, A., 1914: Das Ångströmsche Kompensationspyrheliometer und die pyrheliometrische Skala. *Met. ZS.* **31,** p. 369.

Ångström, K., 1899: Über absolute Bestimmungen der Wärmestrahlung mit dem elektr. Kompensationspyrheliometer nebst einigen Beispielen der Anwendung dieses Instrumentes. *Annalen der Physik und Chemie.* Neue Folge, Bd. **67,** p. 633.

Bossy, L., et Pastiel R., 1948: Etude des proprietés fondamentales des actinomètres. *I.R.M. Belg. Mémoire XXIX.* Bruxelles.

Bäcklin, E., 1924: Bestimmung von Pyrheliometerkonstanten am Physikalischen Institut der Universität Uppsala. *Arkiv f. Mat. Ast. och Fysik*, 19 A No. **10.**

Bäcklin, E., 1925: Über die Konstanz der Ångströmschen Pyrheliometerskala. *Arkiv f. Mat. Astr.* och Fysik, Bd. 19A No. **18.**

Bäcklin, E., und Kellström, G., 1930: Die Ångströmsche Pyrheliometerskala, *Met. ZS.* **47,** p. 52.

Courvoisier, P., 1957: Contributions to Standard Pyrheliometry (introduction by A. Ångström and W. Mörikofer) *SMHI.* Communication., Ser. B. No. 13.

Granquist, G., 1912: Bericht über aktinometrische Arbeiten an Observatorium der Physikalischen Institution Uppsala, Tagungsber. *Int. Strahl. Komm.* Rapperswyl, p. 19. Anhang 4.

Marten, W., 1922: Zur Frage der absoluten pyrheliometrischen Skala. *Met. SZ.* **39,** p. 342.

Nicolet M., 1948: La mesure du rayonnement solaire. *I.R.M. Belg. Misc.* Fasc. XXI.

Rubens H., und Hoffman, K., 1922: Über die Strahlung geschwärzter Flächen. *Berl. Sitzungsber.* p. 424.

Ber. Int. Met. Direktoren-Konferens, Innsbruck 1905 p. 18.

Trans. Int. Union Coop. Solar Res., 1906. Manchester. Bd. 1. p. 239.

Omm., Cimo., 1953: Enquete sur l'activité en actinométrie dans le Monde.

The Microstructure and Colloidal Stability of Warm Clouds

Part I — The Relation between Structure and Stability

By P. SQUIRES, Division of Radiophysics, C. S. I. R. O., Sydney, Australia

(Manuscript received March 22, 1957)

Abstract

Observations on the droplet spectra of different kinds of warm clouds have shown that systematic differences in microstructure exist between the various cloud types. These differences in microstructure are related in a simple way to differences in observed colloidal stability.

1. Introduction

It is well known that clouds warmer than freezing sometimes produce rain, especially in maritime air. However, the factors which determine whether a warm cloud will rain are not well understood. It is generally agreed that the raindrops form by coalescence of cloud droplets; it must be expected that the existence of large droplets in a cloud will assist this process, both because the collection efficiency of large drops is greater than that of small ones (PEARCEY and HILL, 1957) and because, even with a constant collection efficiency the mass rate of growth of a droplet increases like r^4.

This expectation has been confirmed by observations of droplet spectra in various types of cloud.

2. Observations

Cloud droplet spectra have been measured in various kinds of cloud: continental, "transitional" and maritime cumuli, the orographic cloud of the windward slope of the island of Hawaii, and "dark stratus", which is seen at times over the sea. The measurements were made with the sampler described by SQUIRES and GILLSPIE (1952). Before 1953, the droplets were impacted on a layer of magnesium oxide. As no reliable calibration could be derived for this layer, only the droplet concentrations are known definitely. From 1954 on, a layer of soot has been used. The calibration of this layer is known with a probable error which is less than 5 % for $d > 20$ microns but increases to about 15 % for $d = 5$ microns.

In cumuli, the observing runs were made at various levels with the intention of securing representative data for the whole cloud. Some of the data on droplet concentrations in continental and maritime cumuli have been published elsewhere (SQUIRES, 1956). The Hawaiian orographic cloud and the observational procedure used have been described by SQUIRES and WARNER (communicated). It need only be remarked that it forms on the island of Hawaii when the trade wind is fairly strong, and that this slope is quite regular from the coast up to 6,500 ft, averaging about 5 %.

The full results of observations in this cloud have been given by SQUIRES and WARNER (loc. cit.). In "dark stratus" layers which occur at times over the sea, samples were taken on horizontal passes through the middle of the cloud.

The observations before 1954, using a magnesium oxide layer, were made over south-eastern Australia and over the adjacent seas. Later observations using a soot layer were made near Hilo, Hawaii in 1954 and in inland Australia in 1956. "Maritime" cumuli include only those which were observed over the sea in an unmodified maritime air mass. "Continental" cumuli include those observed over the land in an air mass which was estimated to have spent at least two full days over the land surface. "Transitional" cumuli include those forming in an air mass which had been over the land for less than two days.

3. Results

The droplet spectrum has been found to change rapidly and erratically in all clouds sampled. Nevertheless, these variations are not so great as to mask the characteristic differences between the various kinds of cloud. These differences are illustrated in Figs. 1—4, which show the mean spectra found in individual examples of four different cloud types. In each case, the liquid water content and droplet concentration given is that corresponding to the mean spectrum. These four figures illustrate the fact that, as between these four categories of cloud, low droplet concentrations are strongly associated with broad droplet spectra and large average and maximum droplet sizes, and high concentrations with narrow spectra and small average and maximum droplet sizes. Statistical evidence of this association is shown in Fig. 5. Here, the mean droplet concentration found in a single traverse through a cloud has been plotted against the diameter of the largest droplet found in any sample taken during the traverse. Each sample corresponds to about 30 cm^3 of cloud air. Each point in Fig. 5 represents, on the average, eight samples. Fig. 5 shows not only that low droplet concentrations are associated with large maximum droplet diameters, but also illustrates the difference in microstructure between "dark stratus", the Hawaiian orographic cloud, maritime cumuli and continental cumuli. It is apparent that the latter three form a series

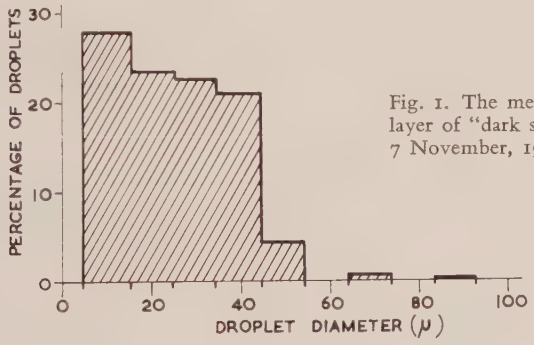

Fig. 1. The mean droplet spectrum (seven samples) in a layer of "dark stratus" at 6,500 ft over Hilo, Hawaii, on 7 November, 1954. Droplet concentration = 24 cm^{-3}; l.w.c. = 0.34 g m^{-3}.

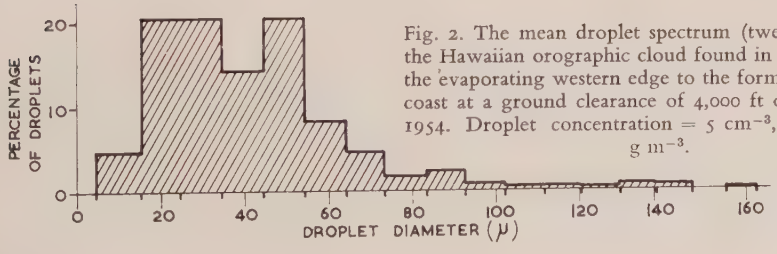

Fig. 2. The mean droplet spectrum (twelve samples) in the Hawaiian orographic cloud found in a traverse, from the evaporating western edge to the forming edge at the coast at a ground clearance of 4,000 ft on 2 December 1954. Droplet concentration = 5 cm^{-3}, l.w.c. = 0.40 g m^{-3}.

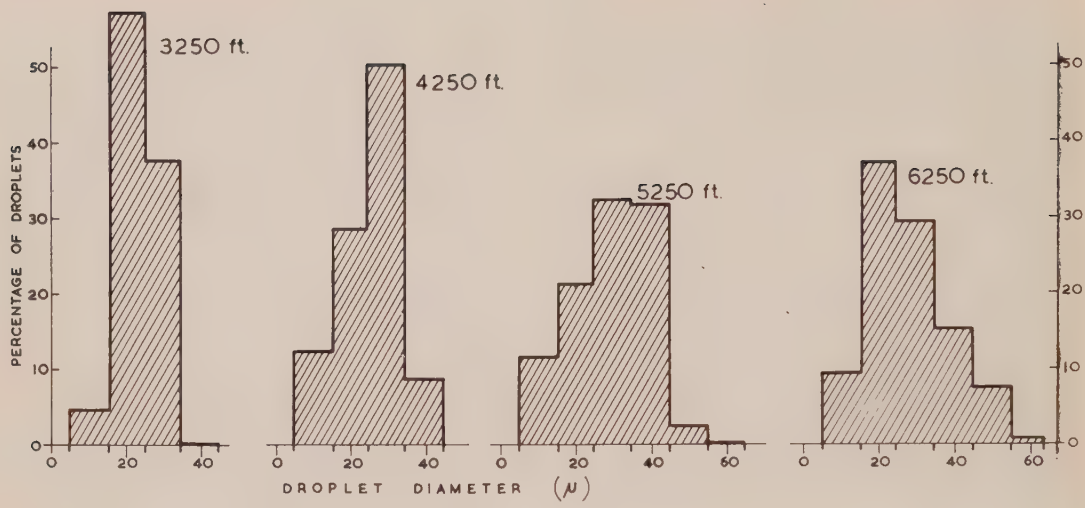

Fig. 3. The mean droplet spectrum at four levels in a tradewind cumulus off the east coast of Hawaii on 23 October 1954. Cloud base was at 2,200 ft, cloud top at 9,500 ft. There was some light rain in parts of the cloud, and turbulence was moderate. Droplet concentrations (n) per cm³ and l.w.c. (w) g per m³:

3250′, n = 74, w = 0.50;
4250′, n = 51, w = 0.53;
5250′, n = 27, w = 0.50;
6250′, n = 30, w = 0.42.

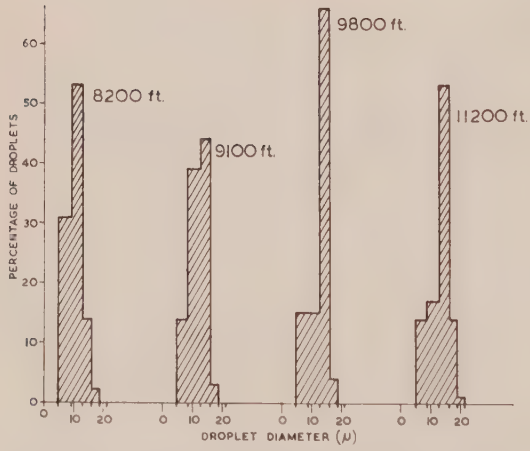

Fig. 4. The mean droplet spectrum at four levels in a continental cumulus over the Blue Mountains north-west of Sydney on 2 November 1956. Cloud base was 7,200 ft, cloud top at 12,000 ft. Droplet concentrations (n) per cm³ and l.w.c. (w) g per m³:

8,200′, n = 490, w = 0.35
9,100′, n = 270, w = 0.29
9,800′, n = 250, w = 0.31
11,200′, n = 350, w = 0.48.

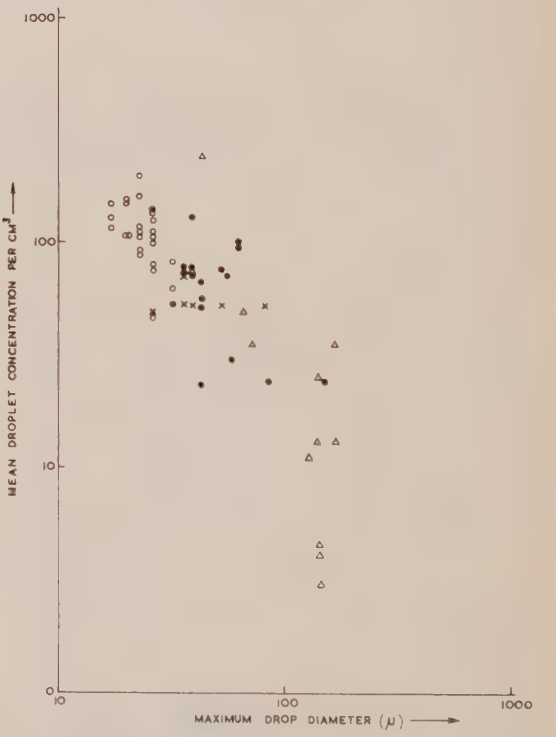

Fig. 5. Scatter diagram relating the maximum droplet diameter found in traverse of a cloud to the mean droplet concentration. Open circles, continental cumuli; full circles, maritime cumuli; triangles, the Hawaiian orographic cloud; crosses, transitional cumuli; crossed circle, layer of dark status.

through which the maximum droplet diameter decreases and the droplet concentration increases. The data used in Fig. 5 incorporate only the observations taken with a soot layer, since the earlier observations with magnesium oxide do not give a quantitative measure of droplet diameters. However, because of the association between droplet concentration and spectrum type, which is shown by Figs. 1—5, it is possible to discuss differences in microstructure in terms of droplet concentrations. This has the fundamental advantage of simplicity, and the incidental advantage that it makes it possible to use the observations made with a magnesium oxide layer, so that a considerably greater total volume of data is available. These earlier observations give only a qualitative measure of droplet sizes but they agree in a general way with those which have been measured since on soot, and in particular, show the same strong association between low droplet concentrations on the one hand, and broad spectra, and large average and maximum droplet diameters on the other.

In Fig. 6, observations in five types of clouds have been summarized. Each histogram shows the percentage of all samples in which the droplet concentrations fell within the specified ranges. The more extensive data of Fig. 6 clearly confirm the evidence of Fig. 5, and the impression given by the examples shown in Figs. 1—4.

The Hawaiian orographic cloud was always wholly warmer than freezing. In the other four groups, data have been included from clouds which had tops colder than freezing, but in no case was the temperature at the level of the cloud top lower than — 3° C, nor was

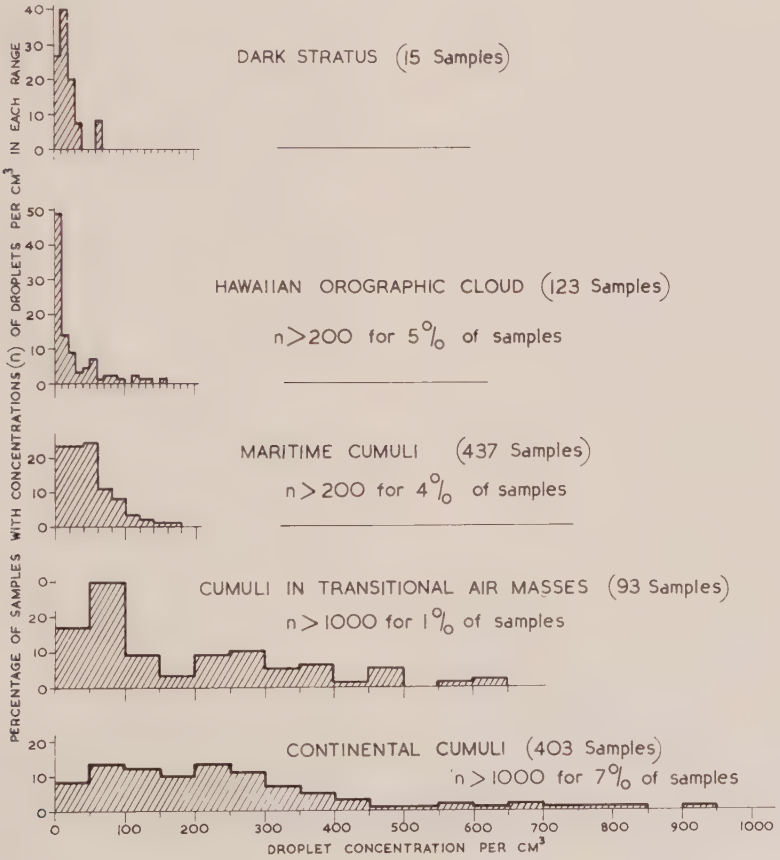

Fig. 6. Histograms of the percentages of samples taken in each of five cloud types for which the droplet concentrations fell in the ranges indicated by the graduations on the horizontal axes. The scale of concentrations is common to the five histograms.

any sign of ice seen in the clouds during the traverses. Only about one in five of the maritime, transitional, and continental cumuli reached above the freezing level and, even in these cases, about 80 % of the observations in the cloud were taken below freezing level. It may be remarked, however, that cumuli which did contain ice, and which have been excluded here, showed no systematic difference in microstructure from warm cumuli.

It will be seen from Figs. 5 and 6 that, although continental cumuli on the whole show high droplet concentrations, a proportion of the samples in these clouds gave concentrations in the range commonly found in maritime cumuli. This is partly due to the fact that dry zones occur in many clouds, in which both the liquid water content and the droplet concentration fall much below their average values. But it partly reflects the fact that continental cumuli do not invariably have high droplet concentrations. On a few days, the median concentration found in them fell below 100 droplets per cm^3.

The cumuli in transitional air masses were sometimes similar to maritime cumuli in microstructure; at other times they had median concentrations of several hundred droplets per cm^3. As a group, they differ from the continental cumuli only in that they show a greater proportion of samples with the low droplet concentrations which characterize maritime cumuli. There is however no clear association between droplet concentrations in cumuli on the one hand, and on the other, the time an air mass has spent, or the distance it has travelled, over land.

4. Colloidal structure and stability

These differences in microstructure can be related in a simple way to known differences in colloidal stability. It is only in recent years that the possibility of warm rain has been generally accepted, and practically all the documented cases of such rain describe cases where warm rain fell over the sea or nearby coastal regions (ALPERT, 1955). Observations off the coasts of Australia and off Hawaii indicate that, in a maritime air mass, warm cumuli which are 6,000 ft deep or more usually rain within half an hour, if they are not already raining when first observed. Over inland Australia, it is rare for cumuli as shallow as this to rain; more commonly, they build to considerable depths, and usually reach well above the freezing level before precipitating. There is some evidence in the literature to confirm these observations. BYERS (1956), summarizing the results of extensive observations on cumuli in the mid-west of the United States and over the Caribbean Sea, states that, for a 50 % chance of precipitating, clouds in the latter area must reach a height, in winter, of 10,000 ft; in the former, of 25,000 ft. BRAHAM et al. (1951) give data concerning the occurence of radar echoes (on 3 cm) in summertime cumuli in New Mexico. As presented, the cloud depths are not directly given, but it is possible to deduce lower bounds for the depth ranges for each group of clouds. BYERS and HALL (1955) give similar data for a 10-cm radar for wintertime cumuli over the Caribbean Sea. From their data, by assuming that the cloud base averaged 2,500 ft above the sea, the cloud depths can be deduced; this assumed height of cloud base would rarely be in error by more than 1,000 ft. The two sets of results are summarized in Table 1.

It is evident from this table that the summertime cumuli of New Mexico are much less efficient in releasing rain than tropical maritime cumuli of similar depths. This is so, despite

Table 1. Cloud depths related to the frequency occurrence of radar echoes.

Caribbean Sea (warm clouds) (after Byers and Hall)		New Mexico (after Braham et al)	
Cloud depth (ft)	Per cent of clouds with echoes	Cloud depth (ft)	Per cent of clouds with echoes
3,500—4,000	2		
4,000—4,500	4		
4,500—5,000	11		
5,000—5,500	13		
5,500—6,000	23	> 5,000—8,000	0
6,000—6,500	28		
6,500—7,000	53		
7,000—7,500	47		
7,500—8,000	73		
8,000—8,500	74		
8,500—9,000	83	> 8,000—11,000	18
9 000 and up	100	> 11,000—14,000	30

the fact that the New Mexican clouds often reach well above freezing level, so that when they do produce rain, it could be as a result of the Bergeron-Findeisen process.

Thus it appears that, in general, warm continental cumuli are colloidally stable. As shown in Section 3 above, they are usually characterized by high droplet concentrations, narrow spectra, and small droplet sizes. However, both of these generalizations are subject to exceptions. It has been pointed out that, occasionally, continental cumuli possess a more or less maritime type of microstructure. The world-wide summary of ALPERT (loc. cit.) shows that warm rain has sometimes been observed far inland. One such case has been observed; a warm cumulus, 5,000 ft deep, was seen to be raining lightly near Broken Hill, some 500 miles west of Sydney, on 13 March 1956. It was here also, on this same day, that the lowest droplet concentrations so far found in continental cumuli were measured. This observation suggests that the occasional instances of colloidal instability in continental cumuli may be associated with the occurrence of a maritime type of microstructure.

The Hawaiian orographic cloud, on most occasions when it was observed, decreased regularly in depth from about 4,000 ft at the coast to about 2,000 ft at its upslope or western edge. Nevertheless, this cloud usually produced quite significant rainfall. The amount of rain decreased steadily inland, but was still appreciable near the western edge of the cloud on some occasions.

Observers have occasionally reported seeing virga fall from "dark stratus" of a depth of 1,000 ft or less. One such case was observed off the east coast of Hawaii on 7 November 1954. A patchy layer of stratus about 500 ft thick based at 6,000 ft (14° C) was producing light rain which was first noticed when the climbing aircraft passed through the rain about 1,500 ft below the cloud.

From these examples, it appears therefore that high droplet concentrations and small average and maximum drop sizes are associated with marked colloidal stability, clouds of considerable depth failing to rain, as in the case of many continental cumuli. Low droplet concentrations, broad spectra, and large average and maximum drop size would seem to be associated with colloidal instability and the release of "warm rain", even from cloud of quite moderate depth.

5. Conclusion

Observations of cloud droplet spectra in a number of different kinds of clouds have shown that marked and systematic differences in microstructure exist, and that as between these differing cloud types, the droplet concentration in a cloud can be used as an index of the type of droplet spectrum, low concentrations being associated with broad spectra and large maximum and average droplet sizes.

Futher, it is shown that these variations in microstructure run parallel with variations in colloidal stability. In agreement with the theoretical expectation concerning the formation of raindrops by coalescence which was mentioned in the Introduction, it appears that a spectrum characterized by relatively large average and maximum droplet sizes is favourable to the operation of the coalescence process.

6. Acknowledgements

The author wishes to thank Mr. K. A. Davidson and Mr. E. Harting for their valuable work on the calibration of the method of measuring droplet sizes, and for their help in making the observations. The measurements were made in aircraft provided and flown by the Royal Australian Air Force.

REFERENCES

ALPERT, L., 1955: Notes on warm rainfall. *Bull. Amer. Meteor. Soc.*, **36**, No. 2, 64—68.

BRAHAM, R. R., S. E. REYNOLDS, and J. H. HARRELL, 1951: Possibilities of cloud seeding as determined by a study of cloud height versus precipitation *J. Meteor.*, **8**, 416—418.

BYERS, H. R., and R. K. HALL, 1955: A census of cumulus-cloud height versus precipitation in the vicinity of Puerto Rico, Winter-Spring 1953—54. *J. Meteor.*, **12**, 176—178.

BYERS, H. R., 1956: Cloud Physics Research—Final report under contract No. AF 19 (604)—618, University of Chicago, January 31, 1956.

PEARCEY, T., and G. W. HILL, 1957: A theoretical estimate of the collection efficiencies of small droplets. *Quart. J. R. Meteor Soc.*, **83**, 77—92.

SQUIRES, P., and C. A. GILLESPIE, 1952: A cloud droplet sampler for use on aircraft. *Quart. J. R. Meteor Soc.* **78**, No. 337, 387—393.

SQUIRES, P., and J. WARNER: Some observations in the orographic cloud of the Island of Hawaii and in trade-wind cumuli. *Tellus*, **9**, 475—494.

SQUIRES, P., (1956): The microstructure of cumuli in maritime and contitental air. *Tellus*, **8**, 443—444.

The Microstructure and Colloidal Stability of Warm Clouds

Part II — The Causes of the Variations in Microstructure

By P. SQUIRES, Division of Radiophysics, C.S.I.R.O., Sydney, Australia

(Manuscript received March 22, 1957)

Abstract

An attempt is made to explore the causes of the differences in microstructure between the Hawaiian orographic cloud, maritime cumuli and continental cumuli, observations on which were discussed in Part I of this series.

1. Introduction

In Part I of this series evidence has been presented to show that the Hawaiian orographic cloud, maritime cumuli, and continental cumuli form a series of cloud types, each of which is more colloidally stable that the one before; further, from the point of view of their microstructure, these cloud types form a series, each of which has typically a narrower droplet spectrum, smaller maximum and average droplet sizes, and a higher droplet concentration than the preceding one.

This parallel between colloidal stability and microstructure would be expected from the theory of raindrop growth by coalescence. It seems reasonable therefore to draw the conclusion that the variations in stability from one cloud type to another are the result of the variations in microstructure. This raises the question of the causes of these variations in microstructure.

It has been pointed out elsewhere (SQUIRES 1952b) that, although the final formation of raindrops in warm rain must occur by coalescence, the factors which determine whether a cloud shall be colloidally stable or not are most likely to operate during the condensation phase of the growth of the droplets.

In Part I of this series it was shown that the systematic differences in the type of droplet spectrum which distinguish these three kinds of cloud are associated with differences in their typical droplet concentrations. It is evident that, if only a few droplets are formed in a cloud, these must be larger than if many are formed, other things being equal. The calculations of DAS (1956) indicate that coalescence of droplets has little or no effect on the droplet spectrum as a whole. Thus it seems reasonable to suppose that the differences in microstructure are not only related to, but are very largely caused by, differences in the number of droplets which form per unit volume; this point of view forms the basis of the following discussion.

The number of droplets which form per unit volume is determined by two factors: the maximum value reached by the supersaturation, and the spectrum of critical supersaturations of the condensation nuclei present in the air. Only nuclei whose critical supersaturations are exceeded can grow by condensation to form cloud droplets. The maximum value of the supersaturation itself is determined partly by the spectrum of nuclei, and partly by the speed of the upcurrent. These two

factors are therefore likely to be among the chief determinants of the microstructure and colloidal stability of warm cloud.

Unfortunately neither of these can be measured in a manner which is effective for the present purpose. With regard to the nuclei, what is required is a spectrum of critical supersaturations of cloud nuclei; since the supersaturations in cloud are extremely small, this presents great difficulties. As for upcurrents, what is required is a knowledge of their speed in the critical region of the cloud where the supersaturation is passing through its maximum. This in itself presents difficulties over and above the instrumental ones, which are formidable.

It seems, therefore, that these crucial factors in the problem of the microstructure and colloidal stability of warm cloud are, for the present, unobservable. It will therefore often be necessary in the following exploratory discussion to rely on crude estimates of these factors.

Table 1 summarizes the data on droplet concentrations derived from the observations discussed in Part I of this series. It shows the contrast between the three types of clouds, and constitutes the quantitative basis of the following discussion.

Table 1. Data on the frequency distribution of values of the droplet concentration in three types of cloud. (Number of droplets per cm³).

Cloud Type	Hawaiian Orographic Cloud	Maritime Cumuli	Continental Cumuli
1st quartile droplet concentrations	4	22	119
Median droplet concentration	10	45	228
3rd quartile droplet concentration	30	70	310
Maximum droplet concentration observed	370	470	2,800
Total number of observations	123	438	403

2. The effect of the upcurrent — the contrast between the Hawaiian orographic cloud and maritime cumuli

The Hawaiian orographic cloud forms in an unmodified maritime air mass. The difference in microstructure between this cloud and maritime cumuli must therefore reflect the influence of factors other than that of the spectrum of condensation nuclei. Chief among these would appear to be (a) the rate of rise of the air forming the cloud, and (b) the total time available for the subsequent evolution of the droplet spectrum, that is, the average lifetime of a parcel of cloud. This average lifetime may be considerably longer in the orographic cloud than in cumuli. Since the cloud mass usually fills the space between the ground and the trade-wind inversion, it is reasonable to take this lifetime to be (at a maximum) some 2 to 4 hours, for the width of the cloud along the wind is some 20 nautical miles, and typical horizontal wind speeds during the period of the observations were 5—10 kt.

However, according to the observaions of Squires and Warner (communicated), there is only a slight change in the droplet concentration in the orographic cloud from near the coast to near its western or inland edge. This indicates that a difference in rate of rise may be the major cause of the contrast between maritime cumuli and the orographic cloud, at least in its lower reaches. Indeed, since the slope of the ground is nearly constant, about 5 %, the average vertical velocity of the air forming the orographic cloud must have been in the region 15—25 cm sec^{-1}. In contrast, the vertical currents in trade wind cumuli have been found by Malkus (1953) to be normally some metres per second; Byers (1956) states that the average growth rate of cumulus clouds and of the radar echoes found in some of them over the Caribbean Sea was "of the order of 300 to 400 ft per minute".

Howell (1949) has illustrated by numerical examples how, in a steadily rising air parcel, the supersaturation (S) of the air at first increases rapidly, but soon reaches a maximum (S_m) and begins to decrease. Howell found that, once a nucleus is activated, that is, grows past its critical size and forms a cloud droplet, there is very little tendency for it to re-evaporate to a nucleus, even though S decreases as the air parcel continues to rise. Since the value of S_m determines how many nuclei will be activated, it also determines essentially the concentration of droplets which will be found at later stages of the process. It is evident that S_m will be influenced by the speed of the up-

current. One of HOWELL's examples illustrates the dependence of this maximum supersaturation (S_m) on the upcurrent; with a fixed number of homogeneous nuclei, S_m increases by a factor of about 5 when the upcurrent is increased ten times. In the atmosphere, with its heterogeneous content of nuclei, the number of drops formed will of course increase as S_m increases, since more nuclei will be activated. These additional drops will restrain the rapid rise of S, so that one might expect that a ten-fold increase in upcurrent would result in an increase in S_m, but probably rather less than five-fold.

As applied to a cumulus, these ideas refer specifically to the region of active upcurrent; in surrounding regions, smaller or even negative upward velocities no doubt occur, but these regions play no part in the original formation of the cloud mass, and are not likely to exert much influence on the microstructure of the cloud as a whole. It is therefore reasonable to discuss this problem in terms of the typical upcurrents found in the cloud, as given above.

The supersaturation, S, is related at any moment to the difference between the liquid water which has become available since saturation was reached, and the total mass of the cloud droplets already formed. The characteristic maximum of S is partly due to the shape of the equilibrium vapour pressure curve over a nucleus. It is also partly due to the fact that the absorptive power of the forming cloud drops is small at first; consequently, water is not removed from the vapour phase rapidly enough to prevent the supersaturation increasing as the air ascends. Leaving aside for the moment the complications which arise from the unknown sizes of the nuclei which form droplets, let us suppose that the droplets are of uniform size, grow from zero radius at the condensation level, and that they have equilibrium vapour pressures equal to that over a plane water surface. Equations relating to the behaviour of S have been developed elsewhere (SQUIRES, 1952a). Using the same terminology and symbols, let r be the radius of the droplets, n their number per gram of air, v the upcurrent, z the height above the condensation level, and S the supersaturation expressed as the excess of the dew-point of the air over its temperature in deg. C.

Then, as shown in Appendix A, it results that the maximum value of the supersaturation, S_m, is given by:

$$S_m = 0.73 \, v^{3/4} \, n^{-1/2}. \qquad (1)$$

Now it is obvious that when the upcurrent is increased, smaller nuclei will be utilized for cloud formation, on the average. Also, the more or less saline droplets already existing at the cloud base on the larger nuclei will have less time in which to exercise their restraining influence on the growth of S. This equation therefore tends to underestimate the relative effect of increasing upcurrent on S_m. In order to use it to compare the maritime cumuli with the Hawaiian orographic cloud, it is necessary to assume something about the spectrum of the nuclei, or rather, of the critical supersaturations of the nuclei. For this purpose we may take the law of distribution of aerosols given by JUNGE (1954) according to which the number of nuclei of radius r to $r+dr$ is proportional to r^{-4}. The number between r_1 and r_2 is then proportional to $(r_2^{-3} - r_1^{-3})$ The total number with radius $\geqslant r_2$ is therefore proportional to r_2^{-3}, provided r_1 is appreciably bigger than r_2. If we assume that the nuclei are all of similar material or mixture of materials, the effective molar mass (M) of a nucleus is proportional to r^3. The critical supersaturation of a nucleus, S_c^*, is proportional to $M^{-1/2}$. The number of nuclei with critical supersaturations less S_m is therefore proportional to S_m^2. Combining this with equation (1) gives the result that, in a given air mass,

$$\begin{aligned} S_m &\propto v^{3/8}, \\ n &\propto v^{3/4}. \end{aligned} \qquad (2)$$

If therefore the characteristic upcurrents in maritime cumuli exceed those in the orographic cloud by a factor of 5 to 10, the droplet concentrations should stand in a ratio of 3.3 to 5.5 or, in view of the underestimation of the effect of increasing v in this treatment, rather more.

Taking into account the rather wide fluctuations of droplet concentration observed in any one cloud, the approximate nature of JUNGE's law of distribution of aerosols, and the errors which can arise from using Raoult's law of vapour pressures, this result seems to be in reasonable agreement with the ratio of the

medians of the measured concentrations, as given in Table 1, namely 4.5. It may be concluded that the difference in microstructure between maritime cumuli and the Hawaiian orographic cloud is sufficiently well explained by the difference in upcurrent.

3. The contrast between maritime and continental cumuli

The contrast between continental and maritime cumuli is even more marked than that just discussed. Byers (1955) attributes the notable difference in colloidal stability between cumuli over the Caribbean Sea and over the mid-west of the United States to the fact that cumuli grow rather more rapidly in the latter region, pointing out that the coalescence process needs time to operate. This difference in rate of growth no doubt reflects a systematic difference in upcurrent.

However, over the group of *warm* clouds sampled during the measurements of droplet spectra, no such systematic difference was in evidence. No measurements were made of upcurrents, but the observer's notes of turbulence, classified on a scale of 1 to 5, show that the maritime and continental cumuli sampled were about equally turbulent. On the whole, the maritime cumuli were slightly deeper than the continental ones; because of their higher bases, continental cumuli of any great depth are likely to reach far above freezing level, and form ice. The possibility therefore appears that, on the whole, the maritime cumuli might have had slightly stronger upcurrents than the continental ones. This difference, if it were real, would be in the wrong sense to explain the observed difference in microstructures. The only measurements which bear on this question are photographic records taken on the ground during some of the 1956 measurements of continental cumuli in inland Australia. These showed that the rates of growth of cumulus tops were mostly in the range 200 to 400 feet per minute; this is quite comparable with the values given by Byers (1956) for cumuli over the Caribbean Sea, namely 300 to 400 ft per minute. Thus it seems unlikely that a systematic difference in upcurrent contributed in any notable way to the observed difference in microstructure between maritime and continental cumuli.

Cumuli vary considerably in their persistence as recognizable individual entities. It might be expected that, in a long-lasting cloud, the microstructure would undergo some evolution, presumably in the direction of a decrease in droplet concentration. The tendency for the droplet concentration to decrease upwards in cumuli (Zaitsev, 1950) could be taken as suggesting this. However, it is quite possible that, even in such cloud, the lifetime of individual parcels of cloud is much the same as in less durable clouds. Certainly, no striking difference in microstructure has been found which related to the persistence of the cloud as a whole. There is indeed a tendency for the clouds of continental air masses to be more durable than those of maritime air masses; this is perhaps a reflection of some difference in the pattern of convection, and if it were relevant at all would apparently work in the wrong direction to explain the observed difference in microstructure.

It seems reasonable therefore to seek the cause in the spectra of the condensation nuclei; this spectrum, together with the upcurrent, must determine the course of events in the critical region near the cloud base where the supersaturation passes through its maximum, and the character of the microstructure of the cloud is determined. It is known that there are certain differences between the maritime and the continental aerosol. According to Landsberg (1938), the mean count of Aitken nuclei found over the continents, 9,500 cm^{-3}, is about ten times that found over the ocean, 940 cm^{-3}. Woodcock (1953) has measured the giant nuclei, that is, those of diameter about 1 micron and larger, in the maritime aerosol and found that they are predominantly sea salt. At a given height above the sea, the number of these giant nuclei is a function of the strength of the surface wind. Twomey (1954; 1955) has made similar measurements in a maritime air mass moving inland. He found that even far from the sea nearly all the giant particles consist of either sea salt or sodium chloride. The concentration of these particles at distances of up to 700 miles inland was found to be sometimes quite comparable with that measured at the coast; intensified mixing over the land had merely redistributed them in the vertical without seriously changing the total number present. However, convective showers

over the land were efficient in removing the salt particles from the atmosphere, and appeared to be capable of reducing the number of these particles by a factor of the order of 100. Thus continental air masses may often be deficient in giant nuclei compared with maritime air masses.

The Aitken count itself has of course no direct bearing on the microstructure of clouds, since the majority of the particles included in it never become cloud nuclei, that is, they are not utilized in the formation of cloud; if LANDSBERG's mean values were taken as typical of the sub-cloud layer, it would appear that on the average only about one Aitken particle in twenty succeeded in becoming the nucleus of a cloud droplet in maritime air and one in forty in continental air. LANDSBERG's figures do however indicate that the continents can be sources of Aitken nuclei; it is possible therefore that the continents also add to the atmosphere a number of particles which, while not as large as the giant sea-salt nuclei, are large enough to be utilized in cloud formation.

The giant sea-salt nuclei reach concentrations of 1 cm^{-3} only with very strong winds over the sea. They cannot account therefore in themselves for more than a small fraction of the cloud droplets. Nevertheless, they may be important in two ways. WOODCOCK (1952) has suggested that, by forming relatively large droplets, they may act to trigger off the formation of rain by the coalescence process. Since however, in the observations discussed in Part I of this series, a large proportion of the samples were taken in cumuli which were not raining, this process alone cannot account for the contrast in microstructure between maritime and continental cumuli. It seems possible however that sea-salt nuclei could influence the microstructure of cumuli in another way. KEITH and ARONS (1954) have shown that, at cloud base, these nuclei have already formed droplets with diameters of several microns, or even tens of microns. Thus the giant nuclei must have the effect of reducing the maximum value reached by the supersaturation a little above cloud base. In this way they could indirectly affect the microstructure by restricting the number of nuclei which become activated and grow to cloud droplets.

There would appear therefore to be two possible ways in which a difference between the maritime and the continental aerosol could account for the difference in microstructure between maritime and continental cumuli:

(a) The addition of cloud nuclei to the air from some continental surfaces.

(b) The reduction of the supersaturation in cloud by giant sea-salt nuclei, which are on the whole more numerous in maritime air.

The following discussion has as its aim to show that the second of these possibilities is improbable; in effect, to show that, with likely values of the upcurrent, the concentrations of giant sea-salt nuclei which occur at cloud base levels are not great enough to produce the effect proposed.

It will be assumed, for the moment, that the only significant difference between the maritime and the continental aerosols is that the former is rich in giant sea-salt nuclei and the latter devoid of them. The argument will be concerned with a comparison of the supersaturation of cloud air in maritime and continental cumuli. It will be shown that, in the region of active upcurrent, and above the level where S passes through its maximum, the supersaturation is typically greater in maritime than in continental cumuli. This is contrary to what one might expect if it were true that the more numerous giant nuclei of maritime air masses were effective in restricting the number of droplets forming in maritime cumuli by depressing the supersaturation.

It has been shown elsewhere (SQUIRES, 1952a) that, in the body of a cloud after S has passed through its maximum value and is slowly decreasing, a fairly good approximation to S is given by:

$$S = (0.024v + 1.7 \times 10^{-6}n - 64.4\Sigma(M/r^2))/\Sigma r \quad (3)$$

where M is the effective molar mass of the nucleus in a drop of radius r, and the summations are extended over all the droplets in 1 gram of air. The numerical values are for 10° C, 800 mb. The first term in the numerator is related to the rate at which water is becoming available, the second to the raising of the equilibrium vapour pressure over the droplets by capillarity, and the third to its reduction by the dissolved nuclei. The denominator is a measure of the absorptive power of the cloud for water vapour. The effect of ventilation of the droplets, which is small, is neglected. Consider a maritime cumulus, with $n \approx 4.5 \times 10^4$

per gram of air (see Table 1), and an upcurrent of 1 m sec^{-1}, or more. The first term dominates in the numerator. Its value is at least 2.4; that of the second is 0.076, but the third term is more difficult to evaluate. It is shown in Appendix B that, under the conditions occurring at the time when the maritime observations were made, it could not have exceeded 0.27.

Hence, from (3), in a typical maritime cumulus, with $n = 4.5 \times 10^4$ droplets per gram of air.

$$(0.024v + 0.08)/\Sigma r > S > (0.024v - 0.19)/\Sigma r \quad (4)$$

In a typical continental cloud, with $n = 2.3 \times 10^5$ droplets per gram of air (see Table 1) the second (capillarity) term in the numerator of (3) is more important, viz. 0.39. The third term, which is essentially negative, need not concern us. We have

$$S > (0.024v + 0.39)/\Sigma r \quad (5)$$

in a typical continental cumulus.

From the data of Table 1, it is obvious that, for a given liquid water content, Σr must be much larger in continental than in maritime cumuli. Thus in the maritime cumulus of Fig. 3, of Part I of this series, the average value of Σr was 71 cm per gram of air, and in the continental cumulus of Fig. 4 of Part I, the average value was 184 cm per gram of air, or 2.6 times greater. As mentioned in Part I, a large proportion of the observations in both maritime and continental cumuli were made using a magnesium oxide layer, so that the values of Σr cannot be deduced. In order to make use of the whole of the observations, one may estimate that, for a given liquid water content, Σr will be very roughly proportional to the two-thirds power of the droplet concentration, treating the drops for this purpose as homogeneous. Since the data of Table 1 indicate that a typical continental cumulus has a droplet concentration about five times as great as a typical maritime cumulus, this would indicate that Σr would be about three times greater in the continental cloud. As mentioned in Part I, the continental cumuli form a rather heterogeneous group. Thus, one may conservatively estimate that, over a substantial proportion, and probably a majority, of continental cumuli, the value of Σr will be at least 2.5 times greater than in a comparable maritime cumulus.

It may be remarked here that Σr does not show much change with height in a cumulus; the slow upward increase in liquid water content implies only a small change in mean droplet radius, and this is largely offset by a tendency for the droplet concentration to decrease slightly with increasing height.

On this basis then, comparing similar maritime and continental cumuli with the same upcurrent, we may write:

$$\frac{S_{mar}}{S_{cont}} > \frac{2.5(0.024v - 0.19)}{(0.024v + 0.39)} \quad (6)$$

from the inequalities (4) and (5). S_{mar} and S_{cont} represent the supersaturations at similar levels in the body of each cloud, that is, above the region where S passes through its maximum. As pointed out earlier, over the groups of clouds in which samples have been taken, it is justifiable to take the upcurrents as being equal, on the average.

The values of the ratio on the right-hand side of (6) are shown in Table 2, for various values of the upcurrent.

Table 2.

Upcurrent v cm sec^{-1}	$S_{mar}/S_{cont}>$
20	0.8
50	1.6
100	2.0
200	2.2
300	2.3

The measurements of upcurrent and cloud growth rates already mentioned indicate that a typical upcurrent is about 1 m sec^{-1} or slightly more; hence it would seem that, in the body of the cloud, in a region of active upcurrent, the supersaturation is typically about twice as great in a maritime as in a continental cumulus.

This discussion applies only to the body of the cloud, that is, the region above the level where S, after having passed through a maximum, is now decreasing slowly. It does not follow from the above argument that the maximum value of the supersaturation (S_m) is twice as great in a maritime as in a continental cumulus. If however the supposition were true that the giant sea-salt nuclei, by lowering S_m, were the prime cause of the low droplet

concentrations in maritime cumuli, and that other differences between the continental and maritime aerosols had little influence on the microstructure of cumuli, the result found above would be surprising. For, as shown in the derivation of equation (2) above, JUNGE's law of distribution of aerosols (JUNGE, 1954) would in that case suggest that S_m should be about $5^{1/2}=2.2$ times *smaller* in the maritime cumuli.

If, as these arguments suggest, the giant sea-salt nuclei are not primarily responsible for the continental-maritime contrast in cumulus microstructure, it seems reasonable to suspect that the chief cause may be found in the first possibility mentioned above, namely, the addition of cloud nuclei to the air from some continental surfaces.

It seems possible, for example, that unmodified maritime air masses may be relatively poor in nuclei in the size range called "large particles" by JUNGE (1954) ($0.8\mu > d > 0.08\mu$) but that when such an air mass moves inland, it may pick up these particles. The conclusion reached by JUNGE (communicated) that the large particles are primarily of continental origin would suggest this. If the concentration of particles of this kind should rise to some hundreds per cm^3 over the continent, the high droplet concentrations found in continental cumuli with low supersaturations are readily explained.

4. Conclusions

An exploratory attempt has been made to evaluate the causes of the differences in microstructure between the Hawaiian orographic cloud, maritime cumuli and continental cumuli. As regards the contrast between the first two, which both form in an unmodified maritime air mass, it has been shown that the relatively slow upcurrent in the orographic cloud affords a sufficient explanation.

The striking difference between maritime and continental cumuli cannot be explained in terms of a difference in upcurrent, or in the total lifetime of parcels of cloud. It seems likely that it originates from a difference between the maritime and continental aerosol. On the basis of an approximate formula for the supersaturation of cloud air, it is concluded that the giant sea-salt nuclei are not primarily responsible for this difference; it seems more likely that the operative difference between the maritime and the continental aerosol occurs in the size region below that of the giant sea-salt particles, namely in that of the "large particles" continental air being richer in nuclei of this size than maritime air.

Unfortunately, a wide gap separates the lower end of the spectrum of giant nuclei, which can be studied individually by impaction methods, from the size range where graduated expansions might be useful in yielding a spectrum of critical supersaturations. Observations of droplet spectra in natural clouds might possibly be a means of bridging a portion of this gap, provided upcurrents can be measured simultaneously.

If indeed it should be found that the contrast in microstructure between maritime and continental cumuli is largely caused by cloud nuclei originating over the continents, this could have important implications for those experiments where attempts are made to modify warm continental cumuli by seeding them with salt particles. The conclusions mentioned in the Introduction indicate that the marked colloidal stability of continental cumuli is at least partly due to the fact that the average and maximum droplet sizes found in them are small and rather uniform compared with those in maritime cumuli. Since natural sea-salt particle concentrations are inadequate to seriously affect the microstructure of cumuli, it does not seem likely that artificially produced hygroscopic particles would. On the other hand, it may perhaps be possible to modify to some extent the microstructure of cumuli forming in a maritime air mass in such a manner as to increase their colloidal stability. On the views outlined above, this could be attempted by adding to the cloud-forming air a sufficient number of cloud nuclei. The number of particles required, of the order of a hundred per cm^3, is much greater than is usually considered necessary in seeding clouds; on the other hand, the particle size required would certainly be much smaller.

Appendix A

An evaluation of the effect of upcurrent on the maximum value reached by the supersaturation.

Using the physical model described in the main text in Section 2, and the symbols de-

fined there, it has been shown elsewhere (SQUIRES, 1952a) that:

$$S = az - bnr^3 \qquad \text{(A1)}$$

where $a = \frac{g}{J}\left(\frac{1}{c_p} - \frac{T}{L\varepsilon}\right)$

$$b = \frac{4\pi}{3}\left(\frac{L}{c_p} + \frac{\varrho R T^2}{JL\varepsilon^2 e}\right)$$

and, neglecting the very small effect of ventilation of the small droplets,

$$\frac{r dr}{dt} = ES \qquad \text{(A2)}$$

where $E = \varepsilon^2 L^2 DJe/RT^3\left(1 + \frac{\varepsilon^2 L^2 DJe}{kR^2T^3}\right)$

where L is the latent heat of water vapour,
D the coefficient of diffusion of water vapour in air,
k the thermal conductivity of air,
ε the specific gravity of water vapour with respect to air,
ϱ the density of air,
R the gas constant of air per gram, and the other symbols have their usual meanings. At 10° C, 800 mb,

$$a = 7.9 \times 10^{-5}$$
$$b = 1.68 \times 10^{4}$$
$$E = 6.6 \times 10^{-8}$$

From (A 1) and (A2) $r\frac{dr}{dt} = Eavt - Ebnr^3 \qquad \text{(A3)}$

if t is measured from the moment of passing the condensation level where $S = 0$, $r = 0$. Putting

$$r = y(Eav)^{1/4}\ (nEb)^{-1/2}$$
$$t = x(Eav)^{-1/4}\ (nEb)^{-1/2}$$

the equation (A3) becomes:

$$\frac{dy}{dx} = \frac{x}{y} - y^2. \qquad \text{(A4)}$$

A series solution of (A4) through the origin has been obtained. The value of S in terms of x and y is given by:

$$ES = (Eav)^{3/4}(nEb)^{-1/2}(x - y^3)$$

which is a maximum when

$$x = y^3 + \frac{1}{3y}$$

This curve intersects the solution curve of (A4) near $x = 0.86$, $y = 0.74$, so that

$$S_m = 0.46\ E^{-3/4}\ a^{3/4}\ b^{-1/2}\ v^{3/4}\ n^{-1/2}$$

or, substituting the numerical values already quoted for E, a and b

$$S_m = 0.73\ v^{3/4}\ n^{-1/2}.$$

Appendix B

An evaluation of the effect of condensation nuclei in depressing the supersaturation in the body of a maritime cumulus.

This effect is taken into account by the last term in the numerator of equation (3) of the main text. Consider first the contribution to $\Sigma(M/r^2)$ due to droplets containing giant sea-salt nuclei. WOODCOCK (1953) gives cumulative distribution curves for the spectra of sea salt over the sea near cloud base for various wind strengths and at a number of widely separated places. TWOMEY (1955) has given similar data which are in good agreement with WOODCOCK's. It seems that the spectrum of giant nuclei at cloud base level in a maritime air mass is fairly well defined by surface wind force alone, irrespective of geographical position. The wind strengths estimated over the sea during the measurements on maritime cumuli both off Australia and near Hawaii did not reach force 7. If therefore WOODCOCK's data for force 7 wind off Hawaii are used, an upper estimate of the effect of the giant nuclei can be derived. It is convenient to replace the observed spectrum by a distribution in groups as shown in Table B1, where the observed spectrum given by WOODCOCK is shown on the left, and the substituted group distribution on the right. It is obvious that the substituted spectrum dominates the observed spectrum for an air density of 0.98 g cm^{-3}, corresponding to 800 mb, 10° C.

Table B1

Observed spectrum of sea-salt nuclei for a force 7 wind near cloud base (after Woodcock)		Substituted group spectrum per gram of air	
Mass of nuclei $\mu\mu g$	Number of nuclei per m^3 of mass greater than that shown in the first column	Mass of nuclei $\mu\mu g$	Number of nuclei of this mass per gram of air
1	800,000		
10	200,000	10	555
100	40,000	100	165
1,000	5,000	1,000	35
10,000	150	10,000	5
100,000	<1	100,000	0.15
		1,000,000	0.001

KEITH and ARONS (1954) have given curves for the growth of sea-salt particles in rising air, up to the cloud base. We may safely take their values as giving lower limits for the droplet radii inside the cloud. The values are quoted for upcurrents of 0.5, 1.0 and 2.0 m sec^{-1}; the effect of speed in this range is small. Taking the smallest values, those for $v=2$ m sec^{-1}, we get the results shown in Table B2.

Table B2

Mass of nucleus (m_s) $\mu\mu$ g	Radius at cloud base (r) μ	m_s/r^2 10^{-4} ×	Number assumed per gram	Product
10	6	0.28	555	0.016
10^2	10	1.0	165	0.017
10^3	17	3.5	35	0.012
10^4	33	9.2	5	0.005
10^5	57	31	0.15	0.000
10^6	87*	132	0.001	0.000
				Total $= \sum\left(\frac{m_s}{r^2}\right) =$ 0.050

* A rough lower bound found by extrapolating by a tangent the curve given by KEITH and ARONS, which is concave towards the axis of r.

The total of $\Sigma m_s/r^2$ is therefore certainly less than 0.050. Treating sea salt as ionically dissociated sodium chloride $M=m_s/29$; hence $\Sigma M/r^2<0.0017$; the contribution to the last term in the numerator in equation (3) from droplets formed on giant sea-salt nuclei is therefore less than 0.11.

As mentioned earlier, only with very strong winds does the concentration of giant sea-salt nuclei reach 1 per cm^3. This is small compared with the concentration of cloud droplets. It remains to make an estimate of the contribution to $\Sigma(M/r^2)$ due to the cloud drops formed on nuclei too small to be observed by the impaction method, that is, below about 1 $\mu\mu$g. JUNGE (communicated) has studied the maritime aerosol in the Hawaiian Islands in two size groups—giant particles ($r=8\mu$ to $0.8\ \mu$) and large particles ($r=0.8\ \mu$ to $0.08\ \mu$). He analysed the two components for NH_4, NO_3, Cl and SO_4. The average total mass of all these constituents in the form of giant particles was 5.8 μg per m^3; in the form of large particles, 0.18 μg per m^3. If, as the analyses of fog and cloud water made by HOUGHTON (1955) indicate, these components are an important fraction of the total aerosol in the "large particle" range, it is evident that the total mass of the large particles can hardly exceed ten times the concentration found by JUNGE—that is, 1.8 μg per m^3. On the basis of measurements at various places, JUNGE (communicated) considers that the large particles are primarily of continental origin; their total mass concentration over the sea would not therefore be affected by wind strength, unlike that of the giant sea-salt particles. If therefore all the cloud drops not formed on giant nuclei are formed on large particles, the total mass of nuclear material cannot exceed 1.8 μ g per m^3 or about 1.8×10^{-9} g per g of air.

It is easily shown that nuclei below JUNGE's lower limit for larger particles ($r=0.08\ \mu$) make no significant contribution. Their masses must be less than 4×10^{-15} g, if a density of 2 g cm^{-3} is assumed. Hence the total mass in the cloud drops (assumed not to exceed 4.5×10^4 per gram in number) in a gram of air could not exceed 1.8×10^{-10} g. Thus the total mass of the nuclei in the cloud droplets, apart from the giant particles, cannot exceed 2×10^{-9} g per gram of air. The effective molar mass must be less than about 10^{-10} per gram of air, since no likely material, even when completely dissociated, has an effective molecular weight of less than 20.

The observations of droplet spectra in maritime cumuli show that only a very small minority (about 1 %) of the droplets are smaller than $d = 4\ \mu$. Hence the total contribution to $\Sigma(M/r^2)$ from droplets formed on particles smaller than giant sea-salt nuclei must be less than $10^{-10}/4 \times 10^{-8} = 25 \times 10^{-4}$. Their contribution to the third term of the numerator in equation (3) is therefore less than 0.16; and the total value of the third term, including nuclei of all sizes, must be less than 0.27.

REFERENCES

Byers, H. R., 1955: Geographical differences in cloud populations. *Archiv für Meteor., Geophys. und Biokl.*, **8**, No. 3, 180—184.

— 1956: Cloud Physics Research—Final report under contract No. AF 19(604)—618, University of Chicago, January 31, 1956.

Das, P. K., 1956: The change in the distribution of drops in a cloud. *Indian J. of Meteor. and Geophys.*, **7**, 55—59.

Houghton, H. G., 1955: On the chemical composition of fog and cloud water. *J. Meteor.*, **12**, 355—357.

Howell, W. E., 1949: The growth of cloud drops in uniformly cooled air. *J. Meteor.*, **6**, No. 2, 134—149.

Junge, C., 1954: The chemical constitution of atmospheric aerosols. Measurements at Round Hill Field Station, June—July 1953. *J. Meteor.*, **11**, No. 4, 323—333.

— (communicated): The chemical constitution of atmospheric aerosols and gas traces. II—Measurements on the Island of Hawaii.

Keith, C. H., and Arons, A. B., 1954: The growth of sea-salt particles by condensation of atmospheric water vapour. *J. Meteor.*, **11**, 173—184.

Landsberg, H., 1938: Atmospheric condensation nuclei. *Ergebnisse der kosmischen Physik*, **3**, 155—252.

Malkus, J. S., 1953: Marine Meteorology: Some results of a trade-wind cumulus investigation. Woods Hole Oceanographic Institution, Tech. Rep. **23**, Ref. No. 53—30, May, 1953. (Unpublished manuscript).

Squires, P., and Warner, J.: Some observations in the orographic cloud of the Island of Hawaii and in trade-wind cumuli. *Tellus*, **9**, 475—494.

Squires, P., 1952a: The growth of cloud drops by condensation. I—General characteristics. *Aust. J. Sci. Res.* A5, No. 1, 59—86.

— 1952b: The growth of cloud drops by condensation. II—The formation of large cloud drops. *Aust. J. Sci. Res.* A5, No. 3, 473—499.

Twomey, S., 1954: The composition of hygroscopic particles in the atmosphere. *J. Meteor.*, **11**, 334—338.

— 1955: The distribution of sea-salt nuclei in air over land. *J. Meteor.*, **12**, 81—86.

Woodcock, A. H., 1952: Atmospheric salt particles and raindrops. *J. Meteor.*, **9**, 200—212.

— 1953: Salt nuclei in marine air as a function of altitude and wind force. *J. Meteor.*, **10**, 362—371.

Zaitsev, V. A., 1950: Water content and distribution of drops in cumulus clouds. Glavaia Geofizicheskaia Observatoria, Trudy, **19**, 122—132.

Some Observations Relating to the Stability of Warm Cumuli

By P. SQUIRES and S. TWOMEY, Division of Radiophysics, C.S.I.R.O., Sydney, Australia

(Manuscript received February 25, 1956)

Abstract

Simultaneous observations of giant sea-salt nuclei and droplet spectra in cumuli have shown that variations in the concentration of these nuclei have no direct effect on the microstructure of cumuli.

1. Introduction

It is known that there is a marked difference between continental cumuli and maritime cumuli in stability and duration and even in appearance. Continental cumuli are "hard" in appearance, with sharp outlines and flat well defined bases; even from clouds several km deep, precipitation is relatively infrequent unless ice forms in them, and clouds of this size often persist for an hour or more without precipitating or dissipating. Maritime cumuli, on the other hand, have outlines which are not so sharp and bases which are often very ragged; their lifetime is generally well under one hour: precipitation usually occurs in warm clouds which are more than 2 km deep, and is often observed in clouds of much lesser depth.

Observations of cloud droplet size and concentration (SQUIRES communicated [a]) suggest that some of these differences in appearance and behaviour can be attributed to difference in the drop-size spectra. Continental clouds, in air which has been over land for two days or more, are characterized by narrow spectra and high droplet concentrations, maritime clouds by broad spectra and low droplet concentrations. The median droplet concentration found in non-icy continental cumuli was 228 cm^{-3} (403 observations); and in non-icy maritime cumuli, 45 cm^{-3} (438 observations). There was no systematic difference in liquid water content between the two types of cloud. Thus the colloidally unstable maritime clouds contain a small number of droplets, some of which are fairly large, while the relatively stable continental clouds contain large numbers of small and almost equal droplets. Rapid evaporation of small droplets may partly explain the sharp outlines of continental cumuli, while the presence of larger droplets, which evaporate less rapidly, could account for the less distinct outlines of maritime cumuli.

In order to explain how widely differing droplet spectra are found in clouds of similar dimensions, updraught, turbulance and liquid water content, it seems logical to consider the effects of the condensation nucleus spectrum A plausible hypothesis is provided by considering the effects of giant sea-salt nuclei. When present in large numbers in ascending cloud air these absorb water, and if this occurred at a rate comparable to the rate of release of water by the adiabatic cooling, the water vapour supersaturation could not rise to a large value and only those nuclei active at small supersaturations could form

cloud droplets; if, however, few or no salt particles were present, a higher supersaturation could be reached and so more nuclei would be activated and more cloud droplets formed. However, this hypothesis neglects the possibility that there are other important differences between the spectra of condensation nuclei in maritime and continental air, namely, in the size range below that of the giant nuclei. It is possible to test the hypothesis which has been described if observations of cloud drop spectra can be compared with simultaneous observations of sea-salt nucleus spectra, and in this paper the results of some such comparisons are presented. Clearly, if this hypothesis were true, one would expect that in air with a large content of giant sea-salt particles, cumuli would tend to have low droplet concentrations and broad spectra; and vice-versa.

2. Observations

During experimental flights simultaneous observations of sea-salt and cloud-drop spectra have been made on several occasions. Cloud drops were sampled on soot-covered glass rods using a cloud droplet sampler (SQUIRES and GILLESPIE 1952) while sea-salt nuclei were sampled by direct impaction on glass slides (WOODCOCK and GIFFORD 1949).

Cloud droplet samples were taken at each of several levels in one or more clouds, while one salt nucleus sample was usually taken near cloud base and another above the cloud tops. Cloud drop sampling was almost instantaneous, but the collection of one complete salt nucleus sample involved exposing several slides and occupied 15—30 minutes. Results for one flight usually consisted of sea-salt nucleus spectra at two altitudes and several dozen cloud droplet spectra. However, the use of spectra is necessarily cumbersome and as the shape of the spectra did not vary greatly (excepting the association between narrow spectra and high droplet numbers, in the case of cloud droplets), the results of each flight have been reduced to the following simpler quantities: in the case of salt nuclei, the concentration per m^3 of salt nuclei greater than 10^{-10} g, measured at cloud base; in the case of cloud droplets, the median value of the concentration of droplets per cm^3. These quantities, denoted by the symbols N and n respectively, have been plotted in Fig. 1 for twelve flights made over land, in air masses which had travelled at least 500 miles since crossing the coast.

3. Discussion

It will be seen from Fig. 1 that the droplet concentrations found in inland cumuli covered a wide range; indeed, even in air masses which had been over land for longer than two days, the value of n was sometimes little more than the median value for maritime cumuli (45 droplets per cm^3). It is apparent also that these maritime-type cumuli were associated, over the land, with the lowest observed concentrations of giant sea-salt nuclei. The higher values of n, on the other hand, were associated with high concentrations of giant sea-salt nuclei, concentrations which were in fact similar to those found at cloud base level in maritime air in conditions of light wind (N of order 1,000 m^{-3}). In maritime air masses, the plot of N against n must be very different from that shown in Fig. 1,

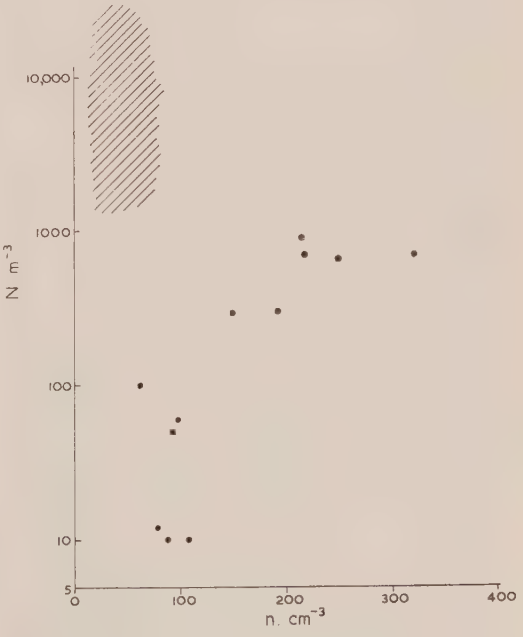

Fig. 1. Scatter diagram showing a positive correlation between the concentration of cloud droplets in inland cumuli (n) and that of giant sea-salt nuclei (N), near cloud base level. Corresponding points for maritime cumuli would fall in hatched area.

for N usually lies in the range 10^3 to 5×10^4, and the value of n (the median droplet concentration found on one flight) has never exceeded about 80 cm^{-3}; as mentioned earlier, it averages about 50 cm^{-3}.

These results are the antithesis of what would be expected to occur on the basis of the hypothesis outlined in the Introduction. If it were true that high concentrations of giant sea-salt particles are responsible for low concentrations of droplets, there would have been a negative correlation between n and N; in fact, however, there was a strong positive correlation. Apparently, therefore, this hypothesis must be rejected. This conclusion agrees with the theoretical conclusion of SQUIRES (communicated [b]) that the supersaturation of cloud air, when computed on the basis of observed droplet spectra, is systematically higher in maritime than in continental cumuli.

Seeing that these observations preclude the possibility of attributing the differing characteristics of maritime and continental cumuli to the action of sea-salt nuclei, another explanation must be sought. The most obvious alternative is to assume that those condensation nuclei which form droplets at the low supersaturations existing in natural clouds are more numerous in continental air than in maritime air. According to LANDSBERG (1938) this is true of Aitken nuclei. Fundamental difficulties, however, have prevented the study of the properties and distribution of that small fraction of Aitken nuclei which are effective cloud nuclei, and it is not known for certain whether they originate from land or sea.

It is interesting to note that the association seen in Fig. 1 between high counts of sea-salt nuclei and high values of cloud drop concentration in continental cumuli can be explained by assuming that cloud nuclei originate over the land surface under dry conditions (e.g. from fires or by the drying out of soluble salts). It is known that rain and convective cloud formation reduce the concentration of sea-salt nuclei (TWOMEY 1955). Continental air with a high concentration of sea-salt nuclei is therefore more likely to have travelled over a predominantly dry surface and become rich in any nuclei formed under such surface conditions. Also, this view is consonant with the observation that the most colloidally stable clouds occur over dry continental surfaces, and with the impression which some meteorologists have gained that dry and wet periods tend to persist, being broken only by a relatively large change in the general weather situation.

Even though giant sea-salt nuclei seem to have little influence on the microstructure of clouds, it may be remarked that they may nevertheless play an important role in the release of precipitation from any colloidally unstable cumuli in which they occur in sufficient numbers.

4. Conclusions

It has been experimentally shown that observed differences in droplet spectra and colloidal stability, between maritime and continental cumuli, cannot be attributed to differences in the concentration of giant sea-salt nuclei.

The observations made agree with the hypothesis that continental clouds owe their higher droplet concentrations and greater colloidal stability to the formation over dry land surfaces of significant numbers of cloud nuclei.

5. Acknowledgements

Acknowledgement is due to the Aircraft Research and Development Unit, Detachment B, of the Royal Australian Air Force, who provided and flew the aircraft used.

REFERENCES

LANDSBERG, H., 1938: Atmospheric condensation nuclei. *Ergebnisse der kosmischen physik*, **3**, 155—252.

SQUIRES, P., communicated (a): The microstructure and colloidal stability of warm clouds. I — the relation between structure and stability. *Tellus* **10**, pp. 256—261.

SQUIRES, P., communicated (b): The microstructure and colloidal stability of warm clouds. II—the causes of the variations in microstructure. *Tellus* **10**, pp. 262—271.

SQUIRES, P., and GILLESPIE, C. A., 1952: A cloud droplet sampler for use on aircraft. *Quart. J. R. Met. Soc.*, **78**, 387—393.

TWOMEY, S., 1955: The distribution of sea-salt nuclei in air over land. *J. Meteor.*, **12**, 81—86.

WOODCOCK, A. H., and GIFFORD, MARY M., 1949: Sampling atmospheric sea-salt nuclei over the ocean. *J. Mar. Res.*, **8**, 177—197.

An Experiment on Artificial Stimulation of Precipitation in the Snowy Mountains Region of Australia

By E. E. ADDERLEY and S. TWOMEY

Division of Radiophysics, C.S.I.R.O., Sydney, Australia

(Manuscript received July 10, 1956, revised November 4, 1957)

Abstract

A long-term experiment on the artificial stimulation of rain over an area has been in progress in the Snowy Mountains region of south-east Australia. The form of the experiment is described, and preliminary results from the first six months' operation are presented.

1. Introduction

This paper presents an interim report on a long-term experiment in the artificial stimulation of precipitation which was initiated in Australia, jointly by the Snowy Mountains Hydroelectric Authority and the Commonwealth Scientific and Industrial Research Organization, in June 1955. The objective is to determine whether cloud seeding with silver iodide nuclei can produce an economically significant increase in precipitation over the Snowy Mountains region. Aerial seeding is employed exclusively to reduce the doubt present in some previous experiments as to whether the seeding material actually entered the cloud systems involved.

The tests will need to be continued for several years before reliable conclusions can be drawn but since they incorporate some novel features in the general design of the experiment, a description of the procedures adopted may be of interest to other workers in this field. Few actual experiments of this kind have been adequately reported in the literature.

2. Design of the experiment

(a) *Method of control*

A basic factor in all attempts to arrive at a quantitative assessment of the changes in precipitation induced by cloud seeding is the reliability with which the precipitation that would have occurred in the absence of seeding can be inferred.

A method frequently used in the past to provide this essential comparison is to locate a "control" area adjacent to the seeded area, the natural rainfall of which is closely correlated in time and amount with that for the seeded or "target" area. Even if such a correlation can be established between two adjacent areas following a careful analysis of data for a sufficient period, and over an adequate network of stations within the areas, any relationship so established is necessarily an historical one and there must be inherent uncertainties in its extrapolation to the present or future. An alternative approach relies on seeding being confined to random periods, so that the intervening unseeded periods are available to provide the essential control data.

This avoids some of the disadvantages of the historical method. It is not dependent upon the existence of long series of records from a closely spaced network of stations, and has the merit, in fact, that any desired cover of gauge stations may be specially installed for the purpose of the tests. This is the method that has been adopted in the present experiments.

(b) *Length of period*

The length of period selected for »on-off« seeding should clearly not be so short as to introduce high variability, and not so long as to prolong unduly the duration of the tests.

In south-east Australia there is for most of the year a fairly regular procession of pressure systems from west to east, with an average period of six to seven days. The frontal surfaces which are the main source of cloud and rain in the Snowy Mountains area are generally located approximately midway between the anticyclone centres.

It was pointed out by Mr. E. B. Pender of the Snowy Mountains Hydroelectric Authority that the selection of a natural period corresponding to the passage across the area of the anticyclone centres would provide a twofold advantage: the measurements of precipitation could be made more expeditiously in the favourable weather usually accompanying anticyclones, and also making the measurements at "null points" would be the next best thing to reading all gauges simultaneously. This convenient natural period has therefore been adopted.

For the purposes of these experiments a period is defined as the interval between the passage of successive anticyclone centres across the 150° E meridian of longitude. During the winter of 1955, however, some periods were as short as three days, and also the raingauge and other readings at the end of some periods had to be made in most unfavourable weather conditions. It seems therefore desirable to further specify that each period shall not be less than 8 days and also that those anticyclones should be excluded which (e.g. by reason of their centres passing a long distance north or south of the Snowy Mountains area) are not accompanied by reasonably fine weather in the catchment area. The division into seeded "on" and unseeded "off" periods is made on the basis of a set of random numbers (FISHER and YATES, 1948). This series is unknown to the individual who decides the end of each period and the beginning of the next.[1]

The regular procession of high pressure and frontal systems across south-east Australia, described above, normally holds from March to December, but breaks down during the summer months (December—February), due to frequent incursions of easterly air and penetrations of monsoonal air from the tropics.

The decision was therefore taken to treat the summer months from December 1st separately for the purpose of analysis. The present paper deals with results from the commencement of operations up to December 1st 1955.

(c) *Estimation of precipitation*

The variability which occurs in the precipitation records of a particular area is a compound one. The total rainfall is itself subject to variations due to natural causes, but there is a further variability as a result of sampling errors. A raingauge measures only a minute sample of the total precipitation over an area, and any increase in the number of raingauges reduces, to some extent, the variability which makes the assessment of cloud seeding experiments difficult. The raingauge cover in the Snowy Mountains area has been greatly increased since the beginning of this experiment. The locations of the raingauges are shown in Figure 2. The precipitation measured at these locations is the total precipitation, both rain and snow. At the conclusion of each period isohyetal patterns are drawn for that period by the Hydrology Section of the Snowy Mountains Hydroelectric Authority, and the total precipitation in acre feet calculated by integration of the isohyets. The precipitation estimated in this way furnishes a better estimate of the true total than that given by individual gauges.

[1] A more desirable procedure would be to seed the control area in the present "off" periods, the effects of seeding would then be twice as apparent and the time scale of the experiments shortened. At present, however, seeding of the control area is not desired by the Snowy Mountains Hydroelectric Authority because of their heavy construction programme in that area.

3. Area of operations

The experiments are taking place over the catchment area of the Snowy River in south-east Australia, an area in which major engineering construction is in progress, under the control of the Snowy Mountains Hydro-electric Authority, to provide water storage for both hydroelectric and irrigation purposes. This general area in relation to south-east Australia is shown in Fig. 1, and its subdivision into "control" and "target" areas in Fig. 2.

The subdivision into "control" and "target" areas was decided by the following a priori considerations: (i) the "control" area included areas to the north where major construction works are at present in progress; the Snowy Mountains Hydroelectric Authority desired that the experiments should have little likelihood of affecting the precipitation in this area; (ii) the "target" area was that part of the main catchment area south of the "control" area, and was of approximately equal area. It included the comparatively small Guthega catchment area in which precipitation is of immediate and direct economic value, as the run-off from this area is utilized by a hydro-electric power station already in operation. This area is enclosed by the broken line in Figure 2.

The orography and climatology of the region seem suitable for an operation of this kind. As the region is approached from the west, the terrain rises rapidly (6,000 feet in 20 miles). The crest of the main range roughly follows a line drawn through the centres of the "control" and "target" areas. Prevailing winds are from the northwest to southwest, and precipitation and deep clouds are most frequently associated with winds from that quadrant, usually in conjunction with frontal or post-frontal synoptic situations. To date, the clouds seeded have been cumuli or stratocumuli.

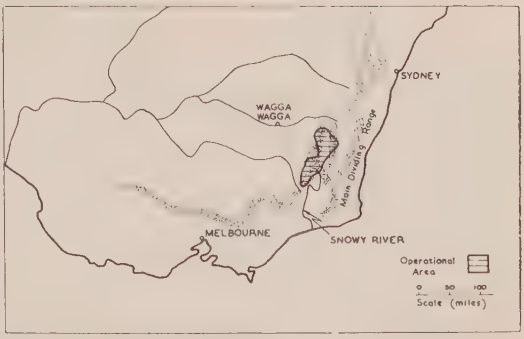

Fig. 1. Map showing Snowy Mountains area in relation to south-east Australia.

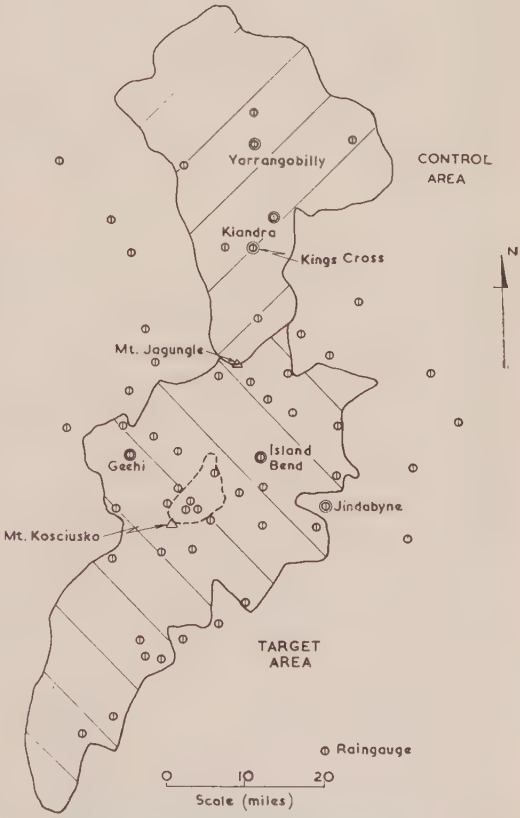

Fig. 2. Snowy Mountains catchment area, showing the target and control areas and other salient features.

4. Equipment

A schematic drawing of the silver iodide smoke generator is reproduced in Fig. 3. A generator unit is suspended from each wing-tip of an Avro Anson aircraft; a pump within the cabin of the aircraft is used to pump a solution containing silver iodide from a tank in the fuselage to the wing-tip units. There

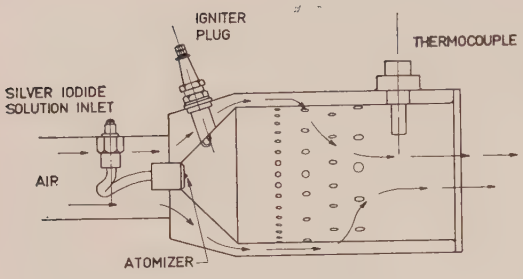

Fig. 3. Silver iodide burner.

the inflammable solution is atomized to a fine spray which is ignited by a "glow-type" spark plug. Thermocouples measure the temperature of each burner, and serve to indicate whether the burners are operating correctly. For reasons of safety, the incandescent vapour is cooled by radial introduction of air, so that the flames are confined to the interior of the burner tube. The solution employed contains silver iodide and sodium iodide in acetone; it is burned at the rate of 500 gm to 800 gm of silver iodide per hour.

The aircraft is equipped with complete navigational aids so that accurate position finding is possible in almost all circumstances —a very necessary requirement for the satisfactory execution of cloud seeding operations of this kind.

5. Operational procedure

In earlier experiments carried out by C.S.I.R.O. convective clouds were seeded with silver iodide nuclei released from an aircraft either within cloud or immediately below cloud base. These experiments indicated that seeding was likely to induce precipitation, providing that (i) the temperature of the top of the cloud was $-6°$ C or colder; (ii) the cloud was compact and at least several thousand feet in vertical extent. Following a successful seeding at cloud base, precipitation was usually observed below cloud base 20—30 minutes after seeding. Less information was available concerning the seeding of stratocumulus layers, but the observed intervals between successful seedings and the appearance of precipitation ranged from 20 to 50 minutes.

With the above considerations in mind, routine seedings are carried out as follows: (i) when visual inspection, or the prevailing meteorological situation, indicates that suitable cloud conditions may be found in the vicinity of the Snowy Mountains region, the aircraft takes off from its base at Wagga Wagga (about 90 miles NNW of the catchment area). At present, daytime operations only are conducted. (ii) As the aircraft approaches the target, wind and temperature measurements are made to augment information provided by the Meteorological Office at Wagga Wagga and an appraisal made of the cloud conditions prevailing. (iii) If conditions are considered favourable, the most suitable level for seeding is decided. The track of the seeding flight is then plotted by laying off a line equal and parallel to a line joining Mt. Jagungle and a point 10 miles south of Mt. Kosciusko. The distance upwind of the seeding track from the latter line, in the direction of the wind at the seeding level, is designed to allow for the expected time interval between a successful seeding and the arrival of precipitation at the ground. Naturally an exact determination is not possible but it is felt that the method used gives the best estimate than can be arrived at by using available data. The distance referred to is obtained by multiplying the wind velocity at the seeding level by 30 minutes in the case of cumulus clouds with bases at or below 6,000 ft, or by 60 minutes in the case of layer-type clouds; when the cloud base exceeds 6,000 ft, 1½ minutes is added for each 1,000 ft by which the base exceeds that height. The best seeding level is considered to be the $-6°$ C isotherm; it is often impracticable to fly at this level, and seeding is usually carried out at cloud base. (iv) A number of passes is then made, following the predetermined track. If weather conditions prevent complete passes being made, the accessible part of the track is traversed. (v) Following the seeding, an attempt is made to assess visually the effects, if any, produced. Precipitation has often been observed over the target following seeding, but it is well known that such observations are of limited value. However, a marked lowering of the cloud base is very frequently observed.

The type of aircraft being used at present curtails the duration of individual seeding flights and also limits the extent to which advantage may be taken of suitable weather conditions. Extension of the seeding time and

fuller use of available opportunities, particularly at night, is clearly desirable. It is planned to increase the duration of seeding during the daylight hours and to introduce night seeding at some date in the future.

6. Results

The precipitation results for periods No 1 to No 27 are given in Table I for both the target area (T) and the control area (C).

The ratios of the cumulative sums of the precipitations in the target and control areas are presented graphically in Figure 4 and in Figure 5 a plot is given of the ratios of target and control area precipitations for each period.

These results indicate that the ratios of target area to control area precipitations are greater during the seeded periods but the number of observations are far too inadequate to determine whether this can be expected

Table 1. Precipitation in target and control areas for periods 1 to 27 (8 June 1955 to 5 December 1955)

Period No.		*T*	*C*
Seeded	Unseeded	Thousands of acre feet	
	1	249,1	190,9
	2	128,7	94,2
3		5,5	3,7
	4	17,1	21,3
	5	105,8	88,1
6		19,1	22,6
7		117,7	98,3
8		22,5	20,5
	9	0	0
	10	333,8	305,3
11		0	0
12		217,7	206,3
13		0	0
14		81,5	46,7
	15	10,9	3,2
	16	132,1	118,0
17		14,1	7,7
	18	74,9	76,9
	19	97,8	100,8
20		105,8	61,9
	21	200,9	179,1
22		102,9	84,0
23		82,6	48,7
24		58,2	37,8
26		99,8	48,5
	27	78,9	71,3

In the number of the periods, No 25 was omitted due to a clerical error. Period No 26 follows immediately after Period No 24.

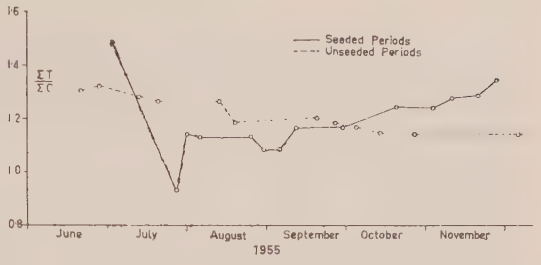

4. Ratios of cumulative sums of precipitation in the target and control areas.

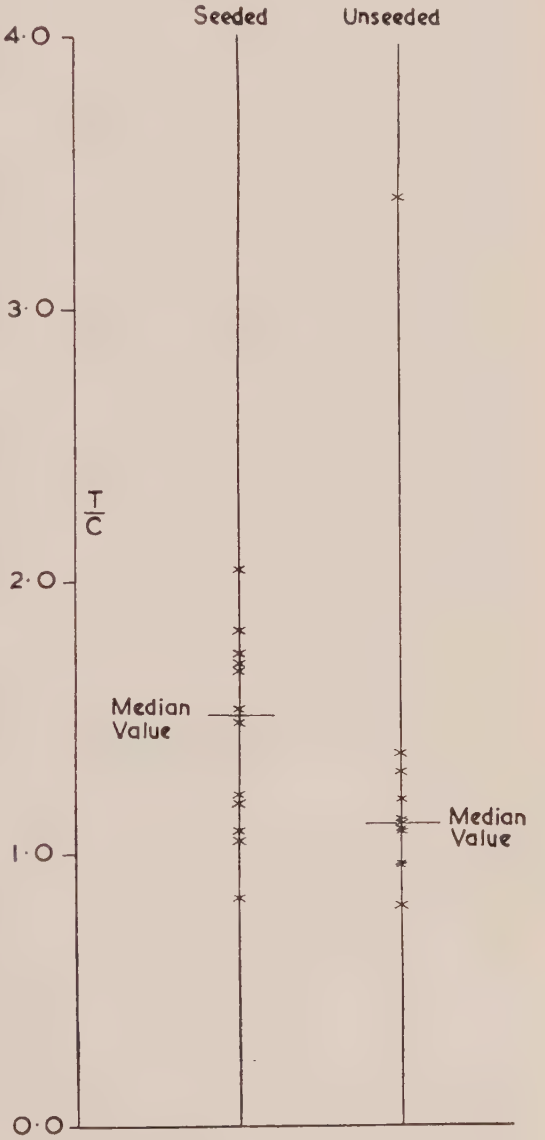

5. Ratios of precipitation in the target and control areas.

naturally or whether there is an effect due to the seeding programme. It is proposed to continue the experiment until a significant answer to this question, one way or the other, is obtained.

7. Discussion

From an operational point of view the dissemination of silver iodide by an aircraft for the purposes of modifying the rainfall in a given area has proved to be quite successful. The procedure adopted is simple and unequivocal in use.

The use of aircraft in this type of experiment reduces the uncertainty as to whether the silver iodide reaches its operating region before becoming inactive and because of its freedom of movement gives greater accuracy in «aiming» the seeding operation.

The design of the experiment would appear to give the following advantages:

(i) The use of random »on-off» seeding allows the use of recently installed precipitation gauge coverage and extrapolation of historical data is unnecessary.

(ii) The integration of an isohyetal map to give an estimate of precipitation is not dependant upon all precipitation gauges being read, and does take some account of the spatial relationships of the recording gauges.

(iii) With the use of periods determined by the passage of high pressure systems there is greater probability that the precipitation gauge readings can be made in fine weather and a delay in reading any particular gauge or gauges is unimportant.

8. Acknowledgements

The onerous task of collecting and collating the precipitation data has been undertaken by Mr. E. B. Pender and his staff of the Hydrology Section of the Snowy Mountains Hydroelectric Authority without whose liberal cooperation this experiment could not have been undertaken. Acknowledgements are especially due to Mr. T. E. Bisits, who was responsible for drawing the isohyetal maps for each period and computing the total precipitations therefrom.

The smooth operation of the experiment owes much to Messrs. A. A. Tapp and J. S. Aitken who are responsible for the navigation and flying of the Anson aircraft and to Butler Air Transport Pty. Ltd. who are responsible for its maintenance and servicing.

Thanks are also due to the Meteorological Office at Wagga Wagga airport for providing synoptic information and forecasts, and to the Commanding Officer of the Royal Australian Air Force establishment at Wagga Wagga, for hospitality afforded to the flying personnel.

REFERENCES

Fisher, R. A., and Yates, F., 1948: *Statistical Tables for Biological, Agricultural and Medical Research*. London, Oliver and Boyde, p. 104.

Current Data on the Chemical Composition of Air and Precipitation XIII

(For further information see Egnér, H., Eriksson, E., *Tellus* **7**, pp. 134—139, **8**, p. 285 and 517)

Code	mm	mg/m² S	Cl	NO_3–N	NH_3–N	Na	K	Mg	Ca	pH	HCO_3^- μval/l	$\varkappa \cdot 10^6$ $\frac{1}{\Omega \cdot cm}$	μg/m³ (= kg/km³) S	Cl	NH_3–N	Na	K	Mg	Ca
		Precipitation Aug. 1957 (D 708)											Air Aug. 1957 (L 708)						
Kn	6	9	228	3	4	135	9	22	39	5.9	18	312	—	—	—	—	—	—	—
		Precipitation Sept. 1957 (D 709)											Air Sept. 1957 (L 709)						
Kn	7	15	314	2	2	155	11	26	34	6.2	10	293	17.2	421.	2.1	346.	15.0	35.0	71.0
BL	106	91	0	21	0	9	8	29	80	5.6	0	9	6.3	13.1	10.6	1.8	1.4	*	1.5
MH	86	53	97	18	5	62	8	3	47	5.3	0	12	17.2	9.8	5.0	1.9	1.7	0.2	0.8
RS	85	49	327	28	3	180	7	11	35	5.3	0	20	11.7	11.9	3.6	2.9	1.2	0.3	0.6
LM	63	41	86	20	4	43	4	3	39	6.4	10	12	—	—	—	—	—	—	—
LX	100	57	45	49	10	46	8	1	34	5.3	0	10	9.1	15.6	5.6	3.2	1.4	0.2	0.7
By	52	33	67	12	26	36	10	1	63	6.7	61	19	0.9	6.3	6.5	1.8	1.0	0.4	0.5
Ae	53	46	69	18	14	25	10	2	122	6.5	85	23	—	—	—	—	—	—	—
		Precipitation Okt. 1957 (D 710)											Air Okt. 1957 (L 710)						
Kn	11	23	295	3	3	278	16	34	36	6.4	21	276	12.1	352.	3.2	283.	11.	27.	62.
Ri	42	12	42	1	2	25	4	5	18	6.1	19	7	0.0	16.0	2.5	1.7	0.6	3.9	5.9
Ki	22	15	16	4	1	7	3	2	19	6.4	27	8	0.3	6.4	0.9	2.0	1.0	0.1	2.1
Ar	31	16	12	1	1	4	2	2	32	6.2	19	7	0.5	3.4	0.9	0.9	0.1	0.3	0.9
Öj	40	28	10	2	1	6	1	5	51	6.3	28	11	2.9	5.6	2.1	0.2	0.1	1.5	2.0
Rö	20	20	6	2	4	8	3	5	31	5.0	0	16	2.1	9.3	1.1	0.7	0.1	0.3	6.7
Of	38	31	9	0	1	6	31	7	29	5.6	—	—	3.5	4.4	2.1	1.2	0.9	1.4	11.
Br	46	19	11	2	6	9	3	8	46	5.4	0	6	15.	3.3	1.0	0.5	0.1	0.4	4.7
ÅF	85	24	110	3	3	60	9	12	93	6.0	5	8	*	*	*	*	*	*	*
ÅH	50	15	29	1	1	22	2	5	30	5.8	3	7	—	—	—	—	—	—	—
Fö	48	78	15	4	2	12	26	6	53	5.7	5	19	—	—	—	—	—	—	—
Sv	35	19	7	2	1	4	5	3	23	5.5	0	8	—	—	—	—	—	—	—
Rä	18	25	3	2	4	4	3	2	55	6.7	110	26	12.	2.3	2.5	0.3	0.1	0.2	4.6
Åm	33	34	12	3	3	7	3	7	25	6.3	27	10	0.3	10.	1.5	1.1	0.6	0.2	4.2
Sa	52	63	39	3	2	13	38	16	78	6.7	65	21	7.3	5.3	1.8	0.7	0.6	3.3	6.8
Ul	65	70	34	13	27	16	6	5	25	4.7	0	19	3.4	3.4	1.4	0.4	0.1	0.4	1.4
Er	39	37	50	5	4	16	26	1	31	4.6	0	19	0.6	8.0	1.0	0.2	0.1	0.6	3.6
St	70	86	35	11	19	23	13	2	58	5.7	5	14	7.4	5.7	3.6	0.6	0.5	0.8	3.9
Fo	60	58	50	7	7	24	9	8	86	6.6	55	18	1.1	10.	1.5	0.5	0.1	1.0	5.0
Kv1	39	440	71	12	34	30	38	23	210	6.9	190	190	50.	3.5	8.1	1.6	2.8	5.0	22.
Kv7	29	55	29	7	14	15	7	7	32	4.5	0	32	*	*	*	*	*	*	*
VK	53	56	38	11	14	24	16	8	46	5.6	0	18	—	—	—	—	—	—	—
La	68	61	98	12	28	53	7	10	37	5.4	0	17	0.3	15.	3.3	0.8	0.1	1.0	5.6
Bo	73	66	19	20	22	550	23	48	49	4.5	0	52	4.0	6.6	1.1	5.6	1.0	1.5	6.4
Vi	60	220	1 980	20	18	2150	86	250	83	4.5	0	360	9.3	25.	1.1	30.	1.0	4.6	4.9
Fa	37	31	19	6	6	17	11	9	32	5.1	0	14	4.9	4.3	1.2	0.3	0.0	0.1	1.4
Fl	80	65	70	13	13	71	12	12	24	4.6	0	23	0.5	8.3	1.4	0.6	0.0	0.0	3.4
Fi	105	20	270	38	57	150	25	47	38	4.6	0	30	—	—	—	—	—	—	—
Am	143	92	240	31	34	170	24	26	76	4.9	0	21	—	—	—	—	—	—	—
Si	158	170	290	45	67	170	33	30	62	4.7	0	24	—	—	—	—	—	—	—
Pl	51	62	240	19	29	160	18	23	22	4.4	0	46	3.4	12.	2.9	1.4	0.2	2.0	10.
Sö	66	78	44	16	9	25	5	9	59	4.7	0	20	—	—	—	—	—	—	—
Sm	26	33	27	2	1	15	27	9	28	5.0	26	20	4.3	9.9	1.9	0.9	0.2	0.4	2.7
Sy	86	83	74	22	41	36	16	11	48	5.0	0	17	3.1	9.0	3.1	1.8	0.6	1.2	10.
BH	51	18	120	11	12	61	220	31	100	6.4	99	43	3.7	6.8	2.8	0.6	0.0	0.0	3.4
Sk	100	35	210	40	79	140	33	20	49	4.7	0	32	5.2	7.1	3.8	1.1	0.4	2.5	3.8
Al	*	*	*	*	*	*	*	*	*	*	*	*	12.	16.	4.3	1.9	0.5	2.5	9.6
Hi	25	30	78	8	14	38	6	6	32	4.8	10	28	—	—	—	—	—	—	—
Ta	23	17	30	2	7	26	4	6	14	5.5	0	17	*	*	*	*	*	*	*

Code	mm	mg/m²								pH	$HCO_3^- - \frac{\mu val}{l}$	$\frac{\varkappa \cdot 10^6}{\Omega \cdot cm}$	$\mu g/m^3$ (= kg/km³)						
		S	Cl	NO_3^-N	NH_3^-N	Na	K	Mg	Ca				S	Cl	NH_3^-N	Na	K	Mg	Ca
		Precipitation Okt. 1957 (D 710)											Air Okt. 1957 (L 710)						
An	—	—	—	—	—	—	—	—	—	—	—	—	—	—	—	—	—	—	—
Yt	101	15	130	0	1	280	70	51	48	6.2	19	28	—	—	—	—	—	—	—
Gj	176	40	600	5	11	400	20	47	39	5.7	2	18	—	—	—	—	—	—	—
Fn	117	67	53	11	18	28	9	10	57	5.6	6	10	—	—	—	—	—	—	—
Få	62	30	40	5	6	27	7	5	9	4.8	0	13	—	—	—	—	—	—	—
Vå	12	25	6	1	1	33	38	6	38	7.0	220	43	0.8	15.	5.1	0.3	0.0	0.4	5.8
Tr	35	15	12	3	4	6	3	3	9	4.9	0	8	—	—	—	—	—	—	—
Ke	45	30	13	5	7	8	3	4	30	5.5	0	10	—	—	—	—	—	—	—
Sd	103	110	270	13	21	190	20	26	29	4.8	0	24	—	—	—	—	—	—	—
Da	55	30	36	1	1	20	30	6	46	6.0	16	13	—	—	—	—	—	—	—
Ås	74	70	120	14	18	67	10	12	30	4.8	0	22	0.3	50.	1.5	0.6	0.0	0.3	3.0
Li	128	420	2 980	30	24	1700	130	390	190	4.6	0	170	11.	43.	1.1	30.	1.0	3.7	7.3
So	46	48	88	3	5	7	14	0	31	5.9	0	8	4.3	0.0	17.0	0.7	0.7	0.0	0.0
Ka	81	0	156	13	17	16	10	0	76	5.5	13	10	2.7	5.0	2.4	0.9	0.4	0.0	25.0
Ku	87	0	0	9	9	10	26	0	44	5.0	0	11	0.0	0.0	2.1	4.7	4.0	0.0	49.0
Jy	71	0	0	13	13	10	5	0	31	5.8	0	12	3.3	16.6	1.5	3.5	1.3	0.0	10.0
Pu	61	385	170	11	11	9	22	0	34	4.6	0	12	0.0	0.0	2.3	3.5	2.5	0.0	27.0
Tv	106	0	770	2	13	82	41	0	50	4.5	0	15	0.0	18.2	81.0	10.0	3.4	0.0	5.2
Vn	78	102	639	14	36	371	31	41	78	5.6	0	43	—	—	—	—	—	—	—
Gr	90	143	183	33	58	108	21	25	154	5.6	0	27	—	—	—	—	—	—	—
Öd	83	110	290	27	57	150	19	22	67	5.2	0	32	8.5	12.	4.2	2.3	0.7	0.6	6.5
Bs	109	154	665	28	38	507	29	65	49	4.6	0	50	—	—	—	—	—	—	—
Ly	85	149	215	32	58	122	25	26	31	4.4	0	42	—	—	—	—	—	—	—
As	104	94	120	34	56	300	28	44	60	5.0	0	39	12.	24.	7.1	3.2	0.0	0.7	7.7
Vd	109	184	278	37	134	136	77	41	158	6.1	16	33	—	—	—	—	—	—	—
Bl	94	135	167	28	51	109	24	22	49	4.8	0	31	—	—	—	—	—	—	—
Ty	59	100	520	32	64	164	70	36	77	5.7	10	43	13.	18.	7.2	3.3	0.8	5.8	38.
Hö	102	157	1 336	30	43	767	40	92	75	4.7	0	72	—	—	—	—	—	—	—
Ad	66	129	203	32	65	119	18	19	69	4.7	0	42	—	—	—	—	—	—	—
Ab	*	*	*	*	*	*	*	*	*	*	*	*	4.0	14.0	3.4	3.2	0.5	3.0	33.
Ed	66	67	220	7	15	150	16	21	66	6.1	27	28	3.1	9.3	2.1	2.0	0.6	1.7	11.
Es	196	159	608	20	51	456	24	41	33	5.8	6	19	7.5	3.2	—	9.1	0.6	0.0	0.0
Le	43	120	150	17	69	59	13	44	100	5.2	0	52	40.	13.	6.5	2.1	0.3	1.5	15.
Ro	56	73	73	14	13	36	12	11	54	4.7	0	28	27.	7.5	4.0	2.1	0.9	1.2	7.5
NA	65	65	190	26	290	160	100	31	150	6.4	280	65	7.5	4.9	4.9	1.6	0.1	0.6	2.9
Ca	—	—	—	—	—	—	—	—	—	—	—	—	—	—	—	—	—	—	—
Va	144	86	936	19	22	—	—	—	—	5.5	0	34	—	—	—	—	—	—	—
Sc	49	97	234	14	34	126	14	16	49	4.8	0	36	19.2	9.8	11.0	4.4	2.1	0.7	1.8
BV	20	40	127	21	72	41	20	26	219	5.2	0	153	31.1	3.8	11.5	0.8	1.1	0.4	1.0
Bn	27	112	104	19	29	24	17	13	248	5.8	73	93	23.0	23.0	12.9	4.2	2.1	0.4	3.4
Au	12	62	12	15	48	5	7	11	62	4.5	0	84	27.0	19.2	16.5	0.7	2.4	8.9	1.1
Fe	23	35	14	4	8	10	5	1	26	4.8	0	20	9.6	5.5	15.7	2.3	3.2	2.1	9.2
Ba	61	79	31	0	3	8	7	0	4	4.5	0	13	17.8	14.9	13.8	0.5	1.3	3.2	2.9
Ho	16	62	18	3	0	4	69	3	63	6.2	118	46	16.7	7.4	0.9	0.6	1.2	0.4	1.9
Rm	17	75	13	10	3	9	7	2	127	6.2	276	60	9.7	5.4	9.5	7.3	1.1	0.5	3.4
Et	11	45	17	3	17	3	4	1	31	5.0	0	40	13.3	2.9	7.7	3.2	0.9	0.1	0.1
He	—	—	—	—	—	—	—	—	—	—	—	—	—	—	—	—	—	—	—
Rz	4	22	10	2	14	2	5	2	44	6.1	16	98	9.2	6.7	18.1	2.2	0.9	0.7	2.1
Wi	4	13	15	1	4	2	17	7	97	6.8	306	211	35.0	2.8	11.5	3.4	1.0	0.4	2.5
Lz	9	12	18	10	34	8	6	1	79	6.6	375	98	18.5	2.7	11.1	1.3	1.2	0.4	1.8
Kl	29	46	0	10	66	0	2	4	45	5.4	0	17	11.0	2.3	9.9	3.2	0.7	0.5	0.2
BL	43	69	49	3	84	21	12	11	100	5.7	9	52	16.4	12.8	11.0	2.4	1.5	*	1.6
DH	58	9	1261	19	22	687	30	80	46	4.5	0	98	13.5	17.4	4.4	4.6	1.3	5.2	1.4
DB	39	62	99	20	37	59	8	2	36	4.6	0	45	16.7	6.3	6.0	1.3	0.7	0.1	1.0
W	45	45	117	20	40	75	11	10	22	4.9	0	46	14.2	3.9	7.2	0.3	1.8	2.9	0.7
SA	66	113	478	38	7	191	91	21	45	4.5	0	48	9.0	9.6	3.8	0.8	0.4	0.3	0.4
U	35	66	119	13	18	50	15	4	60	4.7	0	44	46.1	9.3	4.9	1.5	1.4	2.4	1.7
B	62	66	91	22	10	43	7	3	43	4.8	0	23	5.9	4.9	3.9	0.7	0.5	0.3	0.6

Code	mm	mg/m² S	Cl	NO_3–N	NH_3–N	Na	K	Mg	Ca	pH	HCO_3 – $\frac{\mu val}{l}$	$\frac{\varkappa \cdot 10^6}{\Omega \cdot cm}$	$\mu g/m^3$ (= kg/km³) S	Cl	NH_3–N	Na	K	Mg	Ca
	Precipitation Okt. 1957 (D 710)												Air Okt. 1957 (L 710)						
D	27	54	62	14	12	28	5	1	43	5.0	0	31	15.5	7.2	2.7	0.8	0.5	0.2	1.9
MH	30	84	7	25	25	30	4	2	100	5.7	9	38	25.5	6.9	5.8	2.1	1.8	0.6	0.8
Rs	31	37	124	12	16	74	4	3	36	6.3	15	29	1.7	10.3	6.5	2.6	0.7	0.4	0.6
LM	15	28	43	9	7	26	2	1	27	5.6	2	29	24.3	54.3	12.9	8.2	4.5	1.7	4.5
Lx	23	25	58	10	37	39	13	0	19	6.0	106	28	—	—	—	—	—	—	—
Bg	44	2	37	14	4	15	6	1	81	6.4	34	17	8.7	5.1	6.4	3.2	1.5	0.2	1.6
Ac	31	17	37	11	4	8	4	1	134	6.0	117	36	33.4	12.6	5.8	3.4	2.0	0.3	3.9
Za	*	*	*	*	*	*	*	*	*	*	*	*	*	*	*	*	*	*	*
	Precipitation Nov. 1957 (D 711)												Air Nov. 1957 (L 711)						
Kn	6	21	327	3	4	176	12	29	47	6.5	16	288	15.2	376.	3.9	365.	16.	22.	41.
Ri	51	19	61	3	1	19	4	8	21	5.7	17	12	4.6	13.	1.1	1.9	0.8	4.2	13.
Ki	25	9	4	1	0	7	4	2	12	5.9	4	6	0.8	6.0	0.8	4.2	2.3	2.5	3.9
Ar	25	11	16	3	3	4	5	4	19	6.0	14	9	0.8	1.8	1.0	0.6	0.5	0.7	1.5
Öj	14	16	14	3	2	5	4	2	20	5.7	9	18	4.1	2.0	2.2	0.7	0.8	0.8	2.5
Rö	28	32	20	4	7	15	4	4	28	5.5	0	15	5.3	2.5	2.0	1.0	0.8	0.4	2.9
Of	14	24	6	2	3	3	3	3	9	5.9	2	11	1.1	5.9	1.8	1.6	1.0	0.9	3.0
Br	5	7	7	1	2	2	1	1	7	5.9	16	19	0.9	2.2	1.2	0.8	0.6	0.4	3.9
ÅF	56	24	21	3	1	15	3	5	18	5.8	0	9	1.7	6.6	1.7	0.8	0.8	2.7	46.
ÅH	—	—	—	—	—	—	—	—	—	—	—	—	—	—	—	—	—	—	—
Fö	33	42	30	3	4	12	11	4	69	6.3	33	19	—	—	—	—	—	—	—
Sv	23	22	14	3	3	11	4	4	16	5.7	22	13	—	—	—	—	—	—	—
Rä	33	20	24	5	2	10	5	5	110	6.9	110	24	5.1	6.7	2.1	1.3	1.0	0.6	8.2
Åm	*	*	*	*	*	*	*	*	*	*	*	*	2.0	10.	1.4	1.0	0.8	0.5	4.2
Sa	47	44	30	6	3	15	16	8	39	5.7	2	13	*	*	*	*	*	*	*
Ul	47	45	34	9	17	17	5	10	25	5.0	0	16	6.2	5.2	1.8	0.7	0.7	0.4	1.6
Er	37	28	19	6	8	11	8	5	15	4.9	0	15	3.6	1.8	0.8	0.5	0.6	0.5	2.7
St	33	37	14	8	14	10	9	5	32	5.6	5	16	2.9	9.7	2.6	0.5	0.5	0.2	2.4
Fo	19	32	26	6	6	17	6	6	25	5.3	0	24	4.4	6.3	1.3	0.9	0.8	0.7	3.0
Kv1	26	750	19	8	26	22	27	28	980	4.2	0	320	34.	8.9	9.5	2.1	3.1	3.5	28.
Kv7	21	97	5	2	4	6	6	3	140	5.8	18	50	*	*	*	*	*	*	*
VK	20	43	23	8	16	13	4	4	34	5.8	54	33	—	—	—	—	—	—	—
La	10	49	55	6	30	24	6	6	34	4.9	0	81	1.2	12.	2.3	1.3	0.6	1.0	4.0
Bo	20	35	160	7	6	130	8	19	32	5.8	33	56	*	*	*	*	*	*	*
Vi	27	240	2390	13	11	1450	53	170	110	4.6	0	370	4.7	20.	1.2	5.7	0.6	2.0	3.4
Fa	29	31	33	6	7	21	5	6	23	5.3	0	16	0.5	3.1	1.0	0.6	0.2	3.1	1.9
Fl	22	6	4	0	1	1	1	5	3	5.5	0	1	0.8	2.9	0.7	0.5	0.2	0.5	1.9
Fi	45	45	160	13	27	93	7	47	29	5.1	0	30	—	—	—	—	—	—	—
Am	49	49	84	12	15	40	6	11	40	5.7	8	19	—	—	—	—	—	—	—
Pl	27	42	110	9	21	59	10	13	26	5.0	0	37	4.7	10.	2.6	1.3	0.3	0.8	6.1
Sö	43	44	51	7	7	30	6	10	49	5.5	0	17	—	—	—	—	—	—	—
Sm	43	40	49	6	16	29	6	9	33	5.2	0	16	4.7	6.0	1.5	0.8	0.4	2.8	5.0
Sy	14	26	130	4	10	13	5	4	89	5.9	13	55	4.3	16.	2.3	1.5	0.9	1.3	9.0
BH	38	44	19	4	11	8	3	5	24	4.9	0	16	6.4	1.4	1.6	0.6	0.4	1.5	8.3
Sk	20	42	68	8	30	47	7	9	26	5.4	0	42	5.5	4.8	3.0	1.3	0.3	0.9	4.1
Al	25	37	47	8	30	34	8	7	31	5.0	0	35	13.	7.1	2.5	1.2	0.5	1.0	4.3
Hi	16	24	39	4	7	18	4	5	25	5.7	19	25	—	—	—	—	—	—	—
Ta	30	21	280	2	4	190	7	22	34	5.3	0	59	*	*	*	*	*	*	*
An	—	—	—	—	—	—	—	—	—	—	—	—	—	—	—	—	—	—	—
Yt	73	22	140	4	7	94	8	24	39	6.1	19	14	—	—	—	—	—	—	—
Gj	120	34	72	3	8	90	9	28	45	6.1	9	8	—	—	—	—	—	—	—
Fn	66	36	16	6	12	8	3	4	23	5.5	0	7	—	—	—	—	—	—	—
Få	54	20	9	2	1	9	5	3	13	5.8	2	4	—	—	—	—	—	—	—
Vå	41	27	16	4	4	25	7	5	34	6.3	30	11	6.4	0.9	5.0	1.2	0.8	1.3	2.8
Tr	44	34	52	8	13	25	7	7	19	6.3	10	16	—	—	—	—	—	—	—
Ke	9	14	15	3	4	10	4	3	18	6.3	17	28	—	—	—	—	—	—	—
Sd	100	110	420	13	31	230	10	36	54	5.6	0	27	—	—	—	—	—	—	—

Code	mm	mg/m²								pH	$\frac{\mu val}{l}$ HCO_3	$\frac{\varkappa \cdot 10^6}{\Omega \cdot cm}$	$\mu g/m^3$ (= kg/km³)						
		S	Cl	NO_3—N	NH_3—N	Na	K	Mg	Ca				S	Cl	NH_3—N	Na	K	Mg	Ca
		Precipitation Nov. 1957 (D 711)											Air Nov. (L 711)						
Da	100	42	69	6	2	40	8	7	21	5.2	0	10	—	—	—	—	—	—	—
Ås	49	76	240	13	19	180	12	21	36	4.8	0	41	*	*	*	*	*	*	*
Li	80	330	14000	20	27	4800	170	560	260	4.8	0	410	6.0	11.	1.4	100.	74.	15.	35.
So	29	12	10	2	4	3	0	2	10	5.6	0	7	8.5	22.3	11.	6.6	0.0	5.7	3.9
Ka	28	17	0	7	8	8	5	4	38	6.0	0	15	6.4	9.8	4.0	3.5	0.0	2.5	6.3
Ku	17	39	11	8	7	7	7	3	42	5.5	0	30	6.1	0.0	10.0	5.4	0.0	3.1	10.8
Jy	25	0	14	8	13	9	9	4	42	5.7	22	25	2.2	8.5	9.0	0.0	0.0	1.3	1.7
Pu	11	0	15	2	9	5	0	4	23	6.2	0	20	4.1	18.0	13.6	5.0	0.0	3.9	3.6
Tv	14	0	37	7	9	18	3	6	22	5.2	0	40	0.0	0.0	13.0	0.0	0.0	1.4	0.9
Vn	25	60	259	5	20	146	14	22	56	6.2	14	62	—	—	—	—	—	—	—
Gr	54	87	301	10	27	185	16	22	52	4.7	0	43	—	—	—	—	—	—	—
Öd	38	50	180	9	30	110	8	17	39	5.8	14	35	7.4	14.	4.4	2.0	0.7	2.2	13.
Bs	49	65	623	7	18	350	23	46	32	4.9	0	63	—	—	—	—	—	—	—
Ly	33	56	47	9	22	25	9	15	17	4.7	0	34	—	—	—	—	—	—	—
As	53	66	350	11	30	210	12	33	37	5.1	0	41	12.	17.	3.5	2.1	0.6	0.6	4.8
Vd	79	100	226	11	64	176	44	25	44	5.7	0	25	—	—	—	—	—	—	—
Bl	78	107	189	13	41	110	26	20	46	5.2	0	25	—	—	—	—	—	—	—
Ty	38	50	100	9	37	53	7	18	47	5.6	29	32	15.	26.	7.3	8.0	1.8	3.0	5.7
Hö	67	89	768	10	24	443	27	57	36	4.8	0	60	—	—	—	—	—	—	—
Ad	38	64	75	10	36	64	37	10	39	5.3	0	30	—	—	—	—	—	—	—
Ab	*	*	*	*	*	*	*	*	*	*	*	*	13.	2.8	2.3	1.4	0.5	2.2	11.
Ed	34	47	180	7	15	130	11	19	53	6.3	33	31	11.	7.0	2.1	2.7	0.4	0.9	3.4
Es	60	167	215	11	20	465	27	27	54	6.9	648	49	9.2	2.3	1.2	3.1	0.8	0.3	0.9
Le	37	79	200	12	42	87	8	27	52	5.2	0	47	17.	29.	4.3	1.3	0.6	1.6	8.0
Ro	49	60	190	11	18	100	12	18	64	5.3	0	30	5.6	15.	3.9	3.2	1.3	1.6	16.
NA	57	59	390	9	11	290	17	40	120	5.7	34	49	18.	14.	5.2	4.7	1.1	3.0	17.
Ca	49	104	557	8	13	372	23	42	54	6.4	101	55	13.3	3.2	0.4	16.8	0.6	0.6	1.4
Va	66	79	1485	9	33	—	—	—	—	5.2	0	94	—	—	—	—	—	—	—
Sc	48	81	159	15	27	79	41	9	58	5.5	0	29	20.2	27.8	5.0	16.8	6.0	2.0	1.7
BV	34	106	86	11	19	23	17	15	91	4.8	0	38	52.9	13.3	6.1	0.7	1.7	0.8	0.4
Bn	45	156	79	19	37	23	41	23	270	5.5	0	55	23.0	24.6	5.4	3.4	3.8	1.5	0.0
Au	13	35	33	14	27	6	12	7	55	4.4	0	71	46.0	20.6	8.8	0.9	4.1	5.9	3.8
Fe	26	10	18	15	35	10	21	1	32	4.6	0	37	12.9	6.5	2.4	0.7	3.3	1.1	3.3
Ba	35	63	14	11	24	3	12	2	21	4.8	0	15	16.2	15.5	4.4	0.2	2.2	0.9	0.0
Ho	45	123	79	12	20	12	118	29	168	5.8	40	42	23.6	7.9	3.1	0.6	1.7	0.9	0.0
Rm	26	61	26	13	17	4	11	6	230	6.7	216	56	7.1	2.2	3.2	5.5	0.6	0.2	1.1
Et	29	71	29	15	31	7	16	5	41	5.6	0	32	16.1	6.2	6.6	3.1	2.5	0.8	0.6
He	—	—	—	—	—	—	—	—	—	—	—	—	—	—	—	—	—	—	—
Rz	30	17	29	13	31	4	15	8	63	5.7	4	26	10.5	3.8	5.4	0.9	1.2	0.4	1.4
Wi	50	83	0	16	47	5	47	14	193	5.9	28	38	21.2	7.7	3.3	2.5	1.9	0.7	0.8
Lz	44	100	9	6	4	2	7	7	79	5.9	8	18	11.4	6.0	5.4	0.7	2.2	0.5	1.1
Kl	21	25	8	8	11	2	2	8	28	5.4	0	18	14.1	2.3	3.8	2.0	1.5	0.6	0.0
BL	31	155	29	10	65	4	5	5	89	5.0	0	20	33.7	11.5	5.7	1.9	1.2	0.6	5.6
DH	86	92	1847	30	40	1006	44	123	65	4.4	0	97	5.3	39.0	5.6	8.1	2.9	7.2	2.6
DB	35	72	84	14	27	54	6	6	31	4.5	0	40	11.3	15.1	5.5	1.3	0.9	0.7	0.9
W	53	102	104	21	39	65	13	12	29	4.4	0	42	12.3	15.3	4.3	2.5	1.7	3.6	1.3
SA	42	87	160	24	35	89	22	11	38	4.6	0	46	27.5	15.4	6.2	1.6	1.0	0.5	2.0
U	33	151	83	29	35	18	14	9	86	5.0	0	50	53.5	15.6	5.1	1.2	1.2	1.6	2.5
B	65	134	113	30	40	47	13	10	54	4.6	0	39	6.7	3.0	2.5	1.5	0.5	0.0	1.3
D	40	57	86	24	23	36	7	6	30	4.8	0	29	11.9	7.9	4.9	2.8	0.8	0.0	1.0
MH	20	42	28	11	5	12	4	4	4	4.6	0	40	12.8	8.9	7.1	1.3	1.1	0.0	1.0
RS	82	55	815	23	7	451	17	45	41	5.0	0	42	9.8	38.6	4.7	5.8	0.5	0.7	0.9
LM	59	43	76	18	5	43	4	8	40	5.1	0	15	22.4	37.3	1.5	2.6	1.4	0.0	2.6
Lx	33	27	25	12	6	8	7	3	35	5.2	0	14	10.3	139.8	3.5	95.4	43.8	1.2	5.9
Bg	33	48	48	16	6	17	5	4	63	5.5	6	22	15.7	16.4	5.7	1.5	1.0	0.4	1.5
Ac	73	47	18	29	8	5	2	2	95	6.4	29	11	32.0	62.6	13.1	0.9	1.1	0.7	1.9
Za	27	69	14	4	23	17	4	22	85	5.7	40	41	18.	5.1	5.5	1.3	2.2	4.0	17.

Code	mm	mg/m²								pH	$HCO_3^- \frac{\mu val}{l}$	$\frac{\varkappa \cdot 10^6}{\Omega \cdot cm}$	$\mu g/m^3$ (= kg/km^3)						
		S	Cl	NO_3—N	NH_3—N	Na	K	Mg	Ca				S	Cl	NH_3—N	Na	K	Mg	Ca
	Precipitation Dec. 1957 (D 712)												Air Dec. 1957 (L 712)						
Kn	8	24	298	2	2	195	10	32	29	6.3	25	221	10.9	240.	1.8	212.	8.2	20.	31.
Ri	41	20	120	0	0	49	6	10	11	5.9	2	15	0	1.2	4.0	3.0	1.4	0.3	2.6
Ki	12	7	27	0	0	10	6	5	7	6.4	25	12	3.1	6.4	3.3	12.	3.0	0.4	1.9
Ar	33	17	23	2	5	13	7	4	18	5.7	8	12	2.1	1.2	2.7	0.7	0.5	0.2	1.1
Öj	15	9	7	3	7	9	5	2	13	6.1	11	14	7.1	2.6	6.4	1.5	1.8	1.0	5.0
Rö	28	14	17	3	5	11	4	5	18	5.1	0	14	6.9	7.9	3.5	0.7	0.3	0.1	1.0
Of	33	21	8	4	4	20	9	3	11	5.2	0	9	0.2	4.2	4.9	1.5	0.9	1.3	2.9
Br	9	10	13	2	4	9	3	3	7	5.8	73	23	1.7	0.8	1.9	1.2	0.6	0.1	1.5
ÅF	40	23	43	3	2	32	5	16	14	5.8	8	12	*	*	*	*	*	*	*
ÅH	—	—	—	—	—	—	—	—	—	—	—	—	—	—	—	—	—	—	—
Fö	28	23	36	4	0	18	13	6	70	6.2	40	25	—	—	—	—	—	—	—
Sv	7	8	5	0	1	3	7	2	2	5.9	23	16	—	—	—	—	—	—	—
Rä	1	—	8	—	—	4	—	—	—	—	—	—	5.0	1.3	11.	2.0	1.4	1.0	8.9
Åm	3	15	5	1	2	4	4	2	4	6.5	—	55	7.2	2.8	7.4	4.2	2.9	1.1	6.1
Sa	13	13	11	2	1	7	13	6	19	6.0	6	18	*	*	*	*	*	*	*
Ul	13	33	8	4	7	5	4	3	8	5.7	0	20	11.	5.0	3.8	0.7	0.3	2.6	1.3
Er	10	19	10	1	3	7	4	3	6	5.3	0	18	*	*	*	*	*	*	*
St	17	23	21	5	5	14	9	6	32	5.8	22	28	8.1	1.0	5.5	0.7	0.3	0.3	2.3
Fo	8	12	32	3	3	13	5	5	14	5.7	45	39	4.0	2.3	5.1	2.9	2.1	0.9	3.4
Kv1	20	350	32	9	24	27	42	26	97	4.2	0	330	19.	9.7	8.3	5.3	5.5	9.4	21.
Kv7	20	33	34	6	14	13	5	6	32	4.8	0	37	46.	3.8	33.	7.8	2.0	5.2	19.
VK	14	27	43	7	5	29	8	5	29	5.7	14	35	12.	3.0	5.9	2.2	2.6	1.2	4.0
La	22	36	97	10	22	52	10	8	24	5.9	12	37	8.9	2.5	6.3	4.0	2.9	1.7	3.7
Bo	43	74	580	25	19	400	25	58	50	4.9	0	82	8.8	9.3	4.2	5.7	0.9	1.4	3.8
Vi	21	130	1330	25	16	820	41	120	52	4.2	0	300	8.1	15.	4.5	6.7	1.2	4.1	3.7
Fa	9	2	15	4	2	11	4	3	13	5.2	58	37	6.7	8.1	4.5	2.1	0.5	0.8	1.5
Fl	38	47	72	12	12	36	9	8	13	4.6	0	29	25.	14.	14.	7.6	3.3	3.9	11.
Fi	50	57	160	27	43	100	15	33	14	4.9	0	38	—	—	—	—	—	—	—
Am	52	73	150	23	31	96	19	20	32	5.6	0	34	—	—	—	—	—	—	—
Pl	30	63	170	20	28	95	12	25	17	4.5	0	55	6.6	1.3	7.6	1.4	0.5	0.4	0.6
Sö	20	48	48	13	14	27	9	9	18	5.0	0	37	—	—	—	—	—	—	—
Sm	19	27	22	9	7	11	5	11	7	4.8	0	30	8.1	2.6	6.8	1.8	0.6	0.9	0.7
Sy	37	58	45	17	24	21	8	8	23	4.8	0	26	5.1	4.8	4.2	1.1	0.6	0.6	3.8
BH	24	32	43	12	15	25	7	20	10	4.6	0	33	11.	1.9	14.	1.1	0.3	1.5	2.9
Sk	31	45	200	20	39	120	11	15	25	4.7	0	61	11.	3.7	8.9	2.1	1.0	1.0	1.6
Al	34	75	160	18	35	99	14	18	30	4.2	0	56	31.	4.7	19.	5.2	1.7	2.3	4.6
Hi	17	18	89	5	9	36	9	8	15	5.6	0	40	—	—	—	—	—	—	—
Ta	29	39	460	2	10	220	16	28	25	5.9	15	65	*	*	*	*	*	*	*
An	—	—	—	—	—	—	—	—	—	—	—	—	—	—	—	—	—	—	—
Yt	104	29	700	4	10	460	56	57	56	5.9	30	37	—	—	—	—	—	—	—
Gj	175	110	860	1	10	520	31	70	48	5.8	4	25	—	—	—	—	—	—	—
Fn	148	31	73	4	8	43	6	5	39	5.7	0	36	—	—	—	—	—	—	—
Få	39	19	14	1	1	12	3	9	0	5.0	0	9	—	—	—	—	—	—	—
Vå	39	20	11	3	6	25	5	8	26	6.4	17	11	1.6	1.0	17.	0.4	0.6	4.2	3.4
Tr	5	6	6	1	4	3	3	3	3	6.5	—	27	—	—	—	—	—	—	—
Ke	2	—	9	—	—	9	—	—	—	—	—	—	—	—	—	—	—	—	—
Sd	102	100	630	14	18	360	25	42	47	5.3	0	35	—	—	—	—	—	—	—
Da	87	32	92	1	2	55	12	8	50	5.9	11	10	—	—	—	—	—	—	—
Ås	3	22	29	3	5	23	5	6	80	5.4	—	76	8.0	0.6	5.8	0.9	0.6	1.5	6.6
Li	66	230	5380	32	24	3120	160	350	96	4.7	0	300	5.7	9.3	4.0	9.8	1.2	1.4	2.4
So	4	4	16	—	—	16	6	—	6	6.3	64	32	0.0	6.0	9.0	0.0	4.2	3.6	1.4
Ka	26	24	7	7	8	7	5	3	45	5.8	0	10	10.4	17.0	8.2	0.0	0.0	0.0	1.4
Ku	58	31	10	12	9	6	7	3	10	4.7	0	12	0.0	17.0	9.0	0.0	1.5	0.0	5.7
Jy	38	6	14	9	7	10	8	4	23	5.5	0	11	8.1	1.9	4.1	0.5	1.4	0.0	2.5
Pu	54	36	8	15	14	5	5	2	20	4.6	0	13	0.0	7.7	7.3	1.5	2.9	0.0	3.4
Tv	62	67	98	20	19	76	15	10	29	4.7	0	20	3.8	7.3	3.2	0.0	0.0	0.0	0.0
Vn	32	67	241	13	30	144	13	19	39	5.6	0	48	—	—	—	—	—	—	—

Code	mm	mg/m²								pH	HCO_3^- $\frac{\mu val}{l}$	$\varkappa \cdot 10^6$ $\frac{1}{\Omega \cdot cm}$	$\mu g/m^3$ (= kg/km³)						
		S	Cl	NO_3—N	NH_3—N	Na	K	Mg	Ca				S	Cl	NH_3—N	Na	K	Mg	Ca
	Precipitation Dec. 1957 (D 712)												Air Dec. 1957 (L 712)						
Gr	51	107	309	14	19	203	18	22	55	4.6	0	51	—	—	—	—	—	—	—
Öd	72	57	140	12	34	140	15	21	35	5.4	0	43	11.	3.8	11.	2.7	1.2	3.0	8.1
Bs	47	89	548	14	28	321	28	41	33	4.8	0	63	—	—	—	—	—	—	—
Ly	27	71	126	13	22	69	9	12	29	4.2	0	63	—	—	—	—	—	—	—
As	39	65	500	16	50	310	23	37	58	4.5	0	82	17.	6.1	11.	3.9	1.0	0.7	2.7
Vd	37	71	220	17	35	134	19	17	34	5.4	0	58	—	—	—	—	—	—	—
Bl	46	114	204	16	43	133	16	17	53	4.5	0	52	—	—	—	—	—	—	—
Ty	23	55	160	12	37	97	13	21	37	5.8	22	60	14.	2.4	19.	2.0	0.7	1.6	6.5
Hö	38	128	1255	15	27	742	44	53	114	4.6	0	145	—	—	—	—	—	—	—
Ad	33	80	217	13	33	137	13	15	41	5.2	0	53	—	—	—	—	—	—	—
Ab	86	110	1020	13	13	670	51	11	450	6.3	380	97	11.	3.9	16.	2.0	1.7	2.4	7.7
Ed	79	76	290	7	12	190	18	31	73	5.7	0	29	7.1	0.9	4.8	1.4	1.3	0.3	2.2
Es	158	181	796	21	22	616	68	54	32	5.9	81	29	3.1	3.5	0.7	3.5	0.7	0.4	0.5
Le	60	93	330	11	25	170	23	34	49	4.4	0	55	60.	11.	8.4	1.6	1.3	3.6	7.2
Ro	51	80	250	15	21	110	25	23	66	4.4	0	54	22.	10.	4.5	4.7	1.5	1.6	8.5
NA	103	120	1900	14	62	1210	80	150	200	5.7	36	91	10.	8.8	6.0	5.2	0.3	1.2	4.5
Ca	83	114	1420	15	32	809	51	90	53	5.9	20	71	2.6	7.0	1.7	3.2	0.4	0.5	0.0
Va	131	31	1454	41	54	—	—	—	—	5.7	7	49	—	—	—	—	—	—	—
Sc	52	173	536	32	62	280	24	27	57	4.4	0	69	—	—	—	—	—	—	—
BV	74	260	158	13	30	52	14	33	190	4.8	0	45	67.2	7.6	6.8	1.2	0.7	0.2	2.2
Bn	26	38	114	14	27	32	13	24	230	6.3	75	110	59.4	39.6	13.2	2.1	1.9	0.5	5.5
Au	46	116	74	19	13	16	6	11	65	4.4	0	33	51.8	15.0	12.5	1.5	1.6	2.3	1.6
Fe	41	93	79	13	34	37	11	5	33	4.6	0	28	15.9	6.5	2.3	1.5	0.9	0.7	4.0
Ba	38	62	16	6	2	5	3	3	26	4.7	0	15	45.3	13.0	7.5	4.8	0.7	0.3	1.5
Ho	10	40	20	12	25	6	17	5	37	5.8	42	73	19.4	1.6	4.7	1.4	1.0	0.9	5.3
Rm	20	21	34	9	0	8	6	8	187	6.9	376	86	5.3	0.9	2.5	2.1	0.3	0.2	1.6
Et	16	43	38	5	18	11	10	4	40	4.8	0	46	6.5	9.0	3.9	1.7	0.5	0.2	1.7
He	—	—	—	—	—	—	—	—	—	—	—	—	—	—	—	—	—	—	—
Rz	14	33	25	4	5	2	1	2	19	4.6	0	21	14.6	6.0	4.4	2.3	0.5	0.3	1.6
Wi	31	59	17	4	3	2	3	4	33	5.4	0	26	39.6	3.8	4.1	5.2	0.6	0.4	1.8
Lz	33	82	21	13	0	3	2	4	72	5.7	33	26	14.5	3.9	4.7	0.5	0.5	0.2	2.2
Kl	17	57	22	4	14	4	3	5	40	5.6	19	33	45.3	12.8	8.2	1.2	0.9	0.6	2.4
BL	45	170	17	7	37	16	11	8	120	5.2	0	34	56.6	8.5	6.6	2.6	1.6	0.6	6.7
DH	27	155	1208	14	27	610	40	55	71	4.3	0	251	29.8	16.9	2.8	4.7	1.4	1.4	1.4
DB	44	122	221	19	38	147	10	16	40	4.3	0	70	32.4	10.3	5.4	1.6	0.7	0.3	0.8
W	51	99	247	21	30	128	11	17	31	4.3	0	51	9.8	19.6	1.6	7.9	3.9	4.1	3.9
SA	25	90	103	8	35	67	12	9	41	5.1	0	55	27.7	9.1	6.6	1.4	0.9	0.0	0.8
U	30	107	109	13	33	66	14	11	79	4.5	0	62	11.5	35.5	5.6	2.0	2.5	1.3	1.1
B	105	140	221	26	47	109	14	16	65	5.2	0	25	13.2	6.0	1.5	1.5	0.4	0.3	0.5
D	19	46	123	9	10	66	6	7	33	4.8	0	49	12.3	16.9	2.8	1.8	1.9	0.3	0.8
MH	27	77	66	14	8	36	8	3	69	4.6	0	42	60.0	91.9	6.0	0.4	1.1	0	0.5
RS	109	148	456	21	11	332	35	35	66	4.8	0	28	5.4	23.3	3.1	4.5	1.2	0.8	2.4
LM	38	44	73	11	10	46	4	5	33	5.2	0	21	18.9	29.5	4.2	1.1	1.6	0.5	1.2
Lx	62	65	45	24	9	32	6	6	25	5.0	0	19	23.8	76.9	82.7	70.7	24.6	1.4	3.4
Bg	38	59	186	13	45	140	79	6	91	5.8	146	56	17.4	15.5	3.2	3.5	1.6	1.0	1.5
Ac	63	18	41	29	9	29	7	5	129	5.8	28	22	45.1	19.5	5.4	0.4	1.9	0.8	3.0
Za																			

CO_2-values in Scandinavia November—December 1957 och Januari 1958

(Cf, Fonselius, Koroleff: Tellus 7, pp. 258—265)

Station	November					December					January				
	Date	°C	Wind	Weather	CO_2 ml/10 l	Date	°C	Wind	Weather	CO_2 ml/10 l	Date	°C	Wind	Waether	CO_2 ml/10 l
Ao	14	3.6	WNW 3	7	3.07	13	—16.2	WSW 4	3	3.33	3	—25.0	WSW 3	0	3.34
	21	0.0	W 5	10	3.20	16	— 2.6	W 7	9	3.37	4	—	—	—	—
	22	—0.6	NW 9	✳ 8	2.90	21	—12.0	S 3	10	3.17	19	—10.0	S 2	✳ 10	3.32
						22	— 6.0	NE 2	9	3.15	20	—	—	—	—
Öj	14	1.2	Calm	5	3.16	13	—17.2	Calm	9	3.24	3	—20.2	Calm	3	3.46
	21	—3.0	W 2	10	3.12	16	3.3	W 2	1	3.13	4	—20.2	Calm	1	3.19
	22	0.4	Calm	9	3.04	21	— 7.1	Calm	10	3.12	19	— 9.6	N 4	✳ °10	3.16
						22	— 0.3	N 2	5	3.10	20	—10.6	NW 2	2	3.05
Br	14	3.0	NNW 2	1	2.67	13	—13	W 2	5	3.55	3	—16.0	SW 2	0	3.61
	21	1.0	NNW 1	9	3.18	16	0.0	W 15	✳ 10	3.28	4	—20.0	N 2	0	3.67
	22	—1.0	W 2	10	3.09	21	— 2	Calm	9	3.19	19	— 6.0	NNW 2	✳ °8	3.37
						22	— 3	Calm	5	2.98	20	— 7.0	Calm	1	3.38
Er	14	—	—	—	—	13	— 3.2	NE 5	1	3.34	3	— 5.1	W 4	1	3.11
	21	—	—	—	—	16	1.2	W 4	10	3.51	4	— 5.6	W 7	5	3.09
	22	—	—	—	—	21	7.9	W 12	8	3.25	19	—12.5	Calm	8	3.23
						22	5.0	W 4	8	3.06	20	—10.9	N 1	6	3.06
Fl	14	—0.8	NW 1	= 8	3.05	13	— 4.5	NE 2	✳ 10	3.13	3	—10.0	Calm	0	3.60
	21	—0.0	W 1	8	3.35	16	— 1.2	SE 3	9	3.16	4	—18.0	S 2	0	3.54
	22	—1.2	SW 3	=°10	3.12	21	4.2	W 3	5	3.22	19	— 6.2	W 1	7	3.48
						22	3.2	W 2	● °10	3.10	20	— 4.6	NW 1	0	3.02
Pl	14	1.0	Calm	10	3.08	13	— 3.0	NE 9	✳ 10	3.15	3	—	—	—	—
	21	1.0	Calm	10	3.36	16	1.0	W 2	10	2.92	4	— 9.0	NW 1	9	3.52
	22	1.0	W 2	10	2.87	21	—	—	—	--	19	— 1.0	E 5	△ 4	3.18
						22	4.0	W 2	9	3.07	20	— 1.0	W 2	✳ 5	3.39
Kn	14	—6.0	E 10	✳ 9	3.04	13	—17.0	NE 10	8	2.83	3	—10.0	SW 10	—	2.65
	21	—4.0	W 5	5	2.86	16	— 1.0	S 5	—	2.79	4	— 5.0	N 10	✳ 10	2.81
	22	—6.0	NE 5	✳ 10	2.90	21	—10.0	N 15	10	3.12	19	—10.0	NNE 15	5	2.99
						22	—10.0	N 10	—	3.18	20	— 7.0	NE 12	3	2.95
Ta	14	—	—	—	—	13	—11.2	SW 1	1	3.16	3	—	—	—	—
	21	3.3	W 1	9	3.20	16	— 5.2	SSW 1	9	3.06	4	—24.9	Calm	10	3.49
	22	—5.7	Calm	9	3.33	21	0.0	NW 2	9	3.40	19	—11.6	Calm	=°	3.55
						22	— 7.8	SW 4	9		20	—17.0	Calm	10	3.02
Vg	14	5.1	SSW 4	10	3.11	13	— 6.7	NNE 3	=° 9	3.00	3	— 7.4	N 2	=° 8	3.37
	21	4.0	ESE 1	=°10	3.11	16	1.3	SW 7	✳ 10	3.14	4	— 9.2	N 5	0	3.27
	22	3.0	WNW 5	=°10	2.91	21	— 1.4	E 6	▽ 10	3.25	19	— 5.6	NNE 1	2	3.06
						22	— 4.0	Calm	✳ 1	3.25	20	— 6.4	NNE 1	3	3.09
Vå	14	—5.3	Calm	10	2.96	13	—	—	—	—	3	—	—	—	—
	21	—2.6	E 2	10	3.24	16	3.1	—	5	3.46	4	—	—	—	—
	22	—3.0	SW 2	5	3.49	21	0.0	SW 2	✳ 10	3.30	19	— 5.8	SW 10	10	3.20
						22	— 0.8	NNE 2	10	3.27	20	— 3.7	WSW 13	5	3.10
Sd	14	0.0	Calm		3.37	13	— 6.0	N 5	2	3.63	3	— 4.0	W 2	10	3.39
	21	4.0	W 6	●° 9	2.80	16	4.0	W 5	9	3.22	4	1.0	W 15	5	2.99
	22	4.0	SW 5	△ 9	2.85	21	4.0	WNW 12	● 9	3.07	19	— 3.0	N 2	△ 1	3.34
				●		22	6.0	WSW 15	● 9	3.22	20	— 3.0	W 2	✳ 8	3.21
So	14	—8.6	WNW 1	10	3.31	13	—32.8	SSE 1	0	3.27	3	—33.0	—	0	3.42
	21	—3.1	—	10	3.36	16	— 0.4	SW 4	0	3.40	4	—30.4	SE 1	10	3.42
	22	—1.0	S 1	10	3.35	21	—23.1	W 1	0	3.40	19	—11.3	E 2	✳ °10	3.48
						22	— 7.1	W 3	10	3.43	20	—14.6	NNW 2	10	3.25

Station	November						December						Januari					
	Date	°C	Wind		Weather	CO_2 ml/10 l	Date	°C	Wind		Weather	CO_2 ml/10 l	Date	°C	Wind		Weather	CO_2 ml/10 l
Ka	14	1.0	SE	1	10	3.39	13	— 7.5	SSW	1	10	3.47	3	—18.4	Calm		0	3.50
	21	2.0	WSW	1	10	3.48	16	— 0.8	SSW	4	4	3.10	4	—16.0	SE	2	✳ 10	3.48
	22	1.9	SW	2	10	3.47	21	0.8	W	3	10	3.44	19	— 4.2	ESE	3	✳ 10	3.29
							22	— 1.9	SSW	2	5	3.43	20	—10.8	NNW	2	✳ 10	3.32
Kv	14	0.3	NW	2	0	331	13	—15.6	Calm		5	3.48	3	—19.7	NW	1	0	3.47
	21	2.0	WNW	2	10	3.31	16	— 2.9	WSW	3	10	3.31	4	—27.9	Calm		0	3.47
	22	0.8	WSW	5	● 10	3.31	21	0.0	ESE	2	✳ 10	3.24	19	— 5.9	ESE	5	✳ 10	3.35
							22	— 2.8	WSW	2	0	3.06	20	—10.1	WSW	1	10	3.54
Jy	14	1.0	NNW	1	8	3.27	13	—12.6	SSW	1	5	3.37	3	—16.4	N	2	0	3.54
	21	2.8	WNW	2	10	3.26	16	— 3.1	SW	2	10	3.37	4	—27.7	N	1	5	3.49
	22	0.5	WSW	3	10	3.43	21	3.0	WSW	3	● 10	3.34	19	— 3.6	E	3	✳ 10	3.26
							22	— 0.2	W	2	10	3.54	20	— 9.2	WNW	2	✳ 10	3.45
Pu	14	1.3	NW	2	10	3.31	13	9.4	S	1	5	3.49	3	—12.6	NNW	1	7	3.34
	21	—2.3	W	2	10	3.29	16	— 1.6	SW	2	10	3.42	4	—21.9	NNW	1	0	3.15
	22	3.1	WSW	2	10	3.27	21	3.8	SW	2	10	3.47	19	— 4.2	SE	4	✳ ° 10	3.18
							22	0.8	SW	3	5	3.34	20	— 4.2	W	2	9	3.46
Tv	14	5.0	N	2	0	3.31	13	— 7.0	ENE	2	10	3.35	3	— 9.0	NNE	2	10	3.52
	21	4.0	NW	2	10	3.53	16	2.0	W	3	10	3.39	4	—10.0	E	1	10	3.41
	22	6.0	WSW	4	10	3.41	21	7.0	WSW	7	10	3.24	19	0.0	NW	1	10	2.93
							22	6.0	WSW	4	10	3.47	20	— 3.0	W	1	10	3.36
Öd	14	—	—		—	—	13	— 1.2	NE	6	✳ 10	3.13	3	— 7.8	Calm		3	2.99
	21	2.0	S	1	10	3.13	16	— 4.2	SSW	3	9	3.28	4	— 4.9	SE	4	10	3.28
	22	2.8	S	2	● ° 10	3.53	21	6.2	SW	5	3	3.29	21	— 0.8	S	3	16	3.49
							22	5.1	WSW	3	8	3.30	20	— 0.8	SW	2	9	3.02
As	14	2.8	ESE	2	6	3.11	13	— 0.1	ENE	3	✳ 9	2.97	3	— 5.2	SW	1	2	3.07
	21	2.2	S	2	0	3.36	16	— 4.9	S	2	6	3.23	4	— 5.2	ESE	3	8	3.30
	22	5.0	SW	1	9	3.63	21	5.6	WSW	4	4	3.15	19	0.1	W	5	8	3.15
							22	6.0	—		—	3.35	20	—	—		—	—
Vl	14	—	—		—	—	13	3.9	ENE	15	● ° 9	3.51	3	1.0	SSE	6	—	3.23
	21	0.9	Calm		= ° 8	3.07	16	— 4.3	SE		5	3.13	4	0.1	SSE	11	—	3.10
	22	9.1	NNW	10	2	3.13	21	7.0	WSW		—	3.12	19	2.9	NNW	9	—	2.91
							22	8.3	SSW	10	5	3.13	20	3.9	NW	4	—	2.82